Department of Aeronautics
Imperial college London
MPhil Thesis

Mechanical performance of through thickness reinforcement for damage tolerant aircraft structures

Imperial College
London

Author: Chang Kuan
Supervisor: Dr Ajit Panesar
Supervisor: Dr Giuliano Allegri

Abstract

This thesis is focused on investigating the mechanical performance of Z-pin reinforced laminate under different loading conditions and the development of automatic Z-pin insertion machines.

A versatile surface-based finite element modelling strategy is developed for the analysing of cohesive contact analysis. The modelling approach is developed based on bridging law and modified Coulomb friction law. This modelling method has been validated via comparing against the benchmark work, including the Double cantilever beam test, 4-point End-Notched Flexure test, Mixed-mode Bending test. The tensile fibre failure, modelled using the Weibull Failure criterion, verified through comparing the modelling results to an experimental tensile test result of unidirectional laminate coupon.

The modelling approach carried forward to the analysis of the Z-pin reinforced laminate. A three-dimensional modelling approach was used to address the microstructural features of Z-pinned laminates. These features, including the presence of resin pockets surrounding Z-pin, stacking sequence, Internal splitting. The interface between Z-pin and laminate, as well as internal splitting, were described by customised surface-based cohesive contact. There are a few factors that significantly affect the modelling results, including Frictional coefficient, internal splitting, mode mixities, and each of them was discussed in the parametric study section.

The modelling approach was used to justify the performance of Z-pins in resisting dynamic mode I and mode II delamination has been investigated at a high loading rate. It was found that the Z-pin efficiency in resisting mode I delamination decreased with increasing loading rate compared to the quasi-static loading case, and the loading rate in the mode II test did not significantly influence the maximum bridging force. Moreover, the FE result tends to delay the shift of the failure mode from pull-out to pin rupture.

An automatic Z-pin insertion machine is proposed in the last chapter. Building based on a 3D-printer, the insertion machines able to move, heat, and insert Z-pins by the control of Commercial software LabView.

Keywords:

Bridging law, Surface-based cohesive contact, Three-Dimensional FE model, Dynamic bridging, LABVIEW

Author’s Declaration of Originality

I hereby certify that I am the sole author of this thesis and that no part of this thesis has been published or submitted for publication.

I certify that, to the best of my knowledge, my thesis does not infringe upon anyone’s copyright nor violate any proprietary rights and that any ideas, techniques, quotations, or any other material from the work of other people included in my thesis, published or otherwise, are fully acknowledged in accordance with the standard referencing practices.

I declare that this is a true copy of my thesis, including any final revisions, as approved by my thesis committee and the Graduate Studies office, and that this thesis has not been submitted for a higher degree to any other University or Institution.

Copyright Declaration

Author: Chang Kuan

Supervisor: Dr Ajit Panesar

Supervisor: Dr Giuliano Allegri

Contents

List of Figures

List of Tables

Chapter 1 Literature review

Composite laminate is playing an increasingly important role in the aerospace industry. However, despite the early ambitions of primarily applying composite laminate on the aircraft structure, the poor impact damage tolerance, low through-thickness mechanical properties, and weak strength of the bonded joints are still yet to solve. There are a series of techniques invented to accommodate the potential problem, which includes: 3D weaving, stitching, and braiding, etc. these techniques are effective at increasing the delamination resistance and Impact damage tolerance. However, none of these techniques can apply to prepreg laminates. Attempts to reinforce uncured prepreg will result in excessive fibre damage that degrades in-plane strength properties. The only technique capable of reinforcing prepreg laminates in the through-thickness direction in large commercial quantities is z-pinning.

In the current study, there are a few techniques to insert the Z-pin into the laminate, which can be divided into two categories, manufacture with z-pin insertion before cure and manufacture with z-pin insertion during cure.

1.1 Z-pin manufacturing methodology

1.1.1 Z-pin production and preforms

Any material may be used to manufacture Z-Pins, if it can be manufactured as a small diameter long rod and is strong enough to resist the insertion process into the laminate. Z-pins are typically made of a composite or metal wire. A list of typical materials that making Z-pins are [1]:

- T650/BMI
- T300/Epoxy
- S-Glass/Epoxy
- Titanium
- Stainless steel

In the first stage, carbon fibres are pulled off and sent into a resin bath at an elevated temperature. And then, the material will exit the bath through a nozzle and are drawn together to form a structure like a string. Following that, the material will be sent to the autoclave. The cured material will be cut into single pins and put into the foam in an automated process. Pins are then cut with an acute angle at the ends, and the angle will assist the penetration of the pin into the composite and minimise the distortion of the fibres. Figure 1.1 shown below provides a visual guide of how Z-pin bundles were manufactured [2] . Quality control of the manufacturing and the behaviour of Z-pins has been investigated by Partridge et al[3]

The Z-Pins are embedded in double-layer foam. The foam with pins inserted is called a preform. The two layers of the preform are made by different materials where the low-density preform is usually made by polystyrene, whereas the high-density layer is made of the Rohacell LastaFoam material. The low-density preform is designed to hold the pins before the pinning process and can be crushed easily. Support foam is used to hold the pins prior to the pinning process and designed to collapse. The high-density preform offers stability towards the lower part of the pins to prevent them from buckling during insertion. The preform can be designed to deal with Z-pins at different diameters (ranging from 0.28mm to over 1mm) and also different areal densities ranging from 0.75% (for damage tolerance) to 4%

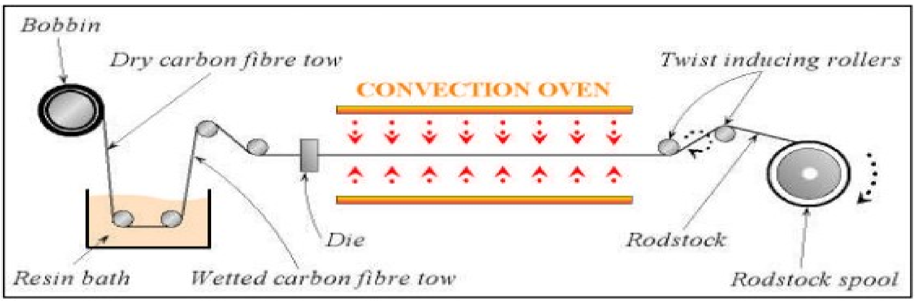

Figure 1.1:Z-pin rodstock pultrusion process [4]

1.1.2 Manufacture with Z-pin insertion before cure

In the contemporary state of art, the most popular method for z-pinning which can be performed on uncured laminates is called Ultrasonic Assisted Z-fiber^{TM} (UAZ^{TM})[11]. The Z-pins are made from either metal wire or pre-cured fibrous composite. The distribution and orientation of pins in the compressible material determines their areal density and orientation in the laminates. For the Z-pin insertion, the Z-pin preform is placed on top of a reinforced un-cured laminate while a layer of release film can be inserted between them to avoid the inclusion of debris and fractured Z-pin dust into the laminate. Finally, the crushed preform and extra lengths of Z-pins are trimmed by a cutter. To improve the efficiency and accuracy, the insertion of the Z-pins into both the compressible material and laminates can be accomplished by automatic tools. The main advantage of the UAZ^{TM} method is larger cross-section area of horn allows the insertion of multiple Z-pins in one press, which results in improved manufacture efficiency. Nevertheless, the main disadvantage is the insertion quality is difficult to control. Due to the insertion resistance provided by the un-cured laminate and the limited support from the foam, the pin insertion angle is always offset from the intended direction and/or the Z-pin may even be damaged. Figure 1.2 gives a schematic of how the Z-pinning process does will work.

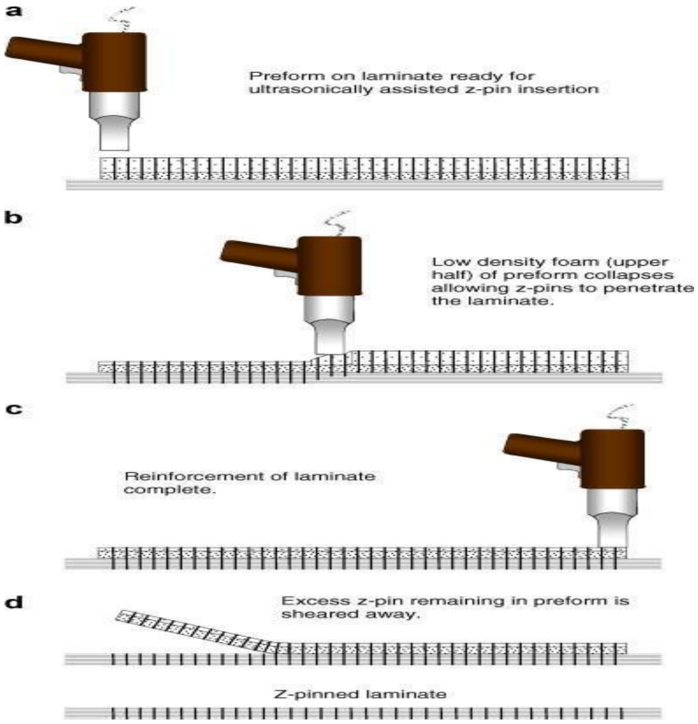

Figure 1.2: UAZ insertion of Z-fibre

To improve the quality and control of insertion, several novel insertion approaches have been proposed since the UAZ^{TM} method. Hexcel[5] invented an insertion method in liquid composite moulding preforms, whereby insertion is assisted by a solid needle. As shown in Figure 1. 3, this approach first employs a vibrating needle to drill a hole through the preform in the Z-pinning position. In the second step, the needle is withdrawn from the laminate. Subsequently, the reinforcing Z-pin is inserted in the pre-drilled hole. EADS ECC[6] improves the efficiency by replacing the solid needle with a hollow one, which is not retracted immediately after drilling a hole. Instead, the Z-pin is pushed into the inner channel of the needle until reaching a predetermined depth. These needles assisted insertion methods can control the insertion quality dramatically because the insertion resistance is decreased along the pre-drilled path. In addition, the usage of dry fabrics is low-cost as they are much cheaper than impregnated ones. However, the insertion efficiency has not shown improvement in comparison with the UAZ^{TM} method.

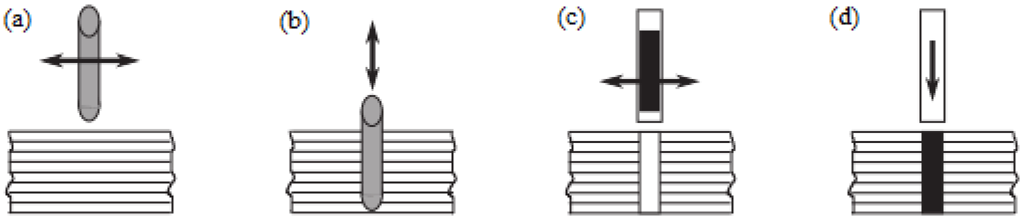

Figure 1.3:Needle-assisted insertion method [5]

An alternative approach was invented and described in [5]. This process consists of the initial stacking of dry fabrics, the impregnation process, the insertion of through-thickness reinforced (TTR) elements, and the cure of the 3D fibre reinforced composite material. The impregnation process may take place either before or after the insertion step. The inserted TTR elements are dry fibre bundles. The machine used for TTR insertion is illustrated in Figure 1.4. During one loop of the TTR insertion, it can be summarised as follows. Firstly, driven by an actuator, the probe 35 firstly drills an insertion path through the thickness of the laminate 30. Then, the movable tube 16, to which the dry bundle (dry TTR element) is fastened by the clamp 12B, moves downwards until its bottom end contacts with the probe 35. Subsequently, the tube together with the dry TTR element, is inserted through the thickness of the laminate, under the guide of the probe. Then, the tube is withdrawn to the original position, and the dry TTR element is left in the laminate. Finally, the dry TTR element will be shear off by its top-end cutter on the top surface of the laminate.

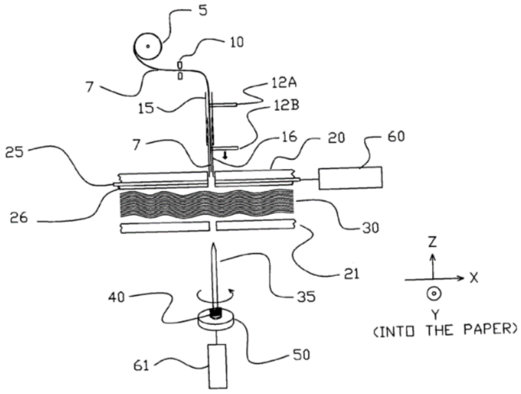

Figure 1.4: Side view of the dry-fibre Z-pin insertion machine [6]

1.1.3 Manufacture with Z-pin insertion during cure

The first manufacture method with Z-pin insertion during cure is disclosed in a patent, U.S. Pat. No. 4808461 in 1989 [7]. In this approach shown in Figure 1. 5, the Z-pins are firstly inserted into a thermally decomposable preform, which is placed on the prepreg laminate. A release film and a bleeder cloth are placed between the preform and the laminate. A steel plate is placed on the top surface of the preform. Then the whole assembly is bagged and placed in the autoclave. As the pressure and elevated temperature are applied on the assembly during the cure process, the thermally decomposable preform collapses while at the same time the steel plate pushes the Z-pins into the composite. After cure, the protruding lengths of the Z-pins are sheared off. In comparison with the insertion-before-cure approaches, this insertion-during-cure method displays significant manufacture efficiency as the insertion of all the Z-pin is completed simultaneously with the cure process. Nevertheless, it is difficult to control the insertion quality, which is deteriorated by many factors that are difficult to control. For instance, the pressure on the preform varies as it collapses during the cure process. This may result in severe misalignment of the Z-pins, Z-pin splitting or even complete rupture.

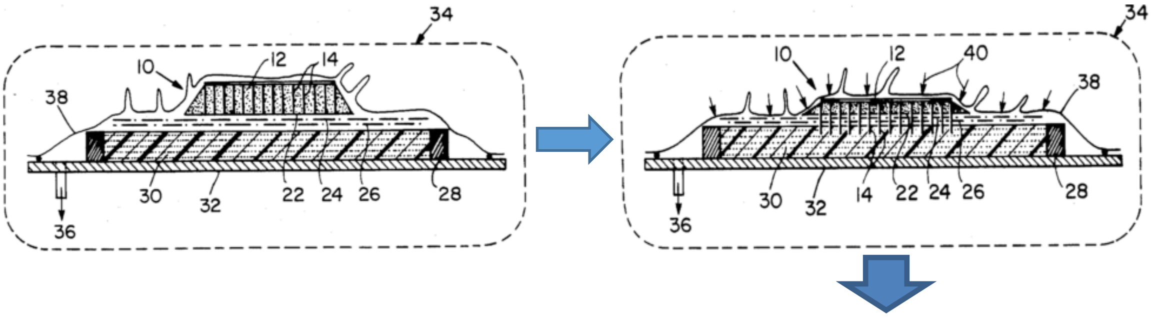

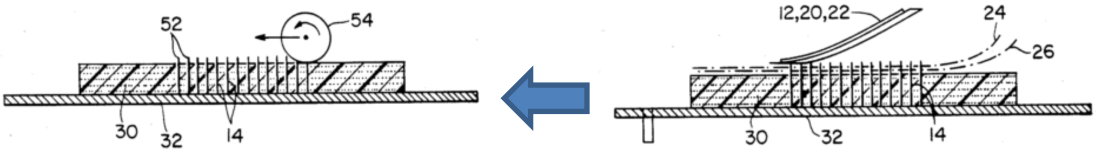

Figure 1.5:Z-pin insertion during cure with thermally decomposable preforms [7]

Choi et al.[8] proposed a similar insertion-during-cure method, whereby the thermally decomposable preform is replaced by a support structure that can be used repeatedly, as shown in Fig. 1.5 [8] . The structure comprises an upper fixture whereby guide pins are installed permanently at the bottom surface, and a lower fixture with Z-pins inserted into its previously machined holes. The distribution of guide pins matches the distribution of holes, and thus determines the areal distribution of the Z-pins. Driven by the vacuum pressure during the cure process, the upper fixture moves towards the lower fixture, and simultaneously the guide pins push the Z-pins into the laminate. In comparison with the first insertion-during-cure method shown in Fig. 1.6, this approach improves the insertion quality dramatically because the preform does not collapse during the cure process. It can supply consistent support for all the Z-pins throughout the whole insertion process. Moreover, the usage of reusable preforms rather than a disposable one is environment friendly and saves materials. However, as the insertion-before-cure method shown in Fig. 1.5 the areal density of Z-pins is determined by the distribution of holes in the preform. This reduces the flexibility of this method as one preform allows achieving only one specific areal density of Z-pins.

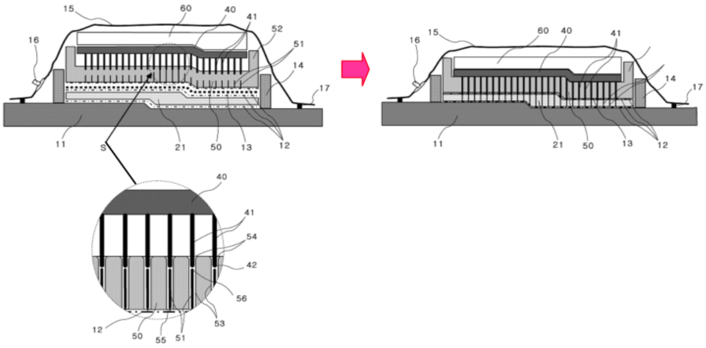

Figure 1.6: Insertion-during-cure method with reusable preform[8]

So, manufacture before the cure process will give a better accuracy to the whole system. A better system is suggested by CSAA[9] and the schematic is included below:

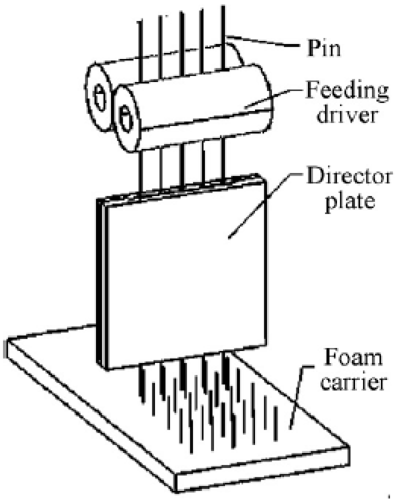

Figure 1.7: Pins feeding device and the director device [9]

Three main sections are combined to make the whole device intact, including the Director device, the cutting device, and pin feeding device. Pins feeding device uses the form of drive roller, and a motor drives the main drive roller. The pressing force between the primary and auxiliary drive rollers provides friction between pins and drive rollers, thereby driving the pins to insert. The implementation depth is determined by the rotation angle of the main drive roller.

1.2 Performance of Z-pin inserted laminate

Laminated composites are susceptible to delamination and one of the most effective ways to accommodate this issue is to insert through-thickness pins, known as Z-pins. However, there are some trade-offs in applying these pins. It is anticipated that the insertion of z-pins into a fibre laminate will lead to both local stress concentration and fibre waviness. In tension, some reduction in tensile strength is expected due to the stress concentration. In compression, the stress concentration and fibre waviness will lead to a reduced fibre micro buckling strength of laminate.

1.2.1 Z-pinned laminate stiffness

The Z-pinning process will affect laminate's stiffness properties and hence global response of z-pinned composite. Therefore, evaluating the engineering stiffness constants and examining the stress distribution around a z-fibre could be a first step towards the development of a design tool for predicting damage initiation and damage propagation in z-pinned composite.

1.2.1.1 Young's modulus

The effect of Z-pinning on the in-plane elastic properties of laminate has been investigated using FE analysis, and all of which have reported reduction on young's modulus in both axial and transverse directions. The reduction in elastic properties is most severe for the unidirectional laminates, and it becomes less severe when the numbers of non 0-degree lamina are increased. In the case of cross-ply or quasi-isotropic laminates which are applied in aircraft structures, the reduction in the axial modulus due to z-pinning is usually under 10%[10]. The reduction to elastic properties is due to microstructural damage caused by z-pinning, particularly fibre waviness, fibre crimp, and swelling that reduces the fibre volume content. A typical way to accommodate this issue is to use extremely fine diameter z-pins and control the curing process to suppress the swelling.

1.2.1.2 through thickness elastic properties

A finite element model has been developed to investigate the effect of z-pinning on engineering elastic constants, and the unit cell approach has been employed for modelling z-pinned laminates. The laminates used in the study had 2% volume fraction of z-pin which is a typical density used in many structural tests, and four very typical stacking sequences were used, they are[0,0]s ,[0,90]s,[45,-45]s,[45,0,-45,90]s. It has been found by adding a 2% volume fraction of z-fibres the through-thickness young's modulus (Ez) was increased significantly. i.e., by 22-35%, for the four different laminates, studied at work. The reduction in the in-plane moduli was contained within 7-10%. Similarly, Dickinson predicts that through-thickness modulus of a carbon/epoxy laminate will increase by 23% when reinforced with only 1.9% z-pins ad rise to 60% with 4.9% z-pins. However, it is assumed that actually improve on elastic modulus will be less than predicted as the calculations assume a perfect bond between z-pins and host composite, which allows the full transfer of interlaminar loads from laminar into pins[11]. Therefore, it is proved that the z-pin technique is beneficial for design against damages caused by out-of-plane loads in terms of stiffness, like impact and stiffeners pull-off. Assessor

1.2.1.3 Flexural elastic properties

The flexural modulus is not changed for the range of pin contents, and pin sizes, the insertion of pins into prepreg laminates causes local damage to the microstructure, including out-of-plane crimping, in-plane distortion, and fracture of fibres and resin-rich regions. It can be minimised by reducing pin diameter and using an advanced manufacturing process [12]

The flexural modulus stays the same as the local damage to the micro-structure only does minor effect on the cross-sectional area, whereas the flexural young's modulus decreases linearly with the increasing Z-pin density.

1.2.2 Strength properties

The in-plane strength properties of the laminate will inevitably be compromised by the presence of Z-pins. it is often desired to use a high-volume content of z-pins to maximize the damage tolerance, meanwhile the strength properties will be worsened at a quasi-linear rate with increasing volume content and size of the z-pins. The following section will take a closer review and make a discussion.

1.2.2.1 Tensile strength

Unidirectional T300/914C laminates were reinforced with pultruded carbon-fibre/BMI rods of diameter 280μm in a square configuration. The rods were spaced 1.75mm centre to centre. The areal density is 2%. The pin orientation angle is ω=0°. The specimens are to be cured under 180°C and pressure. The tensile specimens were loaded in displacement-control in a screw-driven test machine. [11]

A two-sample t-test confirms that there is a significant difference between the pinned and control specimens. The reduction in strength is 27%. The ultimate failure is fibre fracture; it is convinced that one of the major reduction factors in longitudinal tensile strength is due to stress concentration in the vicinity of pins.[11] Additionally, the z-pinning process will lead to breakage of fibres, as the pins are forced into the laminate, they create a small cluster of broken fibres at each pin location, which acts as sites for splitting crack and tensile failure

1.2.2.2 Compressive strength

The laminates made from T300/914C and IMS/924C carbon fibre-epoxy laminates to determine the effect of z-pin arrangement on the compressive strength.
It is found that the compressive strength is reduced by at least 30% due to the presence of z-pins
The compressive strength of z-laminates is reduced by the misalignment of fibres adjacent to z-pins. The tows are therefore failed by kinking at lower compressive loads. The worst fibre misalignments are caused when fibres weave through a field of z-pins, and weaving is more likely to happen and more severe for 23° and 45° orientation angles than 0° orientation angle.
Consequently, it is found that the compressive strength is inversely related to orientation angle. Increasing pin density was more detrimental to in-plane compression strength than increasing pin diameter.

1.2.2.3 Flexural strength

Flexural strength, is the transverse rupture strength material property, defined as the stress in a material before it yields in a flexure test. The flexural strength decreases at a linear rate with increasing pin content and pin diameter. These trends are consistent with reductions in tensile strength due to pinning. It is known that the strength properties is decreased at a linear rate with increasing z-pin content and diameter, and therefore the linear equation: [12]

Equation 1.1

$$\sigma_p = \sigma_0[1 - \alpha D c_r]$$

Can be used to calculate the failure strength σ_p of a z-pinned laminate. σ_0 Is the strength of the laminate without z-pins, α is an empirical material constant, c_r and D are volume content and diameter of the z-pins respectively.

1.2.3 Fracture toughness

Interlaminar fracture mechanics has proven useful for characterising the onset the growth of delamination, and delamination, is the major issue the z-pin insertion is used to accommodate. To fully understand the failure mechanism, the total strain energy release rate, G_T, the mode I component due to interlaminar tension, G_I, the mode II component due to interlaminar sliding shear, G_{II} are needed to be calculated. And following section will take a closer review of how these values are obtained from experiments and analytical model.

1.2.3.1 Theoretical explanation for Z-pin fracture toughness enhancement

Kravchenko[13] has recently produced a new approach for the through-thickness reinforcement of polymer matrix laminated composite by drilling through-thickness circular holes and inserting fibrous carbon rods into the host laminate after it was cured.

The reinforcing rods were bonded with a liquid resin inside the laminate to be reinforced. This approach allows preserving the original surface quality of the host laminate while improved the mode I delamination resistance. The energy balance for Z-pinned laminate is defined as：

Equation 1.2

$$W = U_e + U_k + U_\gamma + U_{Pin}$$

Where W, U_e, U_k, U_γ and U_{pin} are respectively the work performed by external force, stored elastic energy, kinetic energy, energy dissipation due to the introduction of a new crack surface and energy dissipation due to Z-pin bridging effect. By removing the kinetic energy under the assumptions that the tests are quasi-static, the energy release rate for unit crack extension in a Z-pinned laminate is defined as：

Equation 1.3

$$G = \frac{1}{b}\left(\frac{dW}{da} - \frac{dU_e}{da}\right) = \frac{1}{b}\left(\frac{dU_\gamma}{da} + \frac{dU_{pin}}{da}\right)$$

The last two terms respectively represent the intrinsic fracture toughness of an un-pinned laminate G_C and the energy dissipation G_{Pin} due to the Z-pin bridging effect. Therefore, according to Griffith fracture theory, the total fracture toughness is:

Equation 1.4

$$G = G_C + G_{pin}$$

1.2.4 Experimental investigation for Z-pin fracture toughness

1.2.4.1 Mode I loading

Z-pinned DCB test is essential to investigate the Mode I Fracture toughness, and fracture toughness is the most important measure of Z-pinning technology.

Mode I test is refer to the experiment that applying equal and opposite opening forces on the samples ends. The coupon contains a preformed crack with length a_0, and the forces are directly correlated to the displacement . The experiments conducted by [3,14] was taken as an example to deliver the ideas of how Z-pinned coupon would behaves under mode I loading. The experiment set up is shown below, and the typical reaction force versus displacement curve are also presented：

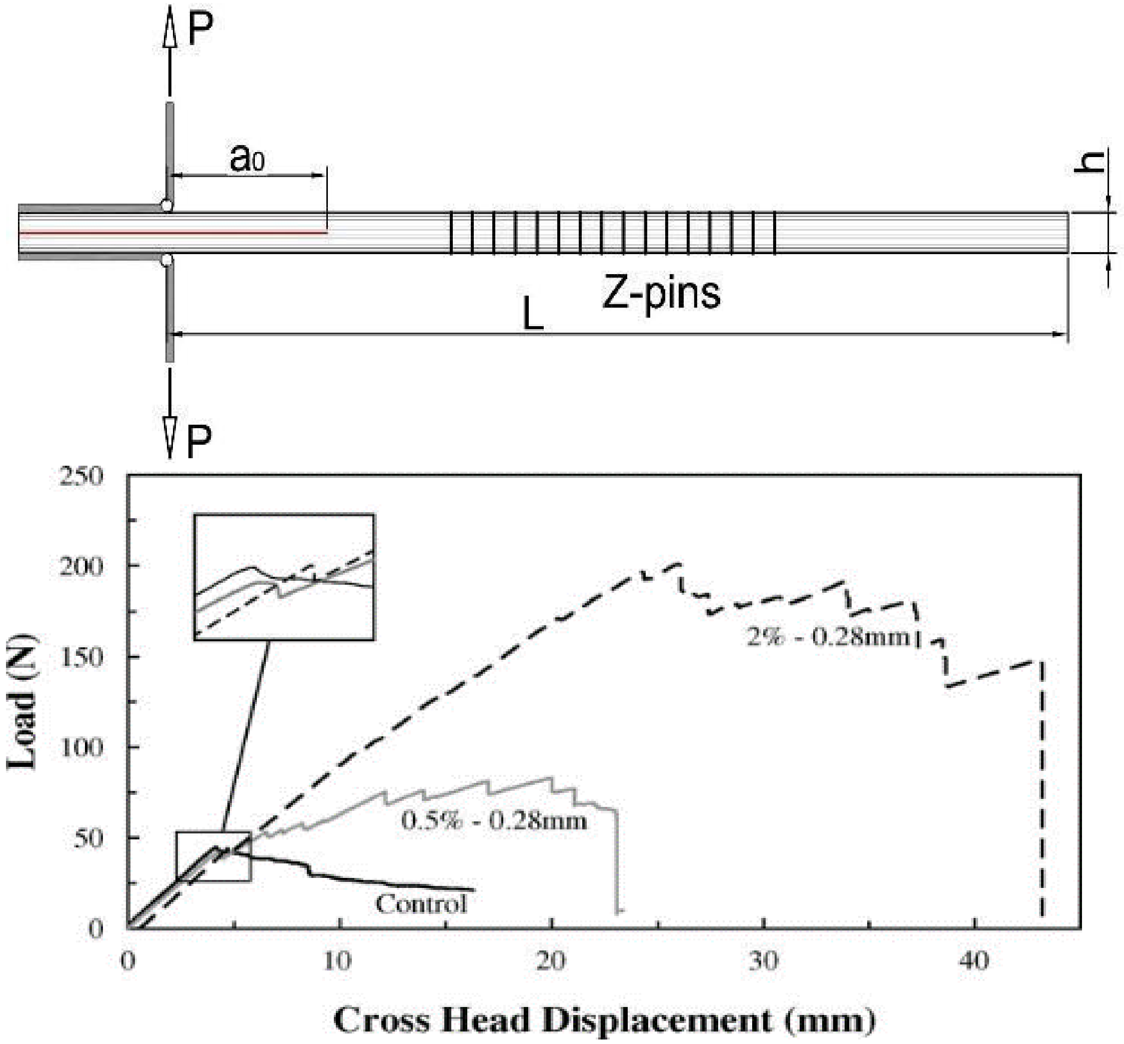

Figure 1.8: Schematic of Z-pinned DCB set-up and load vs displacement curves with and without Z-pins [3,14]

It is noticed that the for the unpinned DCB coupon, the load start to drop continuously once the peak reaction force for debonding has been reached. Nevertheless, in the Z-pinned coupon, the load starts to increase as soon as the crack reaches the first Z-pin row, and the load remained at relative high level after the peak load has been reached, that is due to a matter of fact the bridging zone will consistently withstand the pulling force and translate the load gradually to the new row of pins after the front row been pulled. And a rapid drop was realised at the end which signals that last row of pins been pulled out thus a fatal failure was attained.

Three methods were derived for determining the un-pinned mode I fracture toughness were suggested in the following [15]

They are modified beam theory method(MBT), the compliance calibration method(CC) and the modified compliance calibration(MCC).

- In the MBT method, the toughness is evaluated as:

Equation 1.5

$$G_I = \frac{3P\delta}{2b(a-\Delta_I)}$$

Where Δ_I is a crack length correction factor which used to account for the effects of rotation at the crack tip. P is the equal and opposite force applied to the DCB specimen, b is the sample width, a is the distance between the load P and the crack tip, δ is the displacement at the current displacement. The determination of factor Δ_I need to Plot $C^{1/3}$ against crack length in which the line of best fit crosses the x-axis at some negative value of Δ. The magnitude of this value is the additional crack length, Δ_I

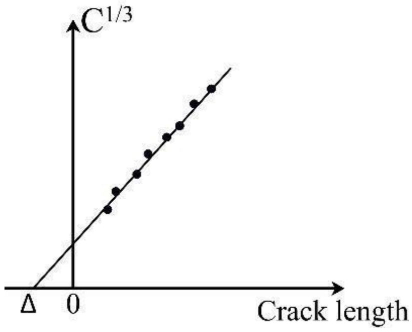

Figure 1.9: Compliance vs the crack length

In the CC method, the delamination toughness is calculated from the slope of a least square plot of log(C) verse log(a).

Equation 1.6

$$G_I = \frac{nP\delta}{2ba}$$

- In the MCC method, the delamination toughness is given by the following equation:

Equation 1.7

$$G_I = \frac{3P^2C^{2/3}}{2A_1bh}$$

1.2.4.2 Mode II loading

According to linear elastic fracture mechanics, the toughness of a structure can be quantified by the energy release rate G, which can be defined as :

Equation 1.8

$$G = \frac{1}{w}(\frac{dU_e}{da} - \frac{dU_s}{da})$$

Where w is the width of the crack front, a is the crack length, U_e is external work performed and U_s is the elastic energy. The potential energy release rate G represent the energy available for the creation of a unit new crack area. For an unpinned ENF specimen, the dissipated energy is assumed entirely consumed by the surface energy of newly created crack under mode II loading. Which is denoted by G_c。Hence：

Equation 1.9

$$G = G_c = G_{IIc}$$

For a z-pinned specimen, the dissipated work includes also included the energy during the z-pin pull-out process. i.e. the elastic energy of the pins, the debonding work between pins and laminate, the friction work during pull-out. So the overall energy would be the energy induced to drive a unit new crack area and the specific energy due to z-pin pull-out (which is governed by the extent of delamination growth Δa

Equation 1.10

$$G = G_c + G_p(\Delta a)$$

Experimentally, 3ENF method can be applied to find out the fracture toughness.

Regarding 3ENF method, the mode II loading test usually have the set-up configuration like shown below[16]:

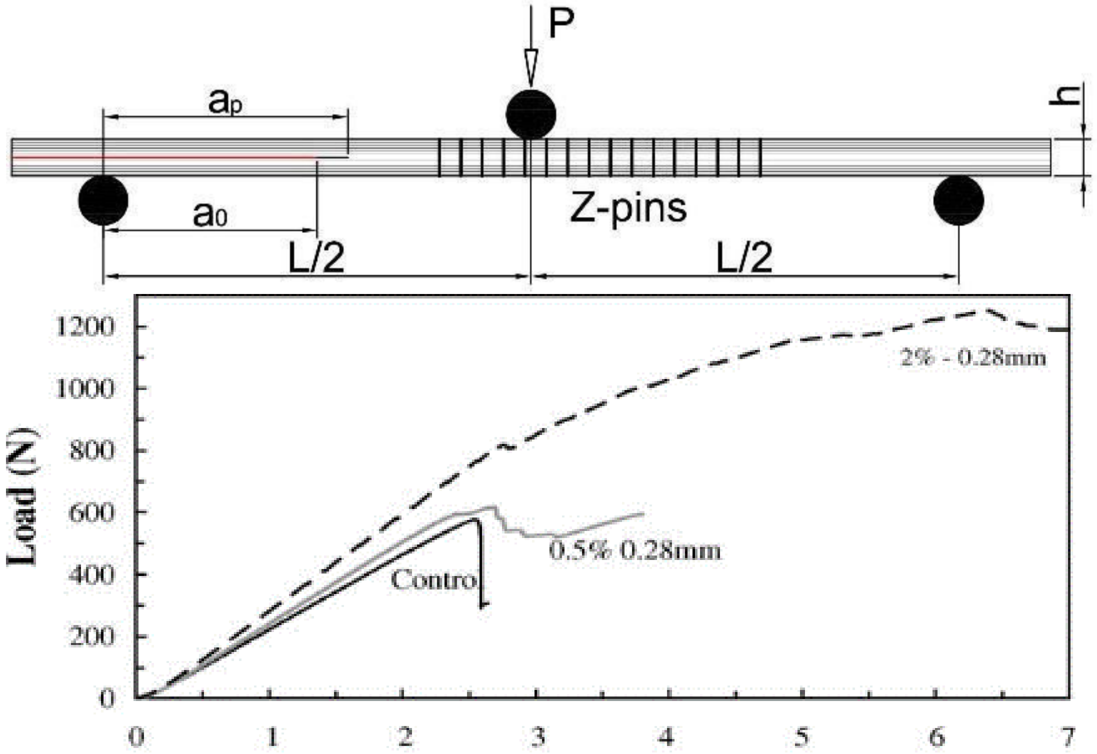

Figure 1.10: Schematic of Z-pinned ENF set-up and load vs displacement curves with and without Z-pins [16]

The main differences in between Z-pinned coupons compared to un-pinned coupons are: higher maximum load, higher crack initiation load, more stable propagation and higher compliance (δ/P).

The fracture resistance under 3ENF loading can be evaluated by three methods. Direct beam theory method, corrected beam theory method and experimental compliance calibration method.

The fracture resistance by direct beam theory method will be illustrated as:

Equation 1.11

$$G_{II} = \frac{9a^2P\delta}{2b(0.25L^3 + 3a^3)}$$

Whereas for corrected beam theory:

Equation 1.12

$$G_{II} = \frac{9a^2P^2}{b^2h^3E_{1f}}$$

And for experimental compliance calibration method:

Equation 1.13

$$G_{II} = \frac{3P^2a^2m}{2b}$$

1.2.4.3 Mixed-Mode loading

In practice, there's not likely to have either pure mode I loading or mode II loading, normally in most of the loading case, the loading condition is an amalgamation of both is what usually been found during practice.

Strong influence of the z-fibres over a large crack wake imply that the crack propagation cannot be described by LEFM, which means that critical energy or stress intensity cannot exist as a constant of the crack growth.

The tendency that the composite laminate is prone to delamination is one of the major drawbacks of many advanced laminated composite structures. And, delamination is subject to and extended by loadings with a wide range of mode mixtures, thus it is important to understand and quantify the mode mixtures.

The test apparatus shown is deployed to determine the delamination toughness at various mix-mode ratios. The test specimen is consisting of a rectangular uniform thickness unidirectional laminated composite specimen, containing a non-adhesive insert at the mid-plane which serves as a delamination initiator.

The length c determines the mode mixture G_{II}/G. The typical load versus displacement curves with the ratio G_I/G_{II} is shown:

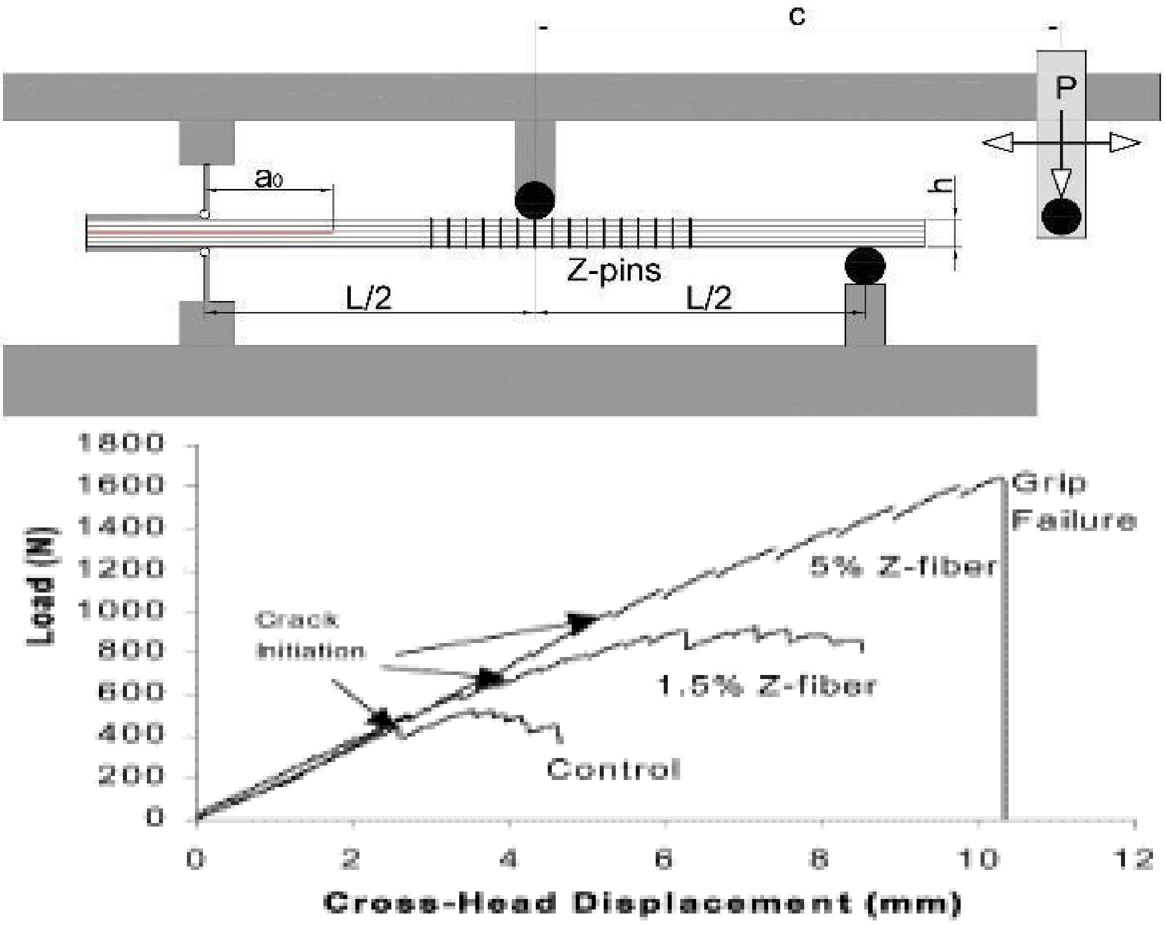

Figure 1.11: Schematic of the Z-pinned MMB Set-up and load vs displacement curves with and without Z-pins [17]

It can be proven that the crack initiation load, ultimate load and deflection displacement corresponding to the loads are all increased due to the presence of the Z-pins.

Equation 1.14

$$c = \frac{12\beta^2 + 3\alpha + 8\beta\sqrt{3\alpha}}{2(36\beta^2 - 3\alpha)}$$

Equation 1.15

$$\alpha = \frac{1 - \frac{G_{II}}{G}}{\frac{G_{II}}{G}}$$

Equation 1.16

$$\beta = \frac{a + 0.5\chi h}{a + 0.21\chi h}$$

Equation 1.17

$$\chi = \sqrt{\frac{E_{11}}{11G_{13}}\{3 - 2(\frac{\Gamma}{1+\Gamma})^2\}}$$

Equation 1.18

$$\Gamma = 1.18\frac{\sqrt{E_{11}E_{22}}}{G_{13}}$$

For a given mode-mixity value, the Mode I and Mode II components of the fracture resistance are determined by Eq. 1.19 and Eq. 1.20 respectively.

Equation 1.19

$$G_I = \frac{24P^2(3c - 0.5L)^2}{b^2h^3L^2E_{1f}}(a + 0.5\chi h)^2$$

Equation 1.20

$$G_{II} = \frac{18P^2(c + 0.5L)^2}{b^2h^3L^2E_{1f}}(a + 0.21\chi h)^2$$

1.2.4.4 Impact resistance

Composite laminates have low capability to resist transverse loads and sometimes the damage from impact is inevitable during manufacturing, installation or maintenance. The Z-pinned structure under static loading has been well investigated whereas few experimental studies focus on characterising the role of Z-pins for composite laminate subject to impact loading.

The effect of Z-pins at different areal densities(0.5%, 2% and 4%) under low-velocity impact was investigated in[18,19], Z-pinning was found to significantly reduce the damage area caused by impact, and highest pin areal density 4% was found to have best efficiency in confining the growth of the delamination.

The effect of laminate thickness on the behaviour of Z-pinned laminate subjected to low-velocity impact was investigated [20] . Quasi-isotropic carbon/epoxy laminated pinned by BMI pins (0.28 mm diameter; 2% areal density) were impacted with the energies varies from 3J to 40J. The results have shown that the effectiveness of Z-pinning in terms of improves the delamination resistance increases with increasing laminate thickness (the amount of reduction in the delaminated areas for 2mm thick sample reduced by 20% whereas the reduction is more than 60% for the 6 mm thick samples)

The influence of how different pin geometries will affect the impact response was explored [21] . Rectangular and circular pins were used to examine the difference, it is found that under the same conditions, Z-pins with rectangular cross-section were more effective than circular pins in improving the delamination resistance to delamination. The difference was primarily reason to the size of the resin rich area nearby the pins, which results in different mechanism of the interface.

The effect of different lay-up under low-velocity impact was studied by recent publication [20]. It is found that the $[0_2/90_2]$s laminates have larger effectiveness after Z-pinning comparing to $[0_2/\pm45]$s and [0/±45/90]s laminates. The difference is contributed the $[0_2/90_2]$s laminate has larger delaminate at a single interface whereas there are multiple but smaller delamination for $[0_2/\pm45]$s and [0/±45/90]s laminates.

1.3 Miscellaneous studies

1.3.1 Experimental Z-pin failure mechanism observation

The major Z-pin failure mechanism that induced by tension and shear was reported by Greenhalgh[22] The authors observed failure of Z-pin due to tensile and shear fracture, damage of Z-pin close to the delamination surface which caused by bending, splitting of Z-pin fibres. Meanwhile, the damage to the laminate caused by Z-pin was observed, including resin-rich pockets, local in-plane waviness of the fibres.

According to authors' observations, it is found that the failure initiation was not affected by Z-pins but the delamination propagation was observed to be stable and significantly delay the failure took place after the crack initiation. Also, the load carrying capability was improved.

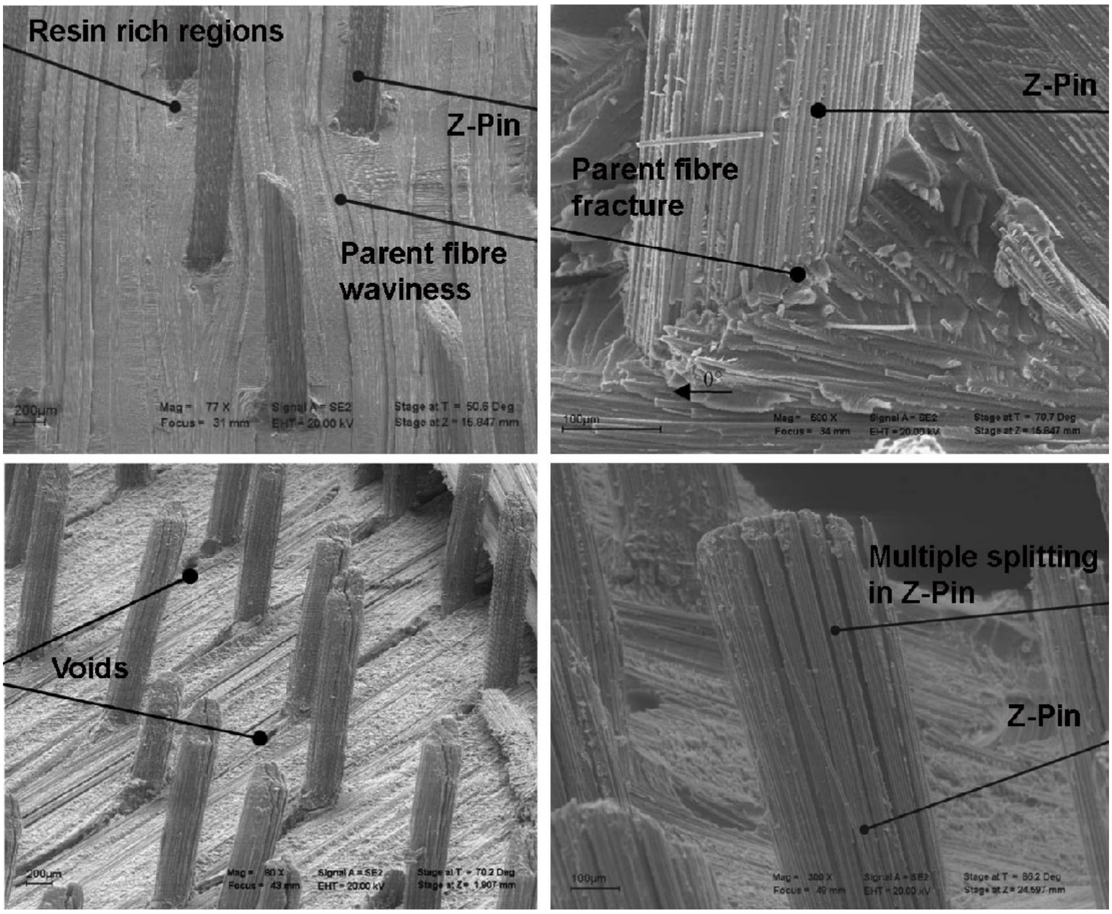

Figure 1.12: Post delamination damage of Z-pin and damage of the laminate caused by Z-pinning [22]

1.3.2 Snubbing effect

The fact that z-pin pull-out process remain stable after the whole z-pin starts to slide, which is called snubbing effect. The formation of the snubbing effect is because large pressure is built up in the z-pin and laminate interface while pin is deflecting, and bigger friction was enhanced in the pin deflection area. The presence of the snubbing effect improves the stability of the pull-out process[23] .

Snubbing has a small effect on predictions of the model for low and moderate crack displacements. At larger displacements, representative of ultimate failure and rod pull-out, snubbing effect becomes very important since it stabilises the pull-out process and strongly affects the displacement and load at ultimate.

The magnitude of snubbing effects is dependent on the amount of lateral deflection of the rod. Ultimate load will be raised if rods are oriented so that they will be loaded against the nap.

1.3.4 Effect of Z-pin density

Two different areal densities were investigated[1] , the specimens with 0.28 mm diameter T300/BMU Z-pins at 0.5% areal density giving a pin to pin spacing of 3.5 mm and secondly, 2% areal density with pin to pin spacing of 1.8mm.

For the mode I loading test, it is realised that the apparent crack propagation resistance ‘G_{IP}’ increases to a plateau at 1200J/m^2 in the 0.28 mm/0.5% DCB specimens and nearly 5000J/m^2 ,in 0.28mm/2% DCB specimens.

For the mode II loading test, the sudden catastrophic failure happens for un-pinned laminate and the specimens with 0.28mm/0.5%, but the delamination develops in a stabilised manner for those 0.28mm/2% specimens

1.3.5 The embedded Z-pin length in laminate

The mode I fracture toughness and fatigue resistance both increase with the Z-pin length up to a critical size [24], beyond which no further improvement occurs due to a transition in the delamination process from single to multiple cracks.

The mode II fracture toughness decreases with increasing z-pin length until a critical size is reached, beyond which there is no further degradation due to a transition in the fracture process.

The rotation mechanism is assisted by debonding, slip and pull-out of z-pins, which occurs more readily when the pin length is reduced

In conclusion, increasing pin length increases their resistance to debonding and slip, and this lowers the amount of rotation of pins before shear fracture. This process reduces the mode II bridging traction loads generated by Z-pins and consequently lowers the mode II fracture toughness.

1.3.6 The effect of loading rate

The performance of z-pins in resisting mode I and mode II delamination has been investigated at a range of different loading rate[57,58] : 0.01mm/s, 5.5m/s and 12m/s

A split Hopkinson bar system was used for the application of high loading rate to z-pinned laminates.

The Z-pin efficiency in resisting mode I delamination decreased with increasing loading rate. Which was caused by the aspects included:

- The friction force that is dependent on fracture surface, pin misalignment and the inertia effect was involved in the bending test.

- The non-linear increase in bridging force during quasi-static pull-out was attributed to the pin misalignment.
- For mode II tests the z-pin mostly failed in brittle manner, the maximum bridging force was not significantly influenced by the loading rate.
- The energy dissipated in this failure process was much lower than that in mode I tests and decreased with increasing loading rate.

The details will be discussed in chapter 4 regarding the dynamic effect

1.3.7 Inclined z-pin on mode II delamination resistance

The bridging behaviour of individual z-pin has been compiled by recent publication[26], indicated that Z-pin provided much higher energy absorption capability at mode I dominated cases(pull out) than mode II(pin rupture) cases, in other words, the advantage of applying Z-pin in mode II cases are way less effective compared to those for mode I cases. Therefore, a series of tests has been carried out to find out how an intended inclination at coupon level will improve the mode II delamination resistance. A series of monotonically increasing insertion angle were used in the study.

The result was interested in two ways, the mode II apparent fracture toughness (the mode II delamination resistance) and maximum reaction force it can tolerant.

For the angles selected in the study, it is shown there is a consistent trend that increasing mode II delamination resistance with increasing z-pin insertion angle as the energy absorption of a single pin specimen showed 200% increase from 0 degree insertion to 60 degree insertion And insertion angle of 45 degrees results in 22% increase in maximum load compared to conventional Z-pin insertion at 0 degrees.

1.3.8 Metallic pins reinforcement

Most used Z-pins are usually in the form of thin pre-cured carbon fibre rod and commonly used material is composite. Metallic Z-pins are the second most used option after composite pins. Compared to composite pins, metallic pins have more advantages on absorbing more fracture energy via plastic deformation, high thermal expansion coefficient as well as electromagnetism.

Recent literature [27] have studied that the mechanical response of the composite laminate with metallic Z-pins are inserted under mode I/II loads test.

It is found that for the Mode I test, the maximum load during pull-out for the 0 degree stainless steel Z-pins is significantly lower than that of composite Z-pins, this can be concluded as the relatively poor interfacial properties between Metallic Z-pins and the laminate, which leads to a small frictional coefficient. However, for the cases of Z-pins with 45 degrees inclination, it is found that the energy absorption for metallic Z-pin is twice that for composite Z-pins under same loading environment. For mode II loading the similar mechanisms were realised while inclined metal Z-pins exhibit higher Mode II fracture energy compared to composite pins, and this will lead to a matter of fact that the bridging zone length for metallic pins significantly longer than that of composite pins.

In conclusion, except for pure mode I loading cases with non-inclined insertion arrangement, the fracture toughness enhancement of inclined metal Z-pins have been shown to be very effective compared to any alternatives including any composite material made Z-pin. Furthermore, Inclined stainless steel Z-pin with ±θ arrangement have shown reduced apparent fracture toughness compared to the orthogonally insertion cases under mode II loading.

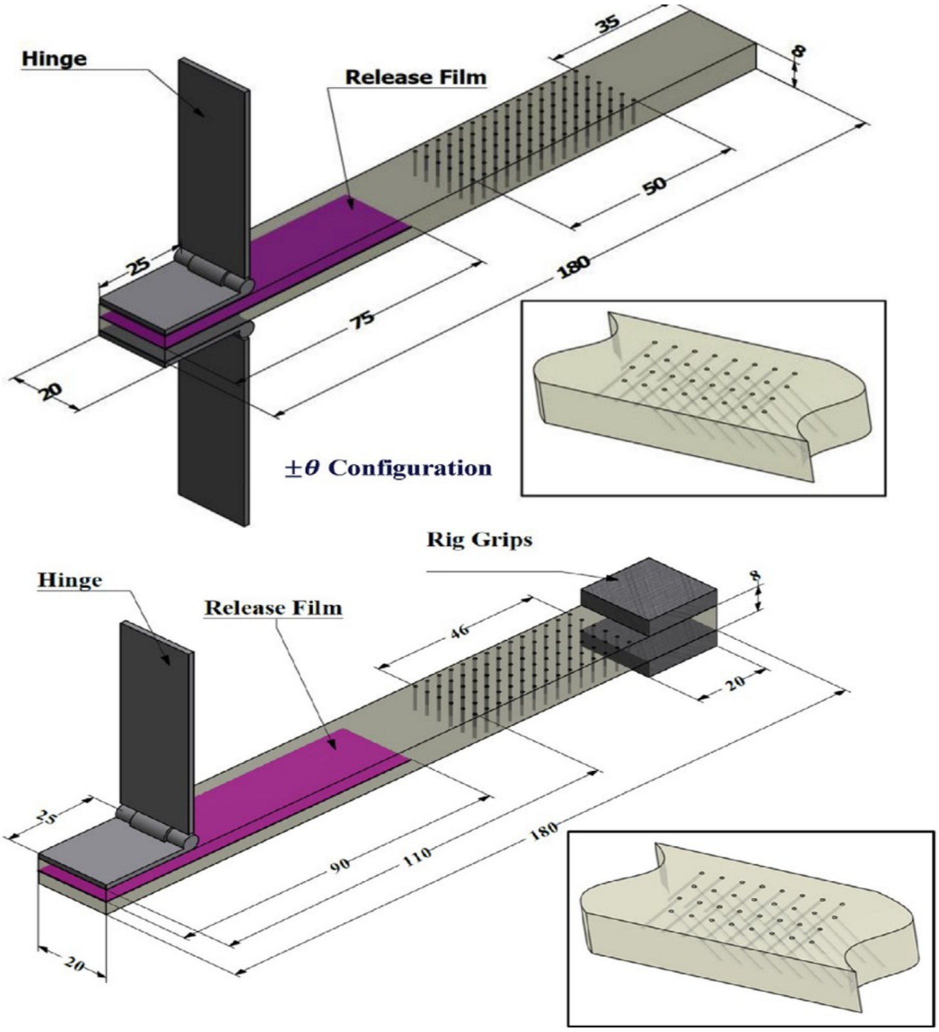

Figure 1.13: Schematic diagram of Z-pinned DCB and ELS specimens [27]

1.3.9 Rectangular Z-pins

Through thickness Fibre-reinforcement is an increasingly demanding topic to be investigated in all the aspects, the ability of the interface to transmit the bridging forces between the pin and laminate is the key to the performance of Z-pin reinforced laminates, and a variety of approaches that have been used to increase the debonding force and the following frictional force by altering the surface properties have been the primary focus to many relevant studies.

By varying the geometry of the pins, the contact areas between pin and laminate will be changed, which would affect the interfacial properties between pin and laminate thus the debonding force and fracture toughness. Julian H, Gerhard S.[28] have presented an experimental study to determine the mechanical response of rectangular Z-pin in hot-cured carbon fibre reinforced laminates under static pull-out loading conditions.

It is shown that in both UD laminates and QI laminates, rectangular Z-pins show a superior debonding force P_d and maximum friction force P_f in comparing to circular Z-pins under same pin volume and areal density. To be specific, with identical pin volume content, an increase in the debonding force of 59% and 149% were found in the UD and QI laminates respectively, an enhancement of 25% and 84% were found during frictional pull-out for UD and QI laminates respectively. The rectangular Z-pins showed a higher pull-out force for both UD and QI laminates, and the superior bridging forces are not solely attributed to the larger surface area of rectangular pins, the difference between the remaining bonded areas after the curing process is another factor which cannot be ignored.

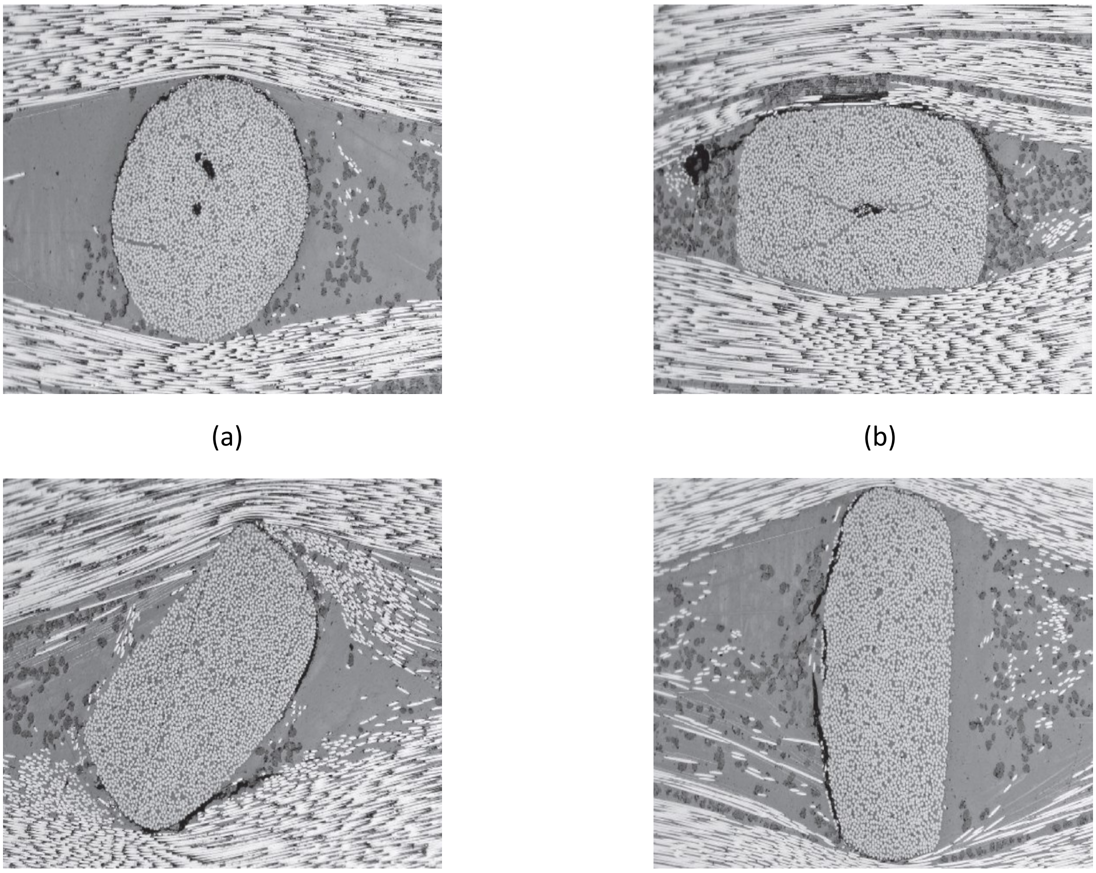

(a) (b)

(c) (d)

Figure 1.14:Cross-section view of an almost completely debonded circular z-pin within a quasi-isotropic laminate (a) as well as a rectangular pin surrounded by laminate plies of different Orientations (b–d) Schematic diagram of Z-pinned DCB and ELS specimens [28]

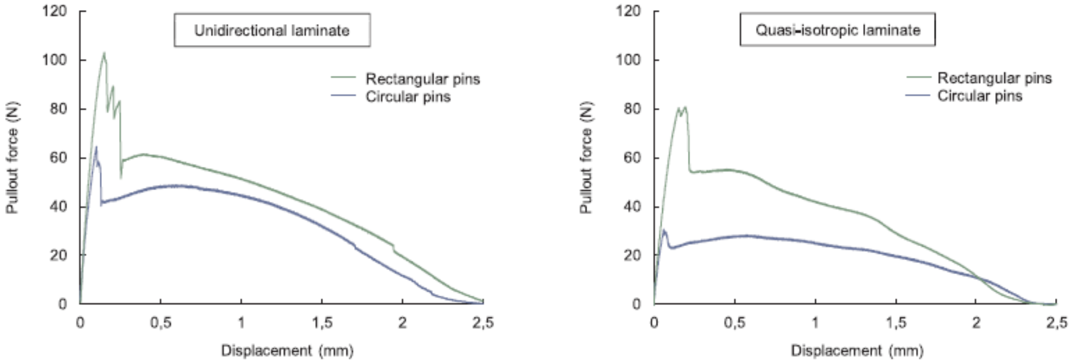

Figure 1.15: pull-out curves for circular and rectangular z-pins in unidirectional and quasi-isotropic laminates

1.4 Electrical based delamination crack monitoring in composites using Z-pins

Delamination cracks are one of the most critical issues in the aircraft structure safety monitoring. Normally, Non-destructive evaluation methods are used to detect the cracks, including ultrasonic, thermography and laser shearography. However, the major issues of these methods in common are the composite assets need to be taken out of service to conduct the investigation.

Structural health monitoring techniques can detect the delamination at the real-time and one of the approaches is via taking advantage of electrical resistivity of the composite material. Zhang et al [29] reported that mode I delamination cracks in carbon-epoxy composites can be detected via electrical resistivity changes by using a single volume content of Z-pins (0.5%) and single type of Z-pins (carbon fibre composite) to monitor mode I cracks.

On top of work done by Zhang et al[29], A.P.Mouritz et al[30] extend the piece of work by applying different pin volume(up to 4%) as well as discuss the influence of the how does different material properties will affect the result.

Z-pins can be used to detect mode I delamination cracks via a measurable increase to the electrical resistivity of the composite, which comparing to unpinned laminate. The theory behind is to detect the delamination propagation via an increase to the resistivity. For Z-pinned laminate, the resistivity of the laminate will be reduced by Z-pins as theses will act as preferential pathways for the current flow. As the delamination cracks propagate, the percentage changes to the resistivity due to delamination crack growth are larger in a Z-pinned composite laminate when compared to an unpinned laminate. It is found that metal Z-pins have less sensitivity comparing to Composite Z-pins and the sensitivity of the resistivity technique to delamination cracking with the volume content of Z-pins made from carbon/BMI composite raised rapidly from 0.5% up to 2%, however, the resistivity of DCB coupon did not increase further when the volume content of Z-pins raised from 2% to 4% due to the transition in the delamination process from a single to multiple cracks growing in parallel.

1.5 Analytical models for Z-pin pull-out

1.5.1 Simple analytical Z-pin pull-out model

A pretty simplified analytical 2D model was proposed by Jain and Main to address the problem concerning pure Mode I pull-out, by separating the pull-out into two stages[]: elastic stretching of the Z-pin before complete debonding and frictional pull-out after complete debonding. In the first stage shown in figure 1.16 (a), the pull-out force is due only from the friction in the debonded interface region, while the Mode I displacement is caused by the elastic stretching of the Z-pin. In the second stage shown in figure1.16 (b),

Equation 1.21 and 1.22 estimate the pull-out force and corresponding displacement δ before the complete debonding, whereas Equation 1.23 and 1.24 compute the pull-out force and sliding displacement after debonding. The pull-out force decreases with the increase of the slippage S.

Rearrange the equation the relationship of parameters can be expressed in Equation 1.25:

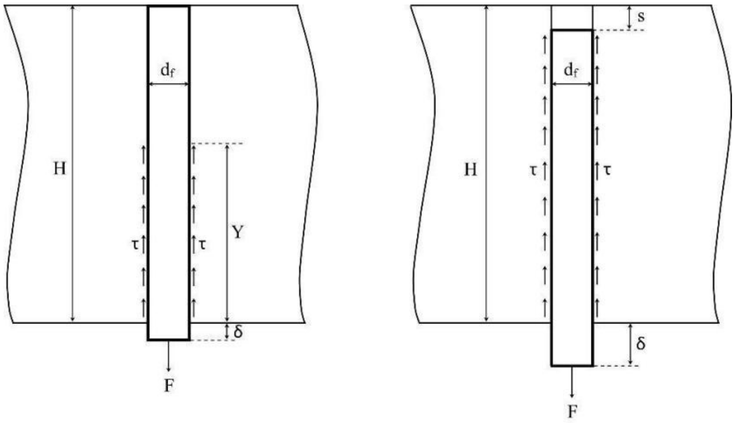

Figure 1.16: Jain's 2D model for pure Mode I pull-out[ ] (a) before complete debonding (b) after complete debonding

Equation 1.21

$$F\big(\delta(Y)\big) = \tau\pi d_f Y$$

Equation 1.22

$$\delta(Y) = \left[Y - \frac{H}{r} ln(\frac{Yr}{H} + 1)\right][1 + \frac{Yr}{H}]$$

Equation 1.23

$$F\big(\delta(S)\big) = (H - S)\tau\pi d_f$$

Equation 1.24

$$\delta(Y) = \left[H - \frac{H}{r} ln(\frac{(H-s)r}{H} + 1)\right][1 + \frac{(H-s)r}{H}]$$

Equation 1.25

τ is the frictional stress, d_f indicates the Z-pin diameter, Y denotes the debonding length, A_f represents the cross-section area of Z-pin and E_f is Young's modulus of Z-pin in the axial direction: (19)The intermediate parameter r can be calculated by:

$$r = \frac{\tau\pi d_f H}{A_f E_f}$$

1.5.2 Model considering snubbing effect

Cox introduced a comprehensive analytical model for the Z-pin bridging mechanism analysis under mixed-mode loadings[23] . The Cox's 2D model describes the Z-pin bridging mechanism in terms of the loading 'with the nap', which indicates that the shear loading is exerted with the Z-pin insertion angle, as shown in Fig. 1.17a, and the loading 'against the nap', which indicates that the shear loading is against the Z-pin insertion angle, as shown in Fig. 1.17b[23,32,33]

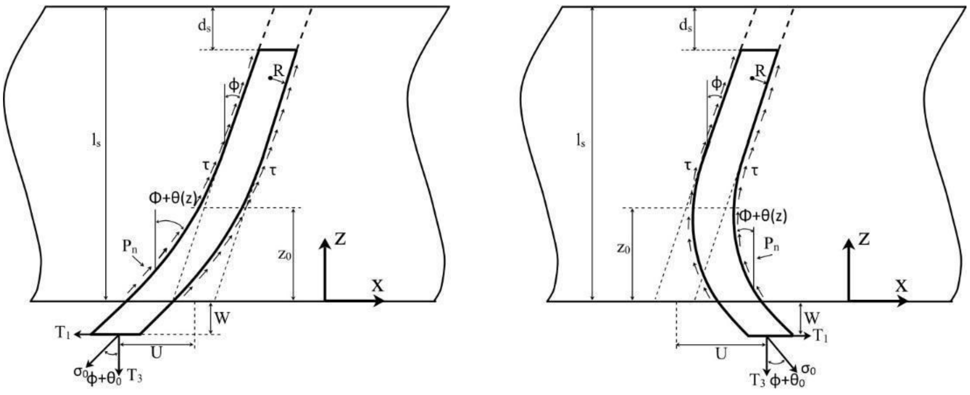

Figure 1.17: (a) Loading "with the nap" and (b) loading "against the nap"[23,32,33].

The constitutive equations are derived based on the following assumptions:

1) The resistance exerted on the defected pin by laminate is assumed to be a constant and regular punch force per unit length, denoted by P_n.
2) Interface debonding between the Z-pin and the reinforced laminate is negligible.
3) The whole pull-out response is also divided into two stages: the pre-pull-out until the slip zone reaches the end of the Z-pin and the pull-out after the slip zone has reached the end of the Z-pin.
4) All strains in the Z-pin are assumed to be either uniform axial extension of uniform transverse shear. This implies that if one fibre fails, then the whole pin will fail catastrophically.
5) The Z-pin is assumed to behave as a linear-elastic/entirely plastic body, which means that the axial shear stress is constant throughout the bridging length of the pin.
6) The ratio of shear stress and axial stress is close to zero.
7) The enhanced frictional stress in the deflected region and un-enhanced fictional stress in the un-deflected region are both assumed to be constant values, denoted by τe and τi respectively.

Based on the above assumptions, the axial stress is expressed as a bilinear function of the slip length in Eq 1.26. For the pre-pull-out stage, the axial stress vanishes at slip length $l_{s.,}$ For the pull-out stage, $l_s= l_r-d_s$, where l_r is the half length of Z-pin and d_s is the pull-out distance of Z-pin end from its original position. The deflected zone is identified by $0<z<z_0$.

Equation 1.26

$$\sigma_t = \frac{2}{R\cos\emptyset}(z_0\tau_e + (l_s - z_0)\tau_i)$$

The deflection angle is given by equation 1.27 where η_1 equals to +1 for loading with the nap while -1 denotes for loading against the nap.

Equation 1.27

$$\sigma_t \frac{\partial\theta}{\partial z} = -\eta_1 \frac{P_n}{A_t \cos\cos \emptyset}$$

The Mode I displacement in the pre-pull-out stage and pull-out stage are expressed by Eq1.28 and Eq. 1.29 respectively. Mode II displacement in the whole pull-out stage can be estimated by Eq1. 50 R indicates the Z-pin radius. The first terms of equation 1.47 and 1.48 indicate the contribution from the deflected zone. The second terms of Eq 1.28 and 1.29 are the contributions from the elastic stretching of the Z-pin. The third term of Eq. 1.28 and second term of 1.29 are the contributions from the Z-pin segment that has already been pulled out of the laminate.

Equation 1.28

$$W = \frac{R}{2}(\int_0^{z_0} \frac{\cos(\emptyset+\theta)}{\cos\emptyset} - 1)dz + \int_0^{l_s} (\frac{\cos(\emptyset+\theta)}{\cos\emptyset}\frac{\sigma_t}{E_t}dz)$$

Equation 1.29

$$W = \frac{R}{2}(\int_0^{z_0} [\frac{\cos(\emptyset+\theta)}{\cos\emptyset} - 1]dz + \int_0^{l_r-d_s} (\frac{\cos(\emptyset+\theta)}{\cos\emptyset}\frac{\sigma_t}{E_t}dz) + d_s\frac{\cos(\emptyset+\theta_0)}{\cos\emptyset}$$

Equation 1.30

$$U = \frac{R}{2}(\int_0^{z_0} (\frac{\sin(\emptyset+\theta)}{\cos\emptyset} - \tan\emptyset)dz + \tan(\emptyset+\theta_0)W)$$

Cox’s model has been employed to explain the response of z-pin reinforced laminates. The model has been employed on the investigation of bridging mechanisms of aluminium Z-pins and carbon-fibre Z-pins in the shear tests. It is found that in both case the Z-pins would be pulled out when loaded with the nap. And all the Z-pins would fail when it is been loaded against the nap. This causes larger axial stresses and thus the rupture of Z-pin axial strength is reached. However, there are many limitations of applying that model, which limits its application. The assumption of uniform axial stress across Z-pin cross section is only entirely valid for pure mode I pull-out. In addition, the assumption that the Z-pin is a perfectly plastic is also almost difficult to justify from the through-thickness reinforcement rods that are made of unidirectional composite.

1.5.3 Model on Z-pinned laminate regarding Mode I loading

Robinson P et al [34] has proposed an analytical model for the application of Z-pinned laminate. An analytical model that describing the bridging mechanism for DCB specimens. By doing that, a simple beam theory was applied to the model, both sides of the DCB arms were seen as cantilever, and the forces exerted by the pins bridging the crack are represented by a distributed loading $\sigma(x)$. This paper separately described the state when the bridging zone was not fully advanced and the state when the first pin start to pull-out and the bridge zone was fully engaged and provide the different states with different analytical solutions.

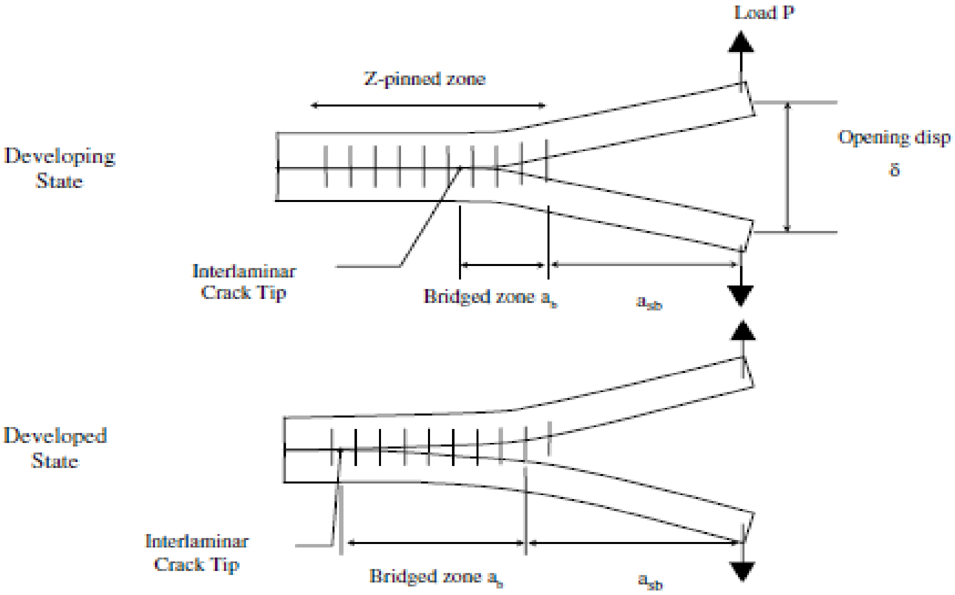

Figure 1.18: Z-pins bridging the crack during the developing state and developed state [34]

Assuming the pin to pull out over an embedded length, t_e, this length defines the opening displacement at which the bridging stress equals to zero. The stress at the critical point before the softening starts, denoted as σ^*.

Therefore the area enclosed by the curve equals to the Fracture toughness of the Z-pinned laminate G_{IC}^{ss} subtracts the fracture toughness of the un-pinned laminate G_{IC}^{u}. i.e:

Equation 1.31

$$\frac{\sigma^* \cdot t_e}{2} = G_{IC}^{ss} - G_{IC}^{u}$$

And bridging stress $\sigma(x)$ can therefore be expressed as a function of the opening displacement δ. Therefore, it can be expressed by:

Equation 1.32

$$\sigma(x) = \sigma^* \cdot (1 - \frac{\delta}{t_e})$$

And substitute back to the differential equation for the equilibrium of a beam can be represented as:

Equation 1.33

$$EI\frac{d^4w}{dx^4} = -B * \sigma^* \cdot (1 - \frac{\delta}{t_e})$$

Where EI is the flexural stiffness of the beam. B is the width of the beam. W is the deflection and the opening displacement δ is equal to 2w as both upper and lower part of the structure are assumed to bend the same vertical displacement, therefore the differential equation becomes

Equation 1.34

$$EI\frac{d^4w}{dx^4} = -B * \sigma^* \cdot (1 - \frac{2w}{t_e})$$

And the applied load P associated with opening displacement δ can be find as

Equation 1.35

$$P = -EI \cdot \frac{d^3w}{dx^3}$$

For developing state, the crack length between the crack tip to the loading point is assumed to be equal to the pre-crack length a_0 and for developed state the length to the interlaminar crack tip a can be expressed as $a_b + a_{sb}$ which indicated by figure 1.18 . The displacement for each corresponding load P can be expressed as:

Equation 1.36

$$\delta = 2(W_{x=a_b} + a_{sb} \cdot \frac{dw}{dx}_{x=a_b} + \frac{Pa_{sb}^3}{3EI})$$

Therefore, for any given applied load, the corresponding opening displacement can be found. The comparison between predicted result and experimental data has been made and good agreement has been achieved

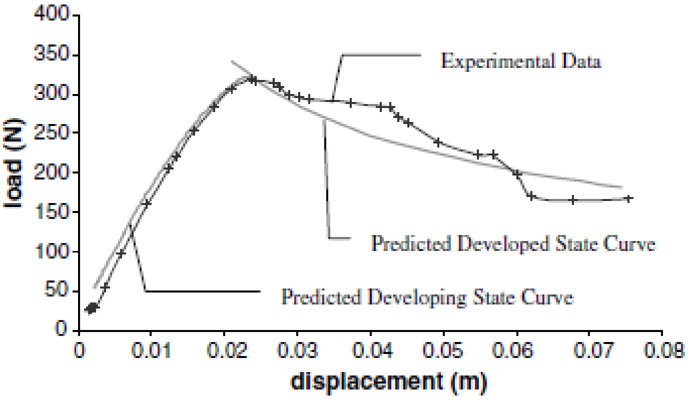

Figure 1.19: Comparison between predicted and experimental load-displacement plots [34]

1.5.4 Model of Delamination bridging via Z-pins

A most recent analytical model has recently proposed another novel analytical model that describes the z-pin as a Euler-Bernoulli beam that inserted in an elastic foundation [35] that represents the embedding composite laminate. In this model, it is assumed that z-pin is pulled out only from one of the embedding laminates. It is demonstrated the case where the z-pin is pulled out asymmetrically. The relative transversal displacement U of two sub-laminates is measured between Z-pin tips. While the opening displacement is equal to the pin pull-out displacement W. The transversal displacement along the Z-pin length is denoted as u(z). The transversal displacement can be described by the equation 1.37. Where N indicates the axial force on the Z-pin cross-section. The resistance force q per length exerted on Z-pin by embedding laminate is proportional to the transverse displacement.

By assuming six parameters, young's modulus E, cross-sectional second area of moment I, axial force N, resistance force q per length, friction force per length p, transverse displacement u(z). for a given z-pinned laminate, equation 1.37 and 1.38 can be derived to yield the bridging force versus displacement curves for various mode mixities using an adaptive collocation method. Each iteration loop of the equations solving process is terminated when Z-pin fails according to Weibull's criterion, or full pull-out is achieved. The analytical result matches perfectly with the experimental results in terms of load-displacement curves and apparent fracture toughness under mixed-mode loadings. What advantages the model is it considers the actual mode mixity and Z-pin misalignment. Which promotes the accuracy. (

Equation 1.37

$$EI\frac{d^4u}{dz^4} - N\frac{d^2u}{dz^2} + q = 0$$

Equation 1.38

$$\frac{dN}{dz} = -EI\frac{d^3u}{dz^3}\frac{d^2u}{dz^2} - p$$

The model is valid for fibrous and brittle Z-pins. The apparent fracture toughness of a Z-pin reinforcement composite is related to the energy dissipated by friction pull out of the z-pins. Considering the special case while the laminate is quasi isotropic, it has been shown that the apparent fracture toughness provided by Z-pin insertion increases with mode-mixity, until a critical value of latter is reached. This is due to the fact the residual friction experienced by Z-pin is initially by coulomb friction in a mixed-mode regime. The friction enhancement increases the axial tension and bending that the Z-pin must support during pull-out. Leading to failure of the through-thickness reinforcement once a characteristic critical mode-mixity is exceeded the critical mode-mixity ratio for Z-pin/laminate arrangement here is 0.4. This figure below shows the mechanism of Z-pin pull-out

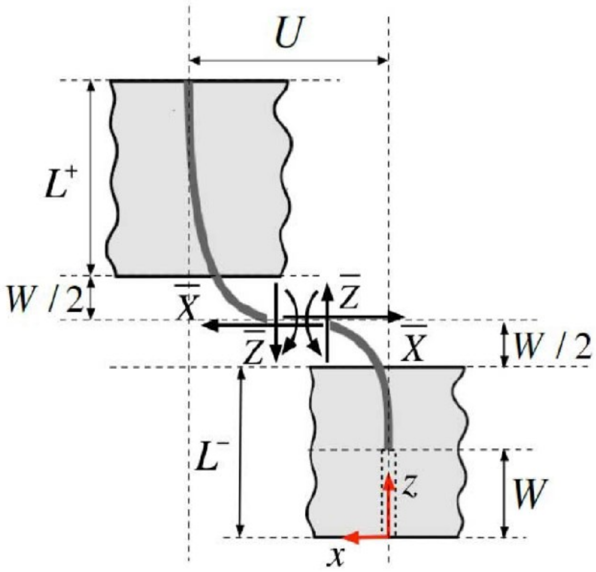

Figure 1.20: Z-pin pull-out mechanism [35]

1.6 Micromechanics in Z-pin pull-out test

Generally, for a single Z-pin pull-out test embedded in QI composite laminates under mode I loading, the following observation will be observed in figure 1.21 :

P_0 – force at end of linear part of the curve
P_1 – first maximum force or the force at first strongly defined drop
P_2 – force right after the first drop
P_3 – maximum force of the frictional sliding phase (or equal to **P2** if the force gradually decreases after **P2**)
P_{max} – the maximum force in the entire process
a0 a1 a2 a3 – displacements corresponding to the above forces, respectively
a_{max} – displacement at the point where force drops to 0
U – Energy consumed in pull-out process, measured from the area under the curve

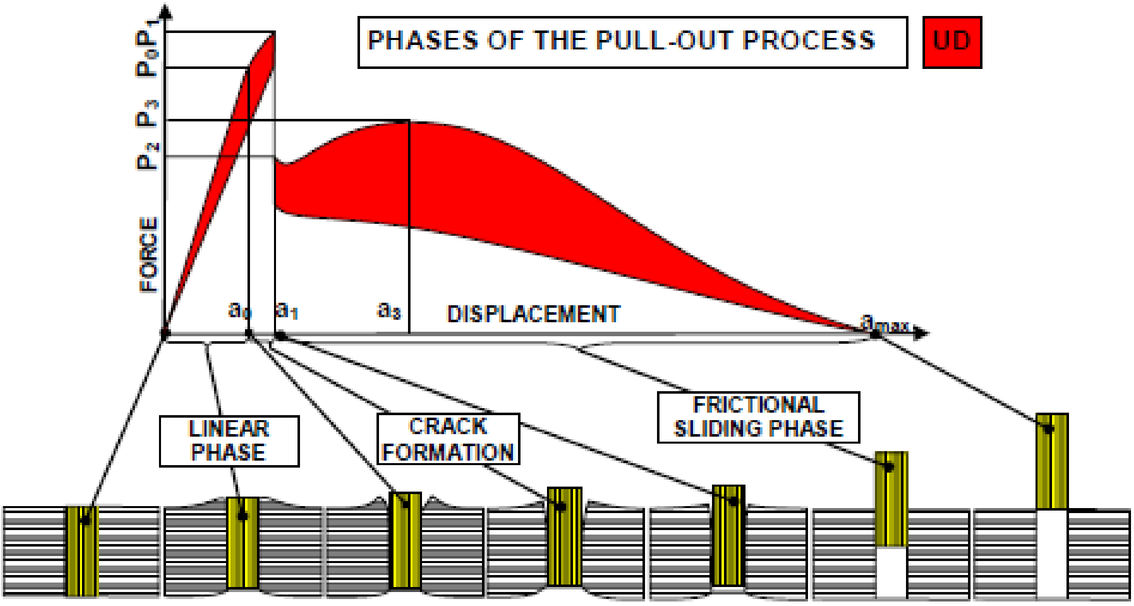

Figure 1.21: Phases of the pull-out process for QI laminate with low mode-mixity [36]

1.6.1.1Linear phase

The beginning of the pull-out process is similar, and the reaction force linearly increases with the pulling displacement. This shows the interface between Z-pin and laminate, playing the functions of holding the pins from getting rid of the laminate. At the end of the elastic stretch phase, an observable peak will be noticed, which indicates the complete debonding of the interface.

1.6.1.2 Crack formation phase

The linear growth will be followed by a rapid drop of the reaction force from the Peak force P1 to P2, this short period of time usually reckoned as crack formation phase. In the duration, Z-pin debonded completely from the surrounding composite, and the rapid drop suggests unstable crack growth.

1.6.1.3 Frictional sliding phase

After the rapid drop of the reaction force, the fully debonded Z-pin starts to slide within the laminate, a coulomb frictional stress starts to develop on Z-pin. The friction force will gradually grow up to a peak value **P3**. Without any insertion angle, the growth of the force during the sliding phase could be explained by the surface roughness of Z-pin. In addition, the residual compressive stress acting at the Z-pin interface will also be another reason for the growth of the friction force.

1.6.2 Pull-out test in QI laminates with higher mode mixities

For the pull-out test conducted in QI laminate, similar pull-out phases can be observed, however the micromechanics-behind is slightly different that of UD laminate. A schematic indication is shown below in Figure 1.22 :

P_0 – force at the end of linear part of the curve
P_1 – first maximum force or the force at first strongly defined drop
P_2 – force right after the first drop
P_3 – maximum force of the frictional sliding phase (or equal to **P2** if the force gradually decreases after **P2**)
P_{max} – the maximum force in the entire process
a0 a1 a2 a3 – displacements corresponding to the above forces, respectively
a_{max} – displacement at the point where force drops to 0
U – Energy consumed in pull-out process, measured from the area under the curve

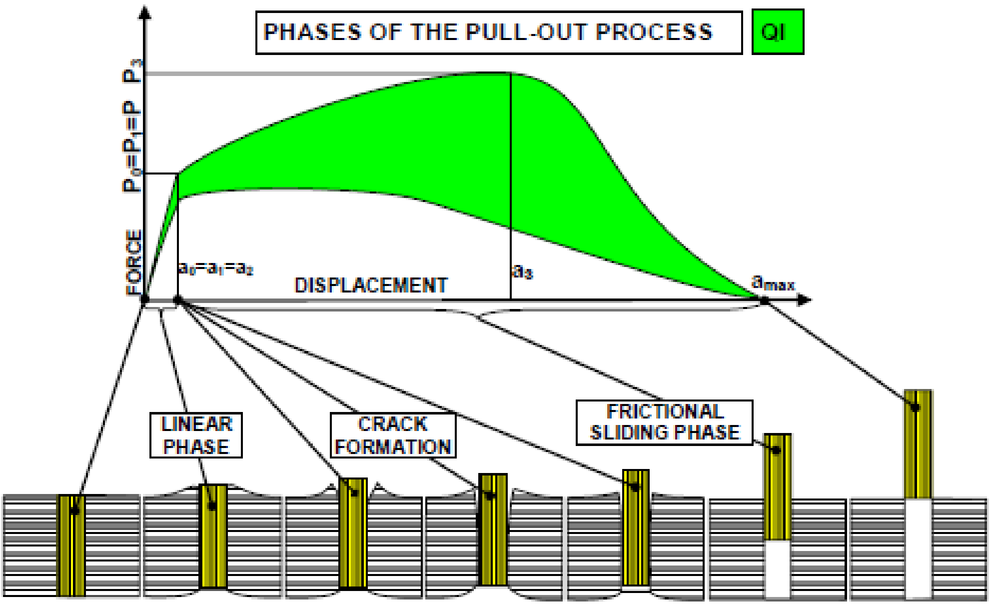

Figure 1.22: Phases of the pull-out process for QI[36]

1.6.2.1 Linear phase

It can be observed that the elastic stretch phase poses a similar behavior compared to QI laminate with lower mode-mixity, despite that the linear phase last significantly shorter and the peak reaction force is observably lower.

1.6.2.2 Crack formation phase

The crack formation phase for QI laminate is quite insignificant in comparison to the UD laminate. That is because the so-called "snubbing effect," due to the load applied on the lateral direction, a large pressure is built up immediately after the Z-pin/laminate interface debonded and Frictional behavior start to dominate fast. Thus, the drop of reaction force is very insignificant and quick.

1.6.2.3 Frictional sliding phase

The growth of the friction force for QI laminates plays an essential role during the whole pull-out Process; this is attributed to the renowned "Snubbing" effect between Z-pin and the edge of the Laminate. This effect will be observed when the Z-pin insertion angle to the normal of the delamination to be 13°-14°; The Z-pin can crush the resin and plough into the resin-rich area under lateral loading, therefore, result in the enhanced friction. Thus, the highest apparent fracture toughness will be obtained for the case with moderate mode mixity due to the reaction force able to reach the highest, and the failure mode is pull-out.

1.6.3 Mode II dominated test

For the mode II dominated test, two phases were observed. It is noticed that the final failure mechanism changes from pull-out to pin rupture failure. Similarly, the schematic indicating how pull-out curve looks like for mode II dominated case in figure 1.23 :

P_0 – maximum of the force at the end of linear part of the curve
P_1, P_2 – forces at subsequent yield points on curve
P_3 – force at the last rapid drop
a_0, a_1, a_2 – displacements corresponding to the above forces
$a_3 = a_{max}$– displacements at the last drop of the force, assumed to be the point of final break of the Z-Pin
U – Energy consumed during shear-out process

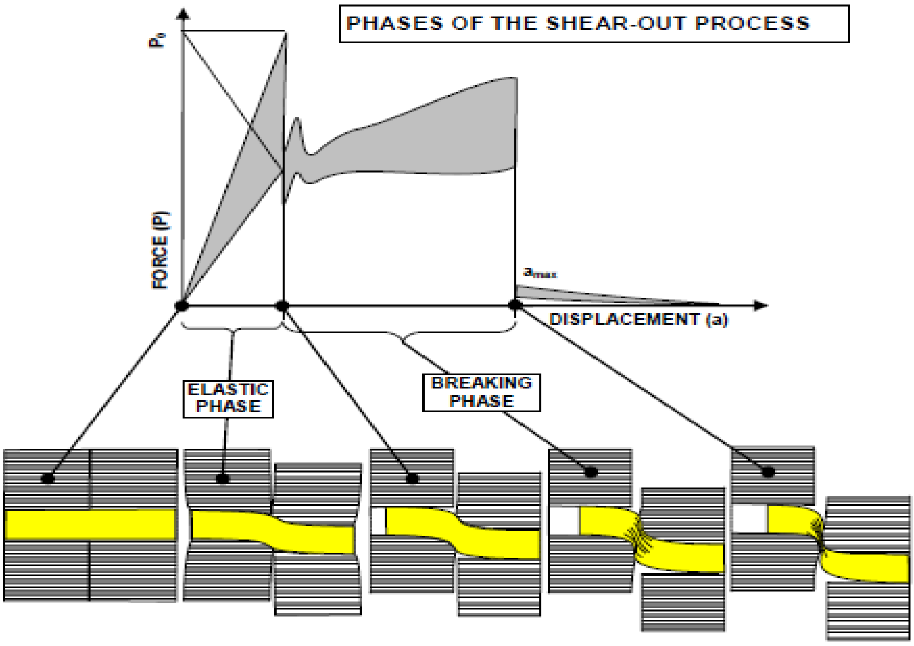

Figure 1.23: Phase of the shear-out process[36]

1.6.3.1 Elastic phase

In this phase, a peak force caused by fully debonding of the interface between Z-pin and laminate.

1.6.3.2 Breaking phase

In this phase, a yield of the curve at 0.2 mm followed by a gradual increase of the force can be observed. And, the final drop of the force would occur, caused by the Z-pin breakage. The whole process is governed by the Z-pin internal structure, it was assumed that during this phase Z-pin gets slowly broken by propagation of the micro-cracks along its fibres, Also a slight pull-out could be expected in this phase, as a rapid growth of the crack opening displacement was usually observed.

The mechanical performance of a single z-pin will be discussed in more details in chapter 3.

1.7 Conclusion

The advantages of Z-pinning on delamination resistance, interlaminar toughness, damage tolerance has been well reported. In a nutshell, through-thickness reinforcement has little effect on the initiation of delamination but significantly improved the fracture toughness and result in stabilization of delamination.

The trade-off of using Z-pinning technology is the decrease of the in-plane mechanical properties, especially the in-plane tension and compression strength. Noticeable damage to the structure was observed , which include fibre crimping, fibre waviness, resin-rich pocket and fibre breakages. Generally, Z-pinning density of 0.5%-4% were applied to most of Z-pinned structure, and the result is substantial growth on the interlaminar toughness with minor degradation in the in-plane properties. The trade-off between Improvement in the delamination resistance and the degradation in the in-plane properties should be put more considerations in the engineering design.

The development in the analytical models provide a simple approach to solve the complex mechanical problem, the models introduced were usually dealing with the long fibres pulling out of a block of isotropic resin, and usually two phases were considered:

1. The debonding state, where the Z-pin fibre is trying to break the interface between fibre and the surrounding resin
2. Slip-out, after the interface between fibre and resin been fully degraded the rest of motion will be governed by friction.

The most recent analytical model considered the ‘snubbing effect’ due to the bending of the z-pin and employed a modified coulomb frictional law followed by the cohesive law. The results suggest that at low mode mixities the pull-out process was dominated by the pull-out failure whereas in high mode mixities, the failure mode shift to pin-rupture.

Chapter 2 modelling set-up and verification

2.1 General review of delamination modelling

Delamination is a typical failure mode happens through the thickness of the laminate when a laminate is impacted, the failure mode is easy to be triggered when the delaminate onset within the laminate, it would not necessarily cause a failure. However, the strength will reduce below a critical level, which no longer meets the standard of application. The major reason the delamination will be induced is due to the fibres in the laminate strengthen the specimen in the longitudinal and transverse direction, but there is no specific fortification can be applied to the through-thickness direction. According to fracture mechanics, delamination has three different independent modes depending on the loading conditions. Critical strain energy release rate is the key criterion that governing the delamination propagation. In this section, three different cases including double cantilever beam, 4 End notch flexure test, mix-mode bending test were investigated against the benchmarks in journals in order to prove the validity of the explicit subroutine.

2.1.1 Virtual crack closure technique

The VCCT is based on the assumption that the energy released in extending a crack by a small amountΔa, is equal to the amount of work required to close the crack back to its original length[37]

In the FEM analysis using VCCT, the strain energy release rate components are calculated by:

Equation 2.1

$$G = \frac{F \cdot \delta}{2A}$$

Where F is the force at the nodes along the delamination front. δ is a row vector that contains the latest relative displacement of the node pairs behind each corresponding crack front node and A is the surface area created by the delamination growth.

Previous investigations have shown that the VCCT results can be mesh dependent; this is due to the oscillatory nature of stresses in the vicinity of the crack front at the bi-material interface. Which beyond the scale this research is concerning. In the following chapter, only homogenous material will be used. Furthermore, it is recommended to use consistent crack tip elements between analyses that are being compared.

2.1.2 VCCT vs cohesive zone modelling

The most common approaches that have been extensively applied to simulation delamination is the Virtual Crack-closure technique and cohesive elements. The range of application of cohesive elements is not limited to structures with small fracture process zones that confined to the crack tip.

Comparing these two methods and find out their applicability will be carrying forward in the following section

The damage occurs in the cohesive zone, and a criterion for the damage applying stiffness reduction is typically used.

The main challenges for Cohesive zone modelling are the definition of traction-separation law and the empirical parameters that been applied, as there are no universal standards for determining its parameter values. Meanwhile, mesh dependency is another important aspect that will severely affect the results of cohesive zone modelling. However, the VCCT can yield accurate results with larger elements. In the nutshell, the properties of the CZM and VCCT methods are compared in the table shown below:

Table 1:Comparison between VCCT and CZM

Method	CZM	VCCT
Damage initiation	Stress concentration initiates fracture	Pre-existing crack is necessary
Damage process zone	Traction-separation law defines softening	No softening
Material parameters	Maximum stress/ power law required on the top of Fracture toughness	Only fracture toughness
Nodal release	After reaching critical energy release rate/separation	After virtual closure reaches critical energy rate
Mesh-sensitivity	Mesh-sensitive	Less mess-dependency

Table 1: Comparison between VCCT and CZM[37]

The key difference between these two methods is that VCCT must have a pre-existing crack whereas CZM does not. A traction-separation law defines the damage nucleation and propagation in a CZM model and furthermore, CZM allows the model capture the damage process zone adjacent to the crack tip, which is beneficial to the modelling work when small plasticity exists during the propagation phase[37].

In that case, CZM will be carried forward for the future of modelling work as it is increasing the complexity of modelling to design pre-existing crack for model like mechanical Z-pin pull-out.

2.2 Geometries based Z-pin pull out model

Z-pinning technology is an effective method of reinforcing laminated composite materials for preventing the laminate from delamination propagation. Research has been conducted extensively to simulate the mechanical response of individual Z-pins at the micro-scale and associated bridging mechanism. The existing modelling strategy accounts for the characteristic features associated with Z-pinning, i.e., the interface between Z-pin and the surrounding laminate block, residual stresses due to post-cure cooldown, and splits within Z-pin. However, all those modelling strategies were based on the particular purpose cohesive elements; the implementation of zero thickness cohesive elements in the model requires an exceptional level of complexity. This paper presents a three-dimensional FE modelling approach based on pure geometries based cohesive contact method. The analysis results are in excellent agreement with the experimental results, meanwhile reducing the complexity in modelling.

Introduction & Background

Through-thickness reinforcement of composite laminates via the z-pinning method results in a large increase of interlaminar fracture toughness. Z-pinning is the use of short and discontinuous rods of high stiffness and strength inserted in the through-thickness direction. The Z-pins exert traction forces, via a combination of adhesion (cohesive contact) and friction that suppress the crack opening displacement.

Numerical models have been conducted extensively to simulate the reaction of the Z-pin bridging mechanism. Jain and Main proposed a simplified analytical 2D model for pure mode I pull-out by separating it into two stages: elastic stretching before the complete debonding and frictional pull-out after complete debonding. Cox introduced an analytical model for mixed-mode bridged delamination. It gives the relation between the bridging traction and cracks opening/sliding as an implicit function. In Cox's [23] model, axial stress can be expressed as a bilinear function of the slip length and take into account of snubbing effect.

Regarding the analysis of single Z-pins, the analytical methods are computationally cheap. However, it is subject to some strong assumptions. Moreover, the analytical model does not consider of the stacking sequence on the Z-pin response. FE modelling must be conducted to precisely investigate the response of Z-pin pulls out. Cui et al[38] established a 2D plane strain model by introducing mode I and mode II traction law to model mixed-mode Z-pin pull out mechanism. Allegri and Zhang[39] proposed an explicit micro-scale model for the response of the single Z-pin. In which they describe bridging tractions as a function of delamination opening/sliding displacement.

Furthermore, the model considers stacking sequence and post-cure down effect. The simulation results for Z-pins in QI laminates subject to mix mode loading are in good agreement with experimental data. However, all the existing models are dependent on the implementation of zero thickness cohesive element at the interface, which grossly increases the difficulties of building the model considering the complexity of the geometry. In this paper, a geometry-based contact model without employing cohesive elements is present.

2.2.1 Constitutive cohesive law for interface

A concise constitutive law for cohesive interfaces is accepted in the following section based on Abaqus subroutine Vuinter, a new state variable is introduced to track the extent of damage accumulation at the interface. The constitutive laws are majorly derived from Abaqus documentation and the work proposed by Jiang et al [40], which are used to account for mixed-mode ration change during the debonding process. The interface model is implemented in Abaqus Vuinter explicit finite element code. Comparison between results from subroutine and the results from Abaqus CAE shows good correlation.

As the matrix between plies in a composite is very thin and may be considered to be, it is appropriate to determine the response in terms of traction versus separation relationship, a simple bilinear softening cohesive-decohesive law that relates the interfacial traction components σ to relative displacement δ components has been adopted. Instead of considering mode II shear and mode III shear separately, a combined resultant shear mode is considered. The bilinear interface formulation adopted in this paper for the mixed mode softening law can be illustrated in a single three-dimensional map as shown below:

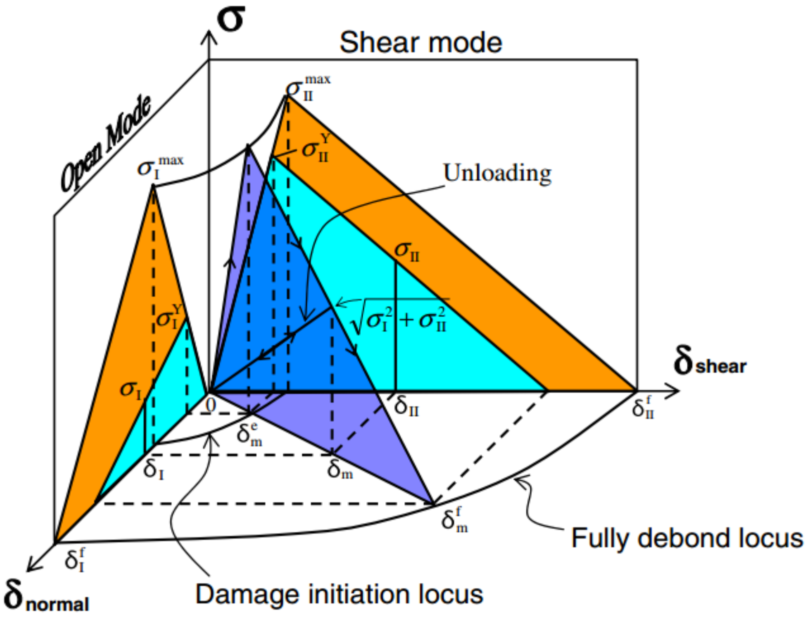

Figure 2.1: Interfacial bilinear mixed-mode softening law[40]

The relative displacement $\delta_1, \delta_{2,}\delta_3$ are the relative displacement components for a pair of interfaces connecting points in local orthogonal coordinate system. δ_1 is the normal relative displacement and $\delta_{2,}\delta_3$ are representing the relative displacements in shear directions.

While the normal opening relative displacement:

Equation 2.2

$$\delta_I = max(\delta_1, 0)$$

The resultant shear relative displacement:

Equation 2.3

$$\delta_{II} = \sqrt{\delta_2^2 + \delta_3^2}$$

Therefore the total relative displacement:

Equation 2.4

$$\delta_t = \sqrt{\delta_I^2 + \delta_{II}^2}$$

The direction cosines are defined as:

Equation 2.5

$$cos\ I = \frac{\delta_I}{\delta_t}$$

And

Equation 2.6

$$Sin\ I = \frac{\delta_{II}}{\delta_t}$$

A quadratic damage initiation criterion under a multi-axial stress state has been successfully used to predict the onset of delamination in previous research, and can be expressed as:

Equation 2.7

$$\delta_t^i = \frac{1}{\sqrt{\left(\frac{KI * cosI}{\sigma_I^{max}}\right)^2 + \left(\frac{KII * sinI}{\sigma_{II}^{max}}\right)^2}}$$

Where KI and KII are the tensile and shear stiffness of the interface.

The stress at the damage initiation point for mode I and mode II in an arbitrary loading direction is illustrated as following respectively:

Equation 2.8

$$stress_I^{yield} = KI * \delta_t^i * cosI$$

$$stress_{II}^{yield} = KI * \delta_t^i * sinI$$

When the interface is further loaded after damage initiation point, its strength will be assumed to degrade linearly until the complete failure of the interface. The interface failures under mixed-mode conditions can be described by the power law:

Equation 2.9

$$G_I = \frac{1}{2} * stress_I^{yield} * \delta_t^f * cosI$$

$$G_{II} = \frac{1}{2} stress_{II}^{yield} * \delta_t^f * sinI$$

Where δ_t^f is used to express the relative displacement between nodes where the interface complete fail. And the following failure criteria is adopted:

Equation 2.10

$$\left(\frac{G_I}{G_{IC}}\right)^\alpha + \left(\frac{G_{II}}{G_{IIC}}\right)^\alpha = 1$$

α is an empirical parameter derived from mixed mode tests, and G_{IC}, G_{IIC} are the critical energy release rates for pure mode I and pure mode II, respectively. Substituting the expression for G_I and G_{II} back to the failure criteria will help to obtain an expression for δ_t^f.

Equation 2.11

$$\delta_t^f = \left(\left(\frac{stress_I^{yield} * cosI}{2G_I} \right)^{\alpha} + \left(\frac{stress_{II}^{yield} * sinI}{2G_{II}} \right)^{\alpha} \right)^{\frac{-1}{\alpha}}$$

A damage parameter D is introduced as:

Equation 2.12

$$D = \frac{\delta_t^f(\delta_t - \delta_t^i)}{\delta_t(\delta_t^f - \delta_t^i)}$$

$$D = max(D^{t-\Delta t}, D^t)$$

Where Δt is the time step and δ_t represent the relative displacement at the current time step. The initial value of D will remain zero until the damage initiation condition is met, it is a monotonically increasing value which starts when the $\delta_t > \delta_t^i$ and reaches the failure value 1 when the fully debonding locus is reached while $\delta_t > \delta_t^f$.

Stress is considered as an output to be updated to Abaqus subroutine. The stress should be updated separately while the damage accumulated.

A penalty contact stress is introduced in case of penetration:

Equation 2.13

$$\sigma_1 = \delta_1 * KI \qquad \delta_1 < 0$$

While before the damage initiation criterion is met the interface relationship is linear, the stress be a product of penalty stress and relative displacement.

Equation 2.14

$$\sigma_1 = \delta_1 * KI \qquad \delta_1 > 0$$

$$\sigma_2 = \delta_2 * \sigma_{II}/\delta_{II}$$

$$\sigma_3 = \delta_3 * \sigma_{II}/\delta_{III}$$

The stress degradation is regarded as a reduction of the peak stress levels:

Equation 2.15

$$\sigma_1 = (1 - D) * \delta_1 * KI$$

$$\sigma_2 = (1 - D) * \delta_2 * KII/\delta_{II}$$

$$\sigma_3 = (1 - D) * \delta_3 * KII/\delta_{II}$$

To clarify the computing procedure, a concise flow chart is provided:

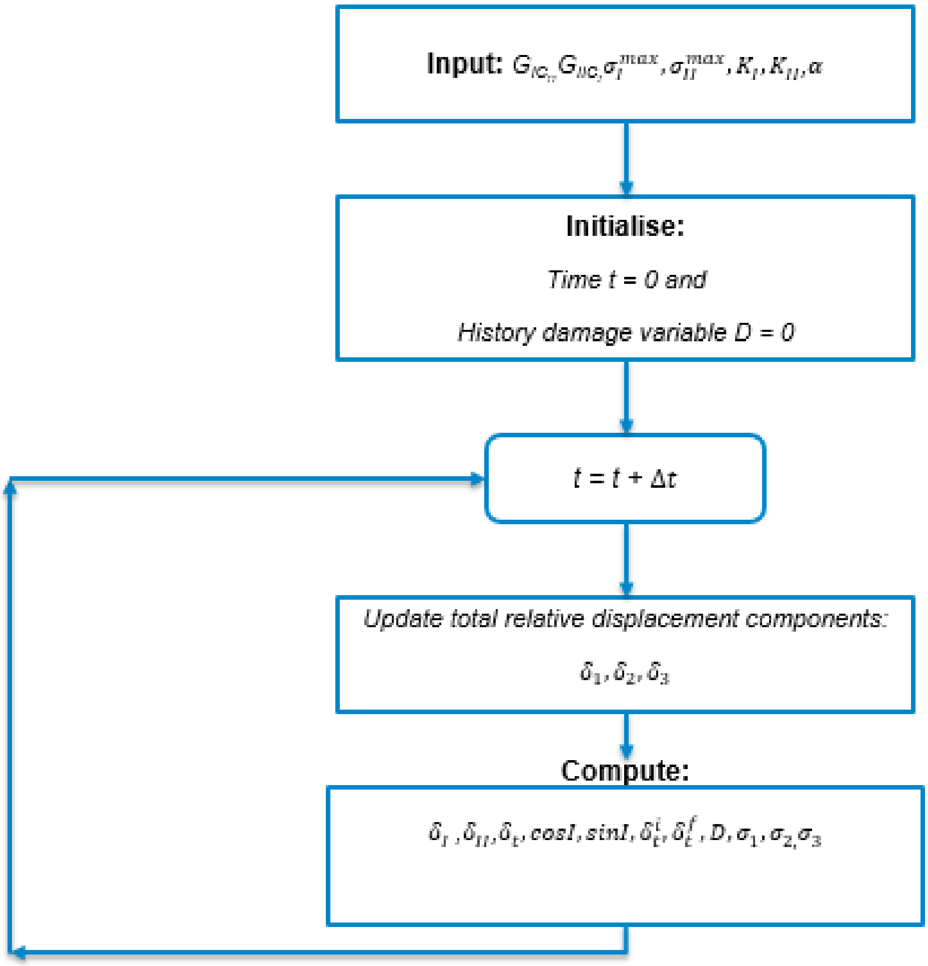

Figure 2.2: flow chart for subroutine Vuinter

2.2.2 Constitutive law for modified Coulomb friction model

The actual geometry of contact surfaces between Z-pin and laminates has large geometrical irregularities and roughness, which are hard to be described explicitly in FE mesh. To address this issue, the interface friction will need to be artificially increased in FE model. A residual friction stress τ_0 is therefore added on top of standard coulomb friction law. The modified coulomb friction can be written as:

Equation 2.16

$$\tau_t = min(\tau_{max}, \tau_0 + \mu\sigma_n)$$

Where the term σ_n is defined as penalty contact stress in normal direction and can be found as:

Equation 2.17

$$\sigma_n = K * max(d, 0)$$

In this expression K is the penalty stiffness of the contact in the model, d is defined as a penetration depth of slave surface to master surface. τ_t is defined as shear stress due to friction, τ_{max} is the maximum allowed shear stress and μ is the coulomb friction coefficient.

The two shear stresses in tangential direction are defined as:

Equation 2.18

$$\sigma_2 = \frac{\tau_t * \delta_2}{\delta_{II}}$$

$$\sigma_3 = \frac{\tau_t * \delta_3}{\delta_{II}}$$

Where δ_{II} is defined as the resultant relative displacement in the shear direction.

A succinct flow chart is provided to ease the understanding.

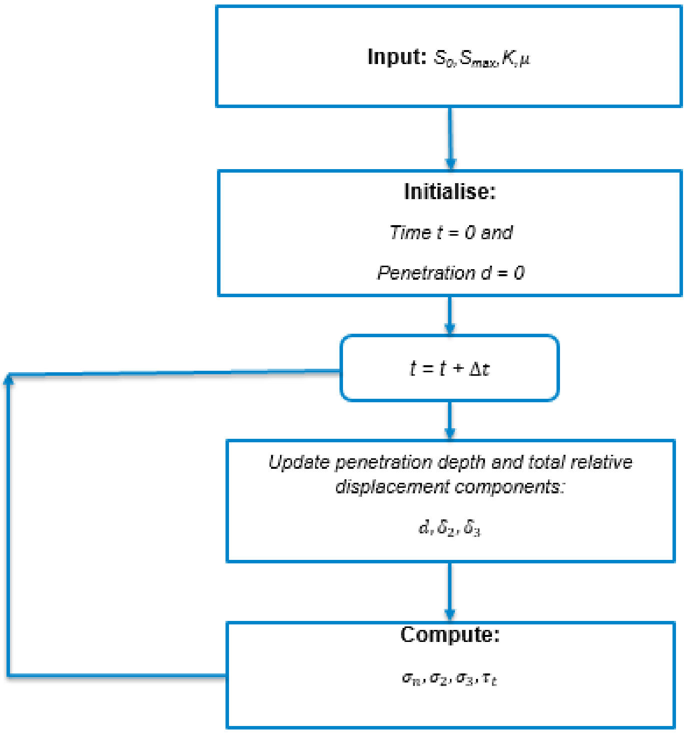

Figure 2.3: frictional subroutine flow chart

2.2.3 Other constitutive law

Pinho S [41] has proposed another way to approach the cohesive problem. In this approach, the relative-displacements and tractions corresponding to the onset of damage are denoted as onset displacements and onset tractions respectively, when the maximum traction N or S (critical normal stress or shear stress) is reached, the damage is assumed to start propagating, the onset displacements are for opening and shear modes respectively:

Equation 2.19

$$\delta_N^o = \frac{N}{K}, \delta_S^o = \frac{S}{K}$$

In this case N and S are the mode I and shear mode maximum allowable tractions respectively, when the traction reaches zero, the energy absorbed must equal the critical energy release rate, this will result in the final displacements in a pure-mode load situation as :

Equation 2.20

$$\delta_N^f = \frac{2G_{Ic}}{k\delta_N^o} \quad \delta_s^f = \frac{2G_{Sc}}{k\delta_s^o}$$

In this case G_{Ic} and G_{Sc} are the pure mode I and pure shear mode fracture toughness.

In mixed mode the damage propagation can start before the critical traction for either pure mode I or mode II been reached. The relative normal displacement and shear displacement can be denoted as:

Equation 2.21

$$\delta_{normal} = \delta_1, \delta_{shear} = \sqrt{{\delta_2}^2 + \delta_3^2}$$

Therefore, the magnitude of the relative displacement,δ, can therefore be represented as:

Equation 2.22

$$\delta_{total} = \sqrt{{\delta_1}^2 + \delta_{shear}^2}$$

The ratio between mode I displacement and mode II displacement can be represented as β, denote the participation of the different modes:

Equation 2.23

$$\beta = max\left\{0, \frac{\delta_{shear}}{\delta_1}\right\}$$

The quadratic delamination criterion is used, which has proven to be suitable to apply for delamination onset prediction in composite material.

Equation 2.24

$$\left(\frac{t_1}{N}\right)^2 + \left(\frac{t_{shear}}{S}\right)^2 = 1$$

As tractions are a function of the relative displacements, the previous criterion may be expressed in term of relative displacements result in:

Equation 2.25

$$\delta_o = \{\delta_S^O \delta_N^O \sqrt{\frac{1+\beta^2}{(\delta_S^O)^2 + (\beta\delta_N^O)^2}} \qquad \delta_S^O \quad for\ \delta_1 > 0$$

The power law criterion was used to express the state of decohesion progress for different mode-mixity and the energy release rates under the certain ratio:

Equation 2.26

$$\left(\frac{G_I}{G_{IC}}\right)^2 + \left(\frac{G_{II}}{G_{sc}}\right)^2 = 1$$

Whereas the mode I and shear mode energy release rates can be expressed in terms of relative displacements. The energy absorbed by each mode I a mixed-mode loading is:

Equation 2.27

$$G_I = \frac{k\delta_1^o\delta_1^f}{2}, G_{shear} = \frac{k\delta_{shear}^o\delta_{shear}^f}{2}$$

Substitute the energy back into the power law we $for\ \delta_1 \leq 0$ can obtain the expression of the final displacement as:

Equation 2.28

$$\delta_f = \{\frac{2(1+\beta^2)}{k\delta_o}\left[\left(\frac{1}{G_{IC}}\right)^\alpha + \left(\frac{\beta^2}{G_{sc}}\right)^\alpha\right]^{-\frac{1}{\alpha}} \delta_s^f\ for\ \delta_1 \leq 0\ \ for\ \delta_1 > 0$$

For most of cases the numerical value of α varies from 1 to 2

2.3 Benchmark applications

2.3.1 Mode I loading: DCB test

Figure 2.4 shows a schematic view of DCB specimen. Two equal and contrary loads, P, are applied at the end of the two-cantilever beam. The specimen has the dimension of 20mm for the width, 3.1 mm thick and has a pre-crack length of 53mm. The mode I fracture toughness during the test is G_{IC}= 0.268KJ/M^2 and the Flexure young's modulus E is 119 Gpa. The maximum mode I traction at the damage initiation point is 60Mpa which defines the interlaminar strength, and the penalty stiffness that were used as K= $1 \times 10^5 N/mm^3$. The minimum mesh seed used in the numerical model was 0.25 mm which ensured that enough cohesive elements were contained in the cohesive zone at any time to obtain correct results. A displacement rate of 0.1 mm/s were used to make sure the model is undergoing quasi-static test mode which make sure the kinetic energy play a negligible role during the test. Each arm of the specimens was modelled by using 8-noded 3D stress elements with 5 elements across the thickness of the beam.

The load vs displacement curves against experimental results were presented in Figure 2.5 together with the analytical solution and Pinho's modelling results

It can be observed that the numerical model has made good agreement with analytical solution and experimental results, however, the numerical model is slightly overestimating the reaction force. While that is due to a trade-off relationship between damping ratio, mass scaling and loading rate.

In terms of mass scaling, a density of 1e-3 kg/mm^3 was used as the density for the laminate and each side of the loading tip experienced a 0.05mm/s constant loading rate.

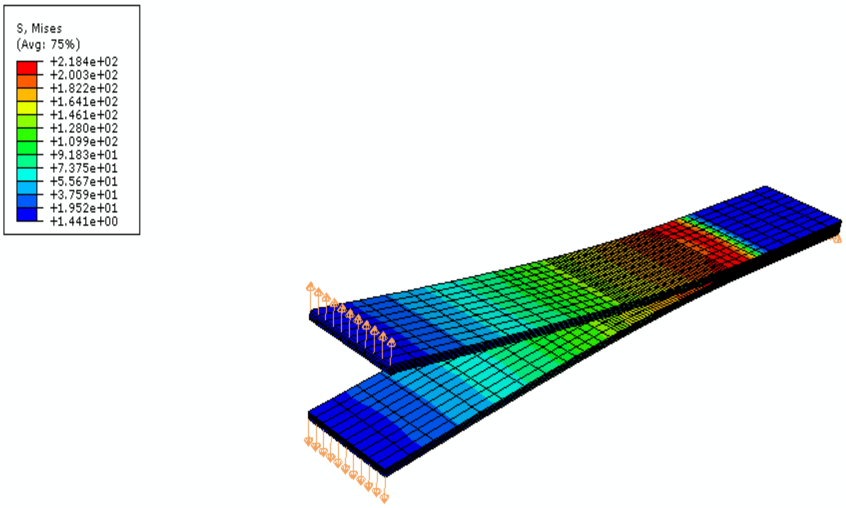

Figure 2.4: side view of double cantilever beam

Compared to Pinho's [41-42] result, a much more reasonable displacement rate was chosen and meanwhile a much less damping and mass scaling were used in order to make sure the result is intact due to the development of computational power.

For a DCB test, the relation between the applied load and the opening displacement can be obtained using LEFM following the ASTM standards. The applied load in a DCB test for the crack propagation can be obtained as:

Equation 2.29

$$F_{applied} = \sqrt{\frac{G_{Ic} b^2 h^3 E_{11}}{12a^2}}$$

Where the b and h are the width and height of the specimen arm, a is using as the crack length. The corresponding opening displacement can be read as:

Equation 2.30

$$u = F_{applied} \frac{8a^3}{bh^3 E_{11}}$$

A comparison was made between analytical vs abaqus default program vs experimental results were presented below, it should be noticed that the experimental results and pinho's experimental results were directly extrapolated from pinho's publication [42]

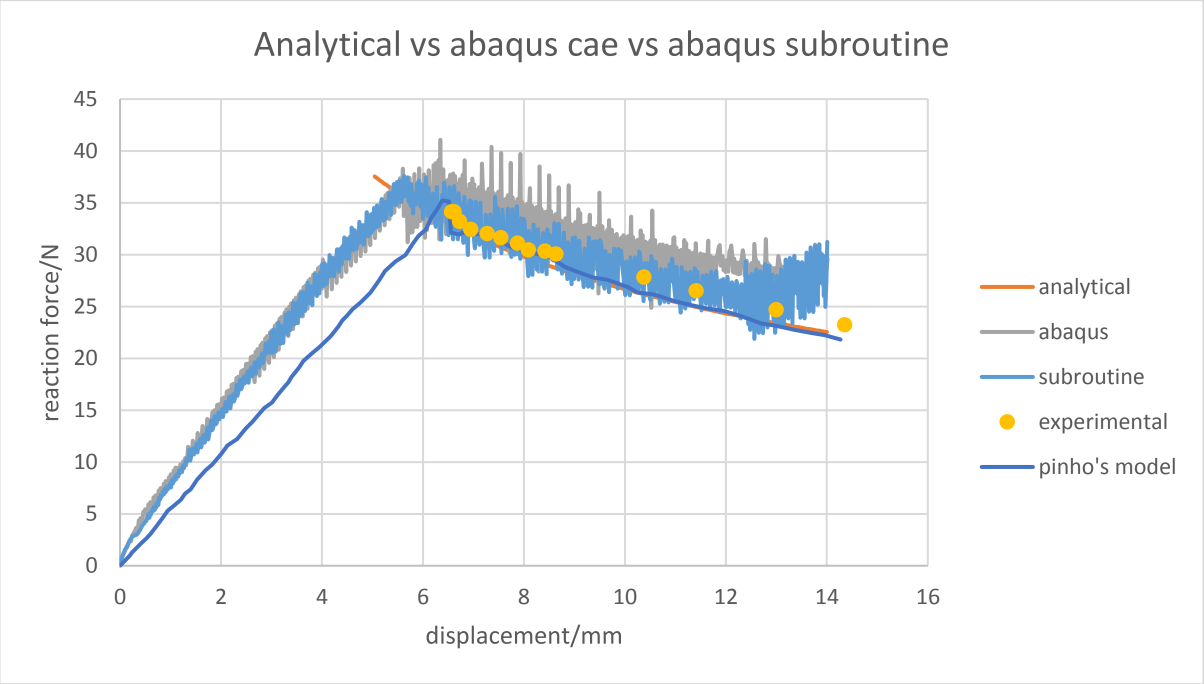

Figure 2.5: experimental load vs displacement for a DCB specimen[42]

2.3.2 Mode II loading: 4ENF test

A 4ENF test was conducted for the sake of pure mode II test to find out the fracture toughness in mode II condition. Similar dimension was used for the experiment where width equals to 20 mm, thickness 3.1mm and pre-crack length 25mm were applied. Part of the loading rig was modelled as well, which of length 80mm. The loading rig was modelled as a rigid body to make sure the simulation is to the point. The fracture toughness $GII = 1.11\ kJ/m^2$, was used in the simulation and the flexural modulus was used as E= 137000 MPA, the maximum mode II traction applied in the model is 60 MPA [42]. Whereas the minimum mesh seed in the experiment is of length 0.25 mm to ensure the delamination growth can be fully captured.[44]

For the ENF test, the relation between the applied loads is:

Equation 2.31

$$F = \sqrt{\frac{G_{IIc} 16b^2h^3E_{11}}{9a^2}}$$

And the corresponding displacement at the midpoint can be expressed as:

Equation 2.32

$$u = F_{applied} \frac{3a^3 + 2L^3}{8bh^3E_{11}}$$

Where L is the length of the specimen

A displacement rate of 0.1 mm/s was applied to the mid-section of the loading rigs.

The experimental vs analytical vs experimental results is presented below.

It can be observed that the numerical results make good agreements with experimental data, the 1 % error is due to the noise and oscillation during dynamic loading.

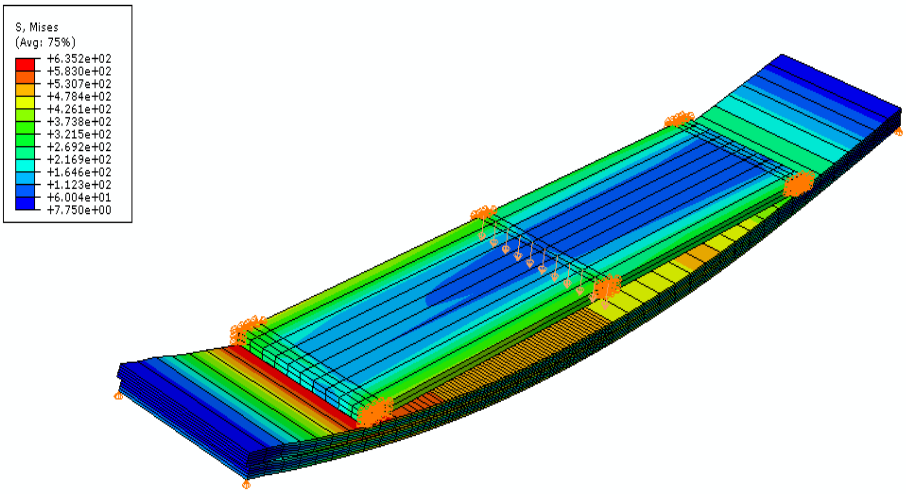

Figure 2.6: side view of end notched flexure specimen

The experimental vs analytical vs experimental results is presented below.

It can be observed that the numerical results make good agreements with experimental data, the 1 % error is due to the noise and oscillation during dynamic loading.

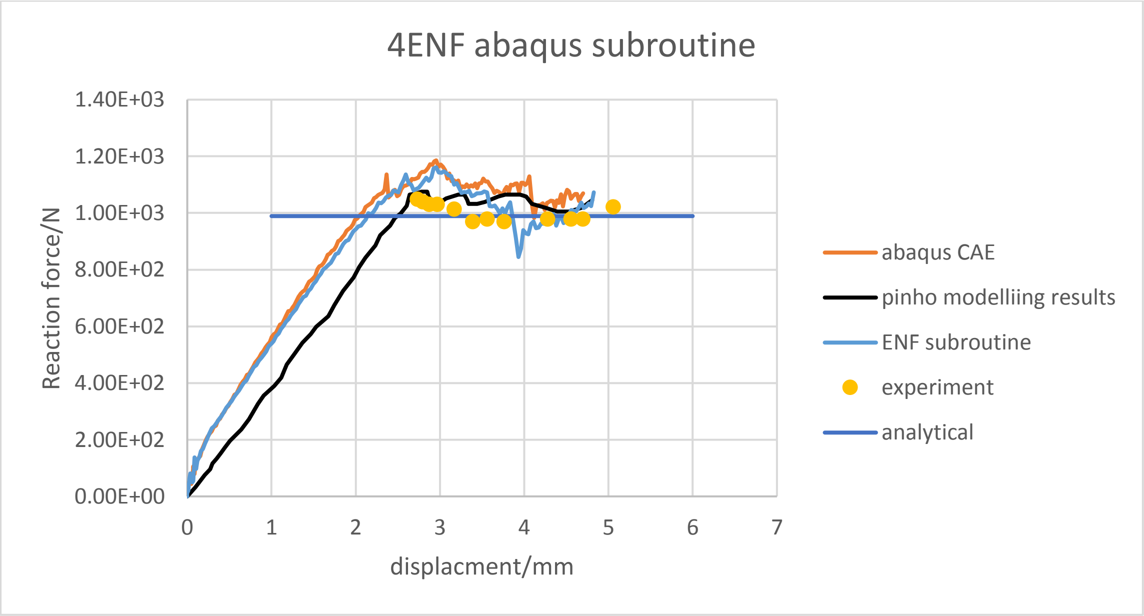

Figure 2.7: Analytical numerical, and experimental load vs displacement for a 4ENF specimen

2.3.3 Mixed-mode loading: MMB test

The simulation of an MMB test was conducted below. The specimen used is of the same dimension as DCB and ENF, with 20 mm width, 3.1 mm thickness and pre-crack length of 33mm. The distance between the loading at the front of the beam and the end is 109mm. The fracture toughness value chosen in this simulation is

$$G_{Ic} = 0.258\frac{KJ}{m^2}, \; G_{IIc} = 1.108\frac{KJ}{m^2}$$

And the power law parameter used in the test is 1.21

The maximum mode I and mode II traction are assumed to be equal, were taken as

N = S = 60 MPA. The minimum length between two mesh seed across the crack tip is 0.25 mm.

The material is considered isotropic with E= 112000 MPA and Poisson ratio = 0.3

It can be seen that a good agreement between the numerical analytical and experimental is shown during the linear elastic region however, in this case, a significant unstable response was found in the stiffness degradation region. This effect is found to be more serious at high loading rates. High value of stiffness used is one of the major drivers that lead this phenomenon to happen. However, if low stiffness was used then the delamination may not be properly captured as the penalty contact method was used[42]

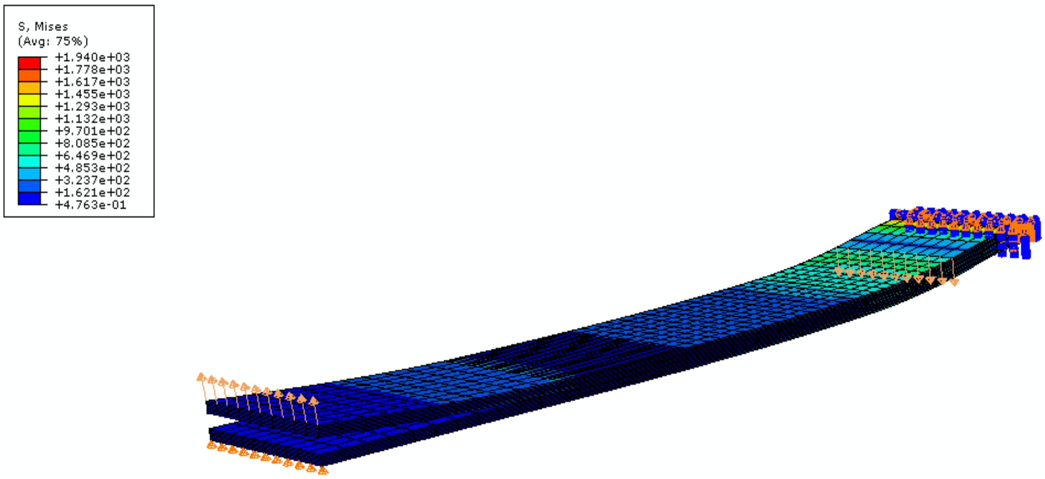

Figure 2.8: side view of mix mode bending specimen

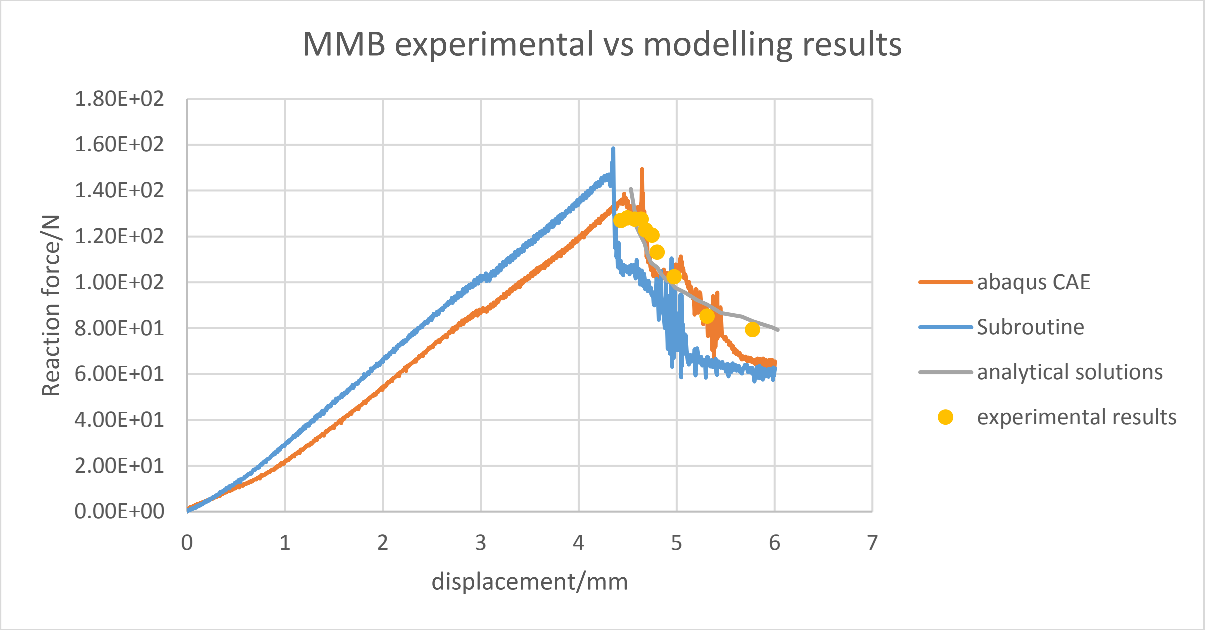

Figure 2.9: Analytical numerical, and experimental load vs displacement for a 4ENF specimen

2.4 Implementation of Weibull failure criterion to user-defined material

The mode II dominated fibre - rupture was described by Weibull failure criterion (Wisnom,1991), a solid of volume V subjected to a stress field σ(x,y,z) has the probability of failure which given by:

Equation 2.33

$$P_F = \{1 - e^{-\int V\left[\frac{\sigma(x,y,z)}{\sigma_s}\right]^m dV} \qquad 0 \quad for \sigma(x,y,z) \leq 0 \; for \; \sigma(x,y,z) > 0$$

Where σ(x,y,z) is the stress within the solid, m is the Weibull modulus and σ_s is a scaling constant. As a given Z-pin subject to an axial force N and bending moment M, the failure will occur when

Equation 2.34

$$\sigma_{max} = X_T \left[\frac{V_0}{V_{eff}}\right]^{\frac{1}{m}}$$

Where σ_{max} is the average peak tensile stress along Z-pin axis and X_T denotes the average fibre failure strength associated to a volume of material V_0 under pure tension. V_{eff} is the effective volume of the Z-pin subjected to tension.

In this case some assumptions have to be made in order to solve the problem. The assumption of equal probability of survival for any elements within the Z-pin and the ASTM standard tensile test specimen have to be made, and the equation can be rearranged as below:

Equation 2.35

$$e^{\left[-V_E\left(\frac{S_E}{S_0}\right)^m\right]} = e^{\left[-V_{ASTM}\left(\frac{S_{ASTM}}{S_0}\right)^m\right]}$$

In this equal V_E is the volume of any individual element within Z-pin, S_E is the fibre-direction tensile stress, V_{ASTM} and S_{ASTM} are the volume of a standard ASTM sample and unidirectional failure stress of ASTM sample separately. M is the Weibull modulus is an empirical parameter which typically has a value range from 25-40. In the user subroutine, **V_E can be found as the cubic value of a characteristic length L_E in any arbitrary elements**.

Equation 2.36

$$V_E = {L_E}^3$$

The only unknown parameter in this case is S_E. Rearranging the equation above will give out the criterion below:

Equation 2.37

$$S_E = S_{ASTM} \times (\frac{V_{ASTM}}{V_E})^{\frac{1}{m}}$$

The user-defined material subroutine can update the strain in six different direction at each incremental step, and the corresponding stresses can be updated respectively by renovating the product of the inverse of the compliance matrix and latest strain component.

Thus, when the latest updated stress in any elements thorough the model exceeds the pre-defined stress limit according to the ASTM data, the fibre rupture failure will happen.

However, according to the size effect [45], the failure stress can be various when the volume of the structure changes as the larger structure can contain more defects, therefore the failure stress will be deteriorated. But the discrepancy will be no more than 10% between perfect carbon-fibre enforced laminate with zero voids and standard coupon scaled specimens and detailed discussion of size effect is beyond the scale of this thesis.

In the following section, a tensile test was conducted. A unidirectional IM7/8552 laminate specimen with thickness of 0.5 mm, width 5mm and gauge length of 30 mm was tested. The experimental results were extrapolated from data in the publication from University of Bristol [46]

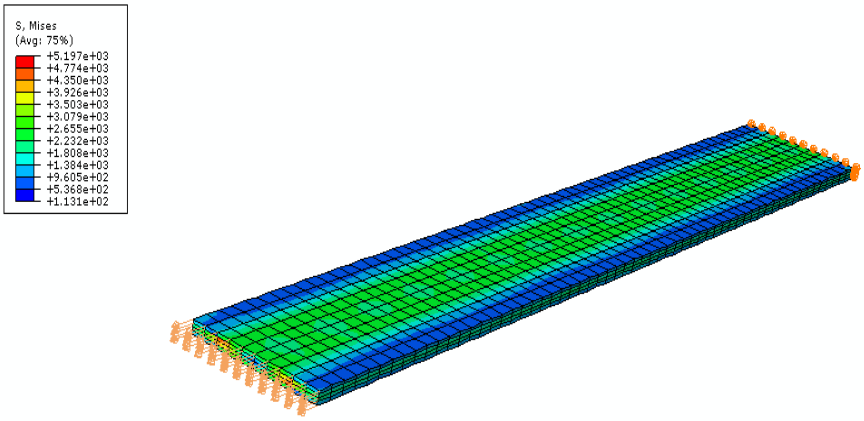

Figure 2.10: Side view of tensile test specimen

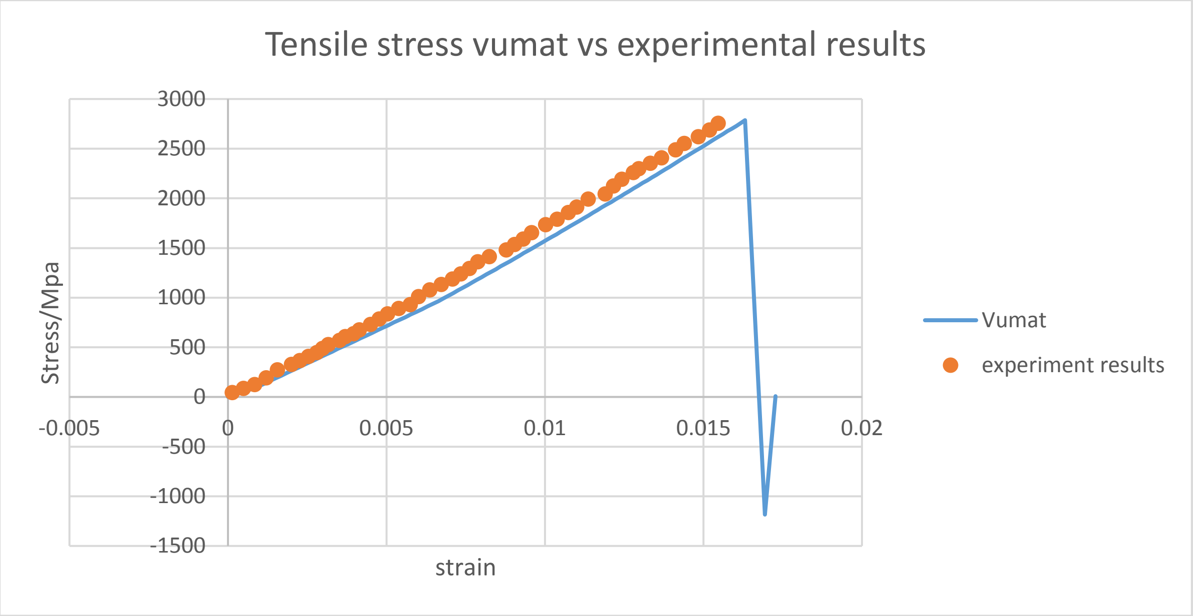

Figure 2.11: Comparison between benchmark experimental tensile tests to Vumat

A rapid load drop was observed immediately after the elastic stretching phase, which indicates that the specimen fail after the critical tensile stress has been reached. Great agreement was achieved by applying the user material in comparing to experimental data as shown in figure 2.11.

Thus, a Vumat subroutine which contains the Weibull failure criteria was developed successfully and applied to the explicit model.

2. 4 Innovative features from the Vuinter and Vumat user-defined subroutine

In the user defined contact subroutine Vuinter, a surface-based cohesive contact approach was developed. The approach was established upon quadratic traction-separation constitutive behaviour and effectively avoid the need to use cohesive elements, thus this method can be applicable to deal with the cohesive contact in complex curvature with ease.

A versatile user-defined material subroutine was also introduced in this section, the user defined material can be used to simulate orthotropic material. Weibull failure criterion was applied to model the fibre rupture failure.

For all the test cases this thesis concerns, the fatal failure mechanism is the fibre rupture failure. The tensile stress reaches the critical value and lead to the catastrophic failure of the overall structure.

However, the user subroutine is versatile enough to be applicable for element failure in different direction. The stress can be updated at six different direction, as long as a comparable ASTM failure stress data was given in desired orientation e.g. transverse, through-thickness, different shear direction. The user-defined material subroutine will be able to update the stress vector until the critical stress finally reached in the corresponding orientation.

Therefore, the application of the user-defined material will not only deal with the fibre tensile failure case but also cover the scenario considering matrix failure

2. 5 Conclusion

In essence, the modelling methodology can be divided into three different procedures, a bridging law that defines the cohesive contact before the interface completely debonded, a modified Coulomb friction law which describes the frictional contact and a user-defined material which can cater to the demand of element failure when shear stress dominated.

In the first part of this chapter, the bridging law and modified Coulomb friction law which applied to the modelling work was introduced, Weibull theory was applied to the Z-pin to describe the failure under critical stress.

In order to validate the subroutine, the FE modelling results were compared to the results in benchmark tests, courtesy to Pinho[41-43] .The benchmark tests, including DCB test for pure mode I case, 4ENF test for pure mode II test, and MMB test for mix-mode loading case. The FE results compared to the analytical solution and experimental data provided in the literature, good agreement has been achieved in general. At the end of the chapter, the user-defined material was also proven sensible in comparing to experimental results.

The FE results have achieved good agreement with experimental results. However, it was also found that the noise will start to affect the result when the frictional contact starts to dominate the contact mode, compared to the modelling results from cohesive element method, the response looks comparatively unstable. Therefore, the subroutine can carry forward for more complex and practical usage.

Chapter 3 High fidelity cohesive model

3.1 Preliminary models and experiments review on Z-pinned structure

It has been widely explored and proved that the interface between z-pin and laminates can be modelled by cohesive elements.

Therefore, a series of modelling have been conducted to approach the problem in order to make great agreement with experimental results.

Cui [38,57] has provided with a plane-stress model that modelling a single Z-pin in UD laminates along the fibre direction. A 0.28 mm diameter Z-pin is inserted into the resin with a depth of 3 mm. The resin size is 0.26 mm wide and 1.5 mm long. A 0.05 mm gap was introduced to prevent contact between lower and upper laminate to make sure the bridging force was purely obtained from Z-pin.

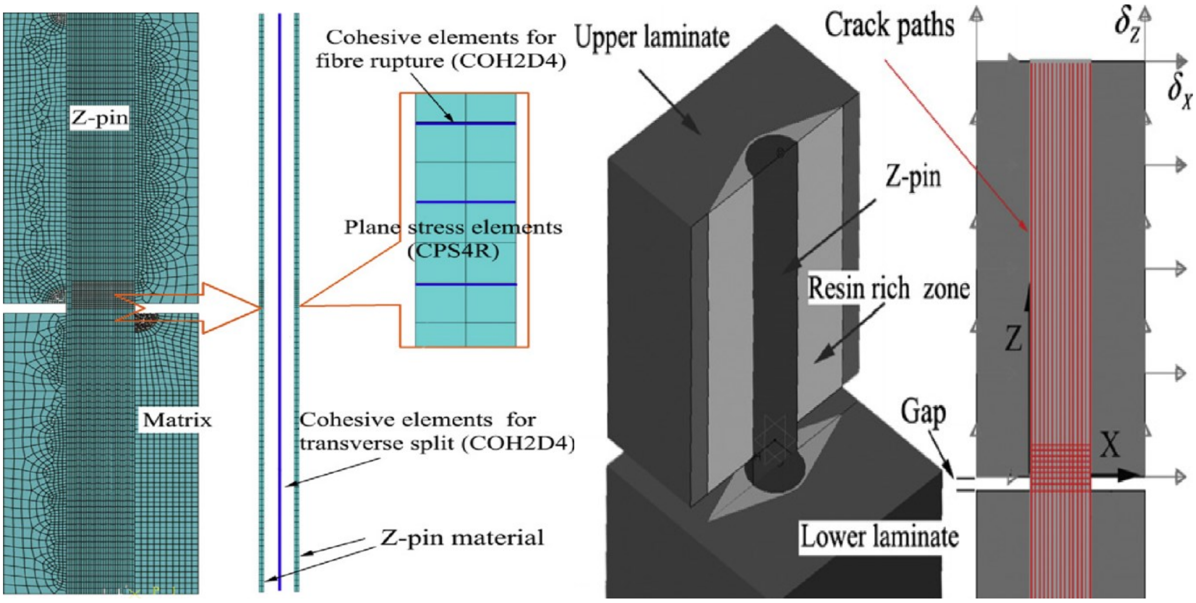

Figure 3.1: Side and cross sectional view of plane stress model[38]

X Zhang [47-48] has proposed models to approach the Z-pinned structure under pure mode I and mode II loading. The significant contributions of the first publication are that it has enabled the pull-out process of Z-pin to be modelled at macro-scale models and enable two separate cohesive laws to be applied on the pin locations and unpinned areas, and second publications proposed an approach which can solve the Z-pin pull-out problem under pure mode II loading.

However, little evidence can prove that the model can be used for mix-mode loading conditions, and cohesive elements were used as the interface between the contact surfaces, which add the complexity of work when the contact surfaces have peculiar shapes. Moreover, not enough critical conditions have been employed to ensure that the program can determine the failure mode be pull-out or pin rupture.

A coupled cohesive zone model that incorporates cohesive law for Z-pinned structure under mixed-mode loading has been developed [38], the author claimed that the model could cope with both interlaminar failure and failure of Z-pins as the failure mode varies from pull-out to pin rupture when different mode mixities applied. However, the complexity of applying the model is ultra-difficult as the cohesive elements have to be divided into shear dominated elements and tension dominated elements, as indicated by the name, the shear elements have high stiffness in mode II and III direction and able to withstand mode II loading whereas has only minor effects on tensional loading. And vice versa, the tension dominated elements can only withstand mode I loading and has a negligible effect on shear strength. Moreover, no specific failure criteria were introduced to cope with the pin – rupture failure.

Giuliano et al[49,50] proposed a micro-mechanical model for describing the delamination bridging action exerted by Z-pins by describing Z-pins as Euler-Bernoulli beams in an elastic foundation. The response of Z-pin is obtained by solving a series of non-linear differential equations that control the equilibrium for a set of prescribed pull-outs and sliding displacements. The failure issue was addressed successfully by applying Weibull's criterion, so it is applicable for fibrous and brittle Z-pins.

This method can be applied to three-dimensional cases; it considered bending of the Z-pin during the pull-out of the Z-pin during the pull-out of the Z-pin under mixed-mode loading conditions and post cure stress influencing the pull-out friction. The apparent fracture toughness of Z-pin was also investigated, it has been demonstrated that the apparent fracture toughness increases with the mode-mixity until a critical value is reached. The reason can be concluded as the residual friction experienced by Z-pin is initially by Coulomb friction in a mixed-mode regime. The friction enhancement increases the axial tension as well as bending that Z-pin has to support during pull-out, the improvement on mode-mixity was peaked once the critical mode-mixity 0.4 has reached and fibre-rupture start to take over the failure mode.

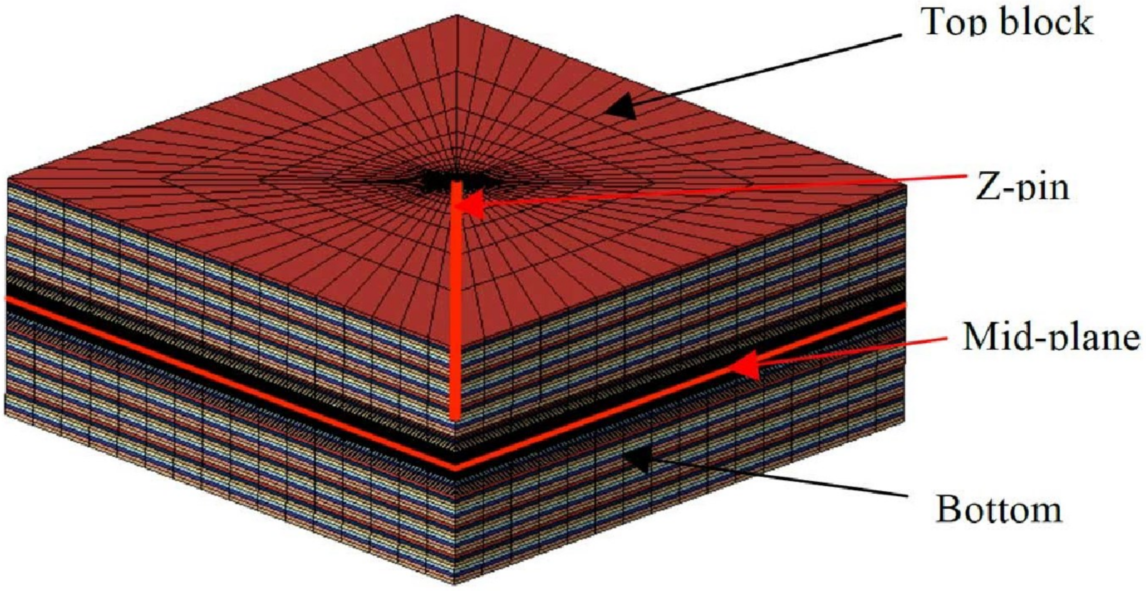

Figure 3.2: Full FE model of Z-pinned quasi-isotropic laminates [49]

3.1.2 Experimental characterisation of a single carbon composite Z-pin

An advanced single Z-pin pull-out, shear-out and mix-mode tests were performed by University of Bristol [51] to investigate the bridging mechanisms of a Z-pin inserted in a unidirectional laminate and quasi-isotropic composite. As illustrated below, the block is divided by a 16μm thick PTFE film.

The mixed mode test rig consisted of upper and lower section with a gap which is used for installing the specimens. The specimens can be placed on the test rig from 0° to 90° at 15° increments to achieve the quoted mode mixities.

Two stages of bridging mechanisms were observed, we see a linear growth in stress per unit displacement travelled in stage I, followed by the friction dominated action in stage II.

The substantial difference between UD and QI specimens were noticed, in UD specimens the debonding is much more significant than that found in stage II. Where a sharp maximum of 86N was reached for UD specimens whereas in QI the debonding phase passed smoothly and moved into frictional contact without seen noticeable peak. That is due to the fact the curing process damaged much more bonding in QI specimen than that in UD specimen, therefore the weakened pin to matrix interface lead to a much lower reaction force in axial direction in QI specimen.

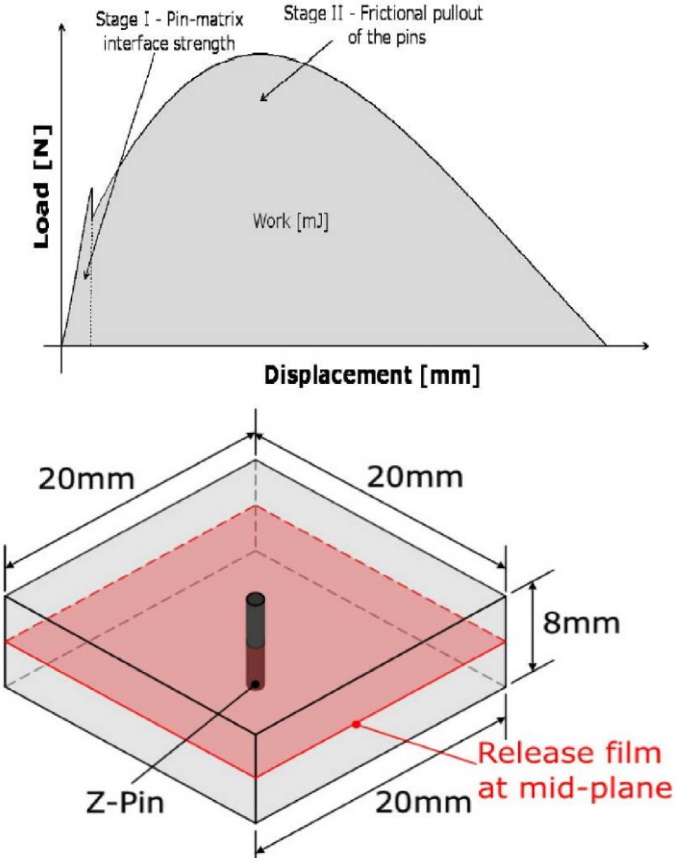

Figure 3.3: Specimen with release film at mid-plane before testing; two stage of bridging mechanism for mode I and mixed mode cases

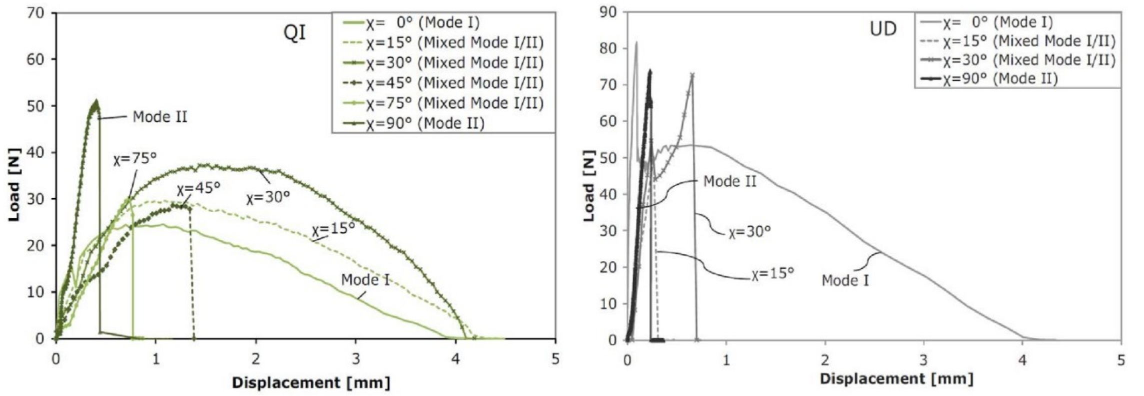

Figure 3.4: Representative QI laminate load vs displacement results Representative UD laminate load vs displacement results.

3.2 Modelling strategies

3.2.1 Modelling strategies briefing

- Ply level mesh was used to model the quasi-isotropic plies in order to define the fibre direction for different plies.
- Each ply of laminate assigns the material properties of Z-pin, the resin pocket and the surrounding QI laminate.
- The Z-pin/laminate interface in the modelling method is described by the surface-based method cohesive contact, whereby it is manually programmed by User subroutine Vuinter. The contact followed by the complete debonding of the cohesive interface was described by a modified coulomb friction law. As frictional contact will dominate.
- Progressive splitting of the through-thickness reinforcement was modelled by assigning a separate cohesive contact pairs within the Z-pin, the purpose of which is to investigate how the micro splitting within the structure affects the overall fracture toughness. The same cohesive law but different parameters were applied to model the splitting.
- Orthotropic user defined material was used to simulate the Z-pin.

3.2.2 Ply level mesh

The material properties for Z-pinned laminate are different from un-pinned ones. The reason is due to the in-plane microstructure of the laminate changes due to the insertion of the pins, the fibres near the Z-pin will be distorted, and the in-plane mechanical properties will change as well. The schematic of the wavy fibre is presented below.

Resin-rich zone was found at each pin location, the resin-rich zone has eyelet shape and elongated in the fibre direction, resin zones develop because the void-age formed when the pin was inserted into the laminate. These voids are filled with resin during the curing process. The shape and dimensions of the resin zone affect the in-plane mechanical properties significantly. In the FE analysis proposed in this chapter, the resin pocket was simulated using isotropic material.

Assuming out-of-plane swelling of laminates caused by accommodating is ignored, and Z-pins are assumed to be perfect solid cylinders, with no fibre crimping along Z-pin length. The in-plane microstructure of Z-pinned laminate is described as a star-like ply-level mesh. For quasi-isotropic laminate evaluated in this case, four different ply orientations were used, that is.

In this case, each ply of laminate is defined by assigning isotropic properties to the resin pocket and 3D orthotropic material properties to the laminate region. The material orientation can be addressed by creating a customised datum axis. Thus, the material orientation of each ply can be assigned correspondingly.

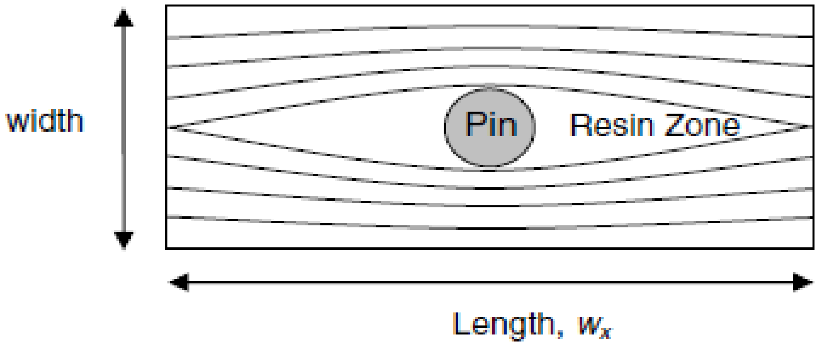

Figure 3.5: Region of wavy fibres and resin-resin zone aside Z-pin [10]

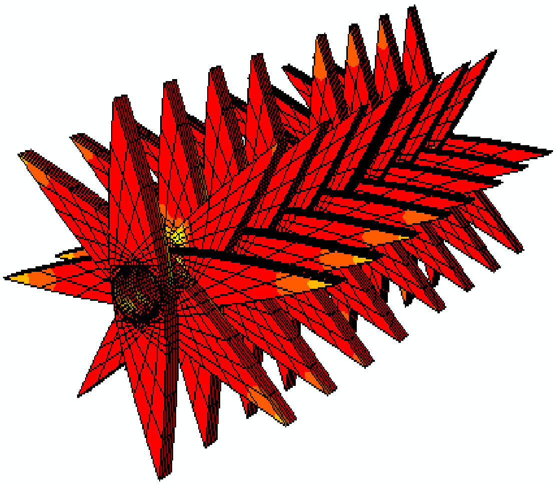

Figure 3.6: cross sectional view of the mesh for resin pocket

To address the fibre waviness, three categories of mesh were created separately and combined in the end. Resin pockets were created first as modelling of the resin need to assign a completely different material property. An Octagonal mesh was developed to address the effect of fibre waviness. The "Outer frame" was developed separately as the material orientation of each lamina supposed to be axial towards the orientation of the given stacking sequence. Different groups of mesh combined to produce the full model. How would fibre waviness be implemented would be addressed in the next section.

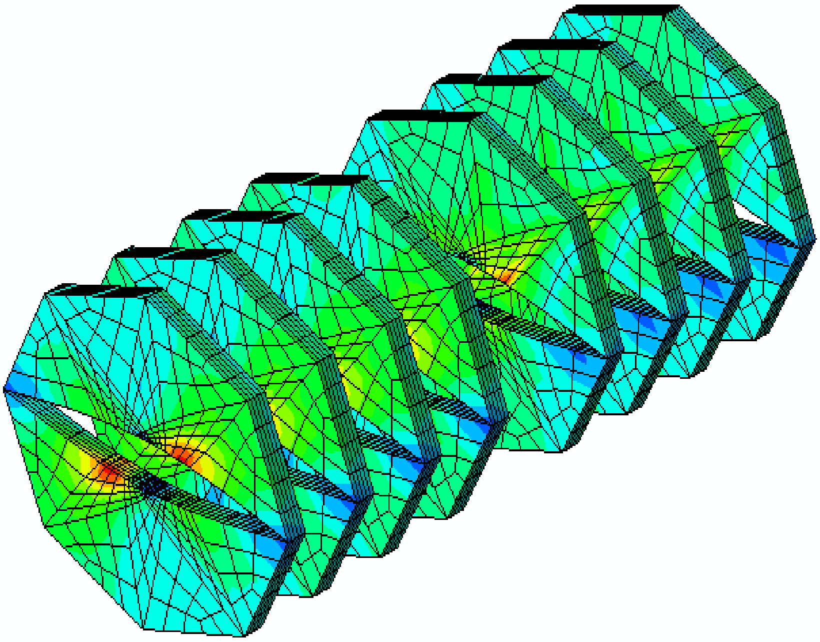

Figure 3.7: cross sectional view of the Octagonal mesh

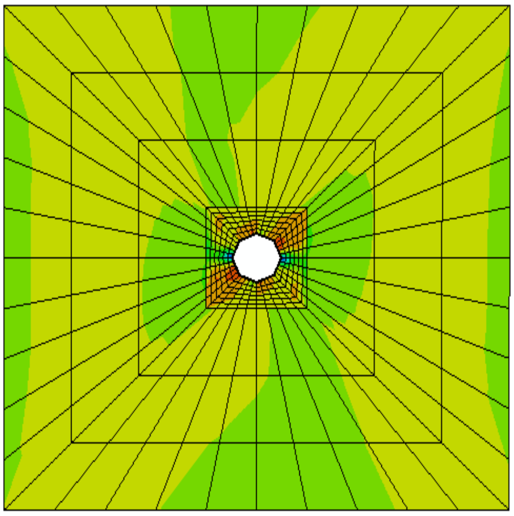

Figure 3.8: front view of the laminate "Outer frame"

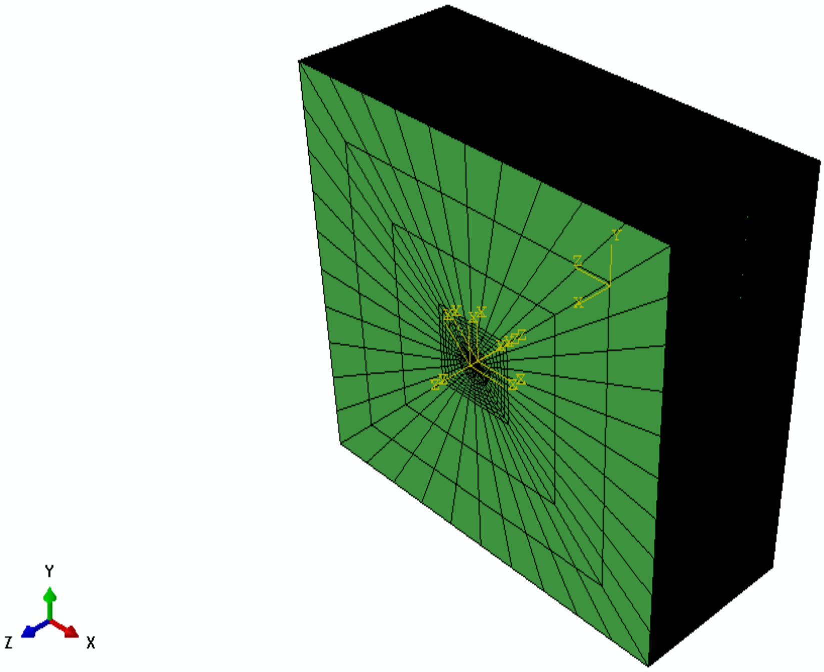

Figure 3.9: Side view of 64 plies full-model

3.2.2 Post cool down effect

In the simulation, a -160 °C temperature differential is imposed to the model prior to the mix-mode loading process. To simulate the cool-down effect from a 180 °C cure temperature to 20 °C room temperature.

3.2.3 Misalignment

Unless very carefully controlled, using the contemporary manufacturing method during the cure will very likely to induce a misaligned angle, where the z-pins embedded in laminates deviating from the orthogonal alignment for a certain angle. Composite with misaligned Z-pins in the laminate would not fully function as it might expected it could be. The relative movement between the top half laminate and the bottom half laminate is given in Eq. 3.1 in the global X-Y-Z coordinate system. θ is the in-plane angle between velocity V and global X-axis.

Equation 3.1

$$[V_X \; V_Y \; V_Z \,] = [V sin\chi cos\theta \; V sin\chi sin\theta \;\; - V cos\chi \,]$$

The actual mode-mixity is defined as the ratio of the delamination sliding velocity (displacement) to the total velocity (displacement). The Z-pin axis is directed opposite to the global Z-axis. The Y-pin axis stays in the global X-Y plane, and the rotation angle ψ obtains it concerning the global Y-axis. The right-hand rule derives the positive direction of the X-pin axis. Then, the relative velocity between the top half pin and bottom half pin at the fracture plane can be resolved in the local Z-pin coordinate system by Eq. 3.2.

Equation 3.2

$$\left[V_{X_{pin}}\, V_{Y_{pin}}\, V_{Z_{pin}}\right] = [-cos\zeta cos\psi \ -cos\zeta sin\psi\ sin\zeta\ sin\psi \ -cos\psi\ 0\ -sin\zeta cos\psi \ -sin\zeta sin\psi\ - cos\zeta\ ][-Vsin\chi cos\theta \ -Vsin\chi sin\theta \ -Vcos\chi\,]$$

Consequently, for the direct method of defining Z-pin misalignment, the mode mixity φ is derived by:

Equation 3.3

$$\phi = \frac{\sqrt{{V_{X_{pin}}}^2 + {V_{Y_{pin}}}^2}}{\sqrt{{V_{X_{pin}}}^2 + {V_{Y_{pin}}}^2 + {V_{Z_{pin}}}^2}}$$

$$= \sqrt{cos^2\chi cos^2\zeta + sin^2\chi(sin^2\psi + cos^2\psi cos^2\zeta) - 1/2sin2\chi sin2\zeta cos\psi}$$

Therefore, in order to obtain the actual mode-mixity for a single Z-pin, the pull-out angle χ can be obtained from Eq. 3.3 Then the corresponding boundary condition in the X-Y-Z coordinate system can be defined according to Eq. 1. As shown in Eq 3. 4, the actual mixed-mode angle ω can be equivalently expressed in terms of either the actual mode mixity or velocity components. (16)

Equation 3.4

$$\omega = tan^{-1}\left(\frac{\emptyset}{\sqrt{1-\emptyset^2}}\right)$$

In the Proposed FE model, the Z-pin misalignment is introduced by applying different displacement in axial and lateral direction. The figure gives the indication of a single pin misalignment is showing below.

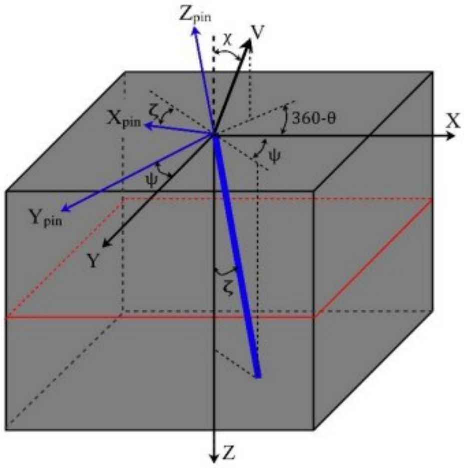

Figure 3.10: Z-pin misalignment schematic [49]

3.2.4 Material definition and boundary conditions

	UD laminate (IM7/8552)	**Z pin (T 300/BMI)**	**Resin 8552**
Young modulus E_x (GPa)	161	144	4.57
Young modulus E_z (GPa)	11.38	7.31	4.57
Shear modulus G_{xz} (GPa)	5.17	4.45	1.67
Shear modulus G_{yz} (GPa)	3.98	2.63	1.67
Poisson ratio, v_{xx}	0.32	0.25	0.37
Poisson ratio, v_{yz}	0.436	0.39	0.37
Thermal coefficient,α_{zz}	3.0×10^{-5}	3.0×10^{-5}	7.5×10^{-5}
Thermal coefficient,α_{xx}	0	0	7.5×10^{-5}

Table 2: Material properties of laminate-pins and resin [52]

- The analysis consists of two steps, curing step and pull-out step
- The full analysis consists of two steps, namely cure (thermal) and pull-out (mechanical). In the cure step, a 160°C temperature reduction is imposed to all the nodes of the model to simulate the post-cure cool-down
- For the pull-out step the back surface is fully constrained, and the front surface is subject to a uniform displacement.
- The resin is assumed as an elastic/perfectly plastic material, with yield stress equal to 90 [53] Mpa

3.2.5 User subroutine flow chart

The explicit user subroutine which contains Contact explicit code Vuinter and user material Vumat were successfully validated by the benchmark test shown in the section above. The general Operational flow chart of these two codes can be presented below:

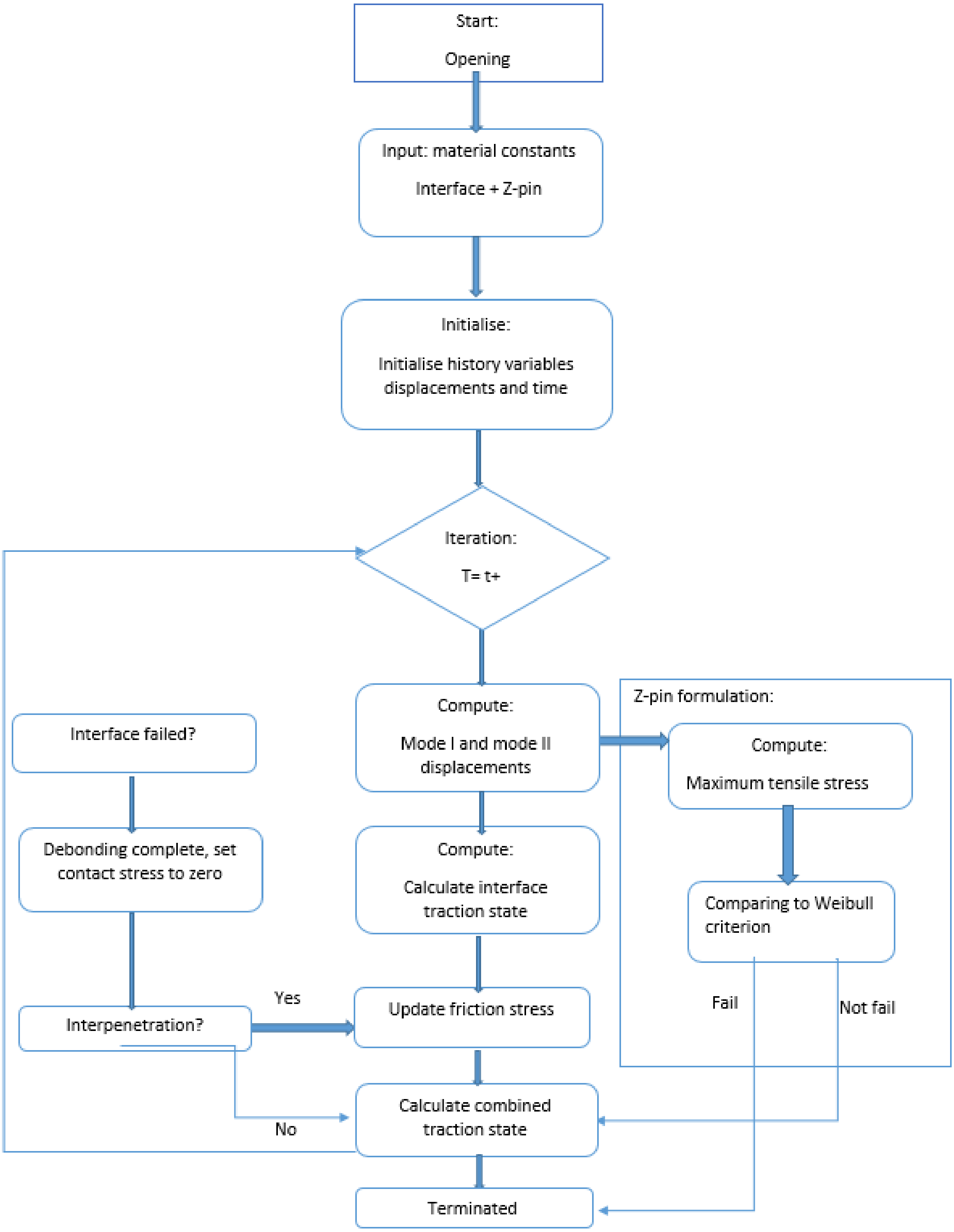

Figure 3.11: Flow chart for Vumat and Vuinter combined routine

3.2.6 Mass scaling

In order to simplify the process of pull-out, mass scaling was applied to the present modelling methodology. Correct application of mass scaling will help the model significantly reduce the computational time while retaining the necessary degree of accuracy required for a particular modelling case.

In quasi-static simulation, the mass scaling can be achieved by reducing the time period of the analysis or increase the density to a certain level. The criteria for how an appropriate time increment should be chosen is dependent on the Dilatational wave speed C_d , which is determined in Abaqus explicit by calculating the effective hypoelastic material moduli from the material constitutive response. Young's modulus E, Poisson's Ratio,v. The expression for the wave speed C_d can be expressed by:

Equation 3.5

$$c_d = \sqrt{\frac{\hat{\lambda} + 2\hat{\mu}}{\rho}} ,$$

Where $\hat{\lambda}$and $\hat{\mu}$ refers the lame constant and ρ denotes the density.

And an approximation to the stability limit is often expressed as the smallest transit time of a dilatational wave across any of the elements in the mesh. Therefore, the time increment has the expression of:

Equation 3.6

$$\Delta t \ \leq \left(L_e \sqrt{\frac{\rho}{\hat{\lambda} + \ 2\hat{\mu}}} \right)$$

Where L_e is a characteristic length associated with an element. And therefore, the amount of increments n, required is $= \frac{T}{\Delta t}$, thus:

Equation 3.7

$$n \approx T_{max} (\frac{1}{L_e} \sqrt{\frac{\hat{\lambda} + \ 2\hat{\mu}}{\rho}})$$

Where T_{max} is the time period of the event being simulated.

Therefore, a criterion for the material given in the present modelling can be calculated. The final time increment chosen to carry forward the modelling is 5e-7s

3.2.7 Fibre waviness

The presence of resin pocket will affect the direction of the surrounding fibre. Therefore, the orientation of the surrounding fibre should be taken into consideration. In other works of literature, fibre waviness was addressed in a complicated way. With the aid of the Commercial software MATLAB, the fibre waviness angle was calculated at each coordinate and assigned separately. Considering the complexity of the stacking sequences, the approach is tricky to apply.

A brand-new approach was proposed in the current study. The material orientation of the fibre surrounding the resin pocket was assigned to be tangential to the curvature of the eyelet resin pocket.

It is worth to mention that it is crucial to simulate the effect of the fibre waviness without altering the orientations of fibre that unaffected by the resin pocket. In hindsight, An Octagonal mesh part was created in the vicinity of the resin pocket region. The rest of the laminate will be "adhered" to the model and merged to become the full model.

This approach eases the complexity of modelling the laminate micro-structural feature fibre waviness, considering the size of the Octagon comparing to the full model, the error from the estimation can be negligible.

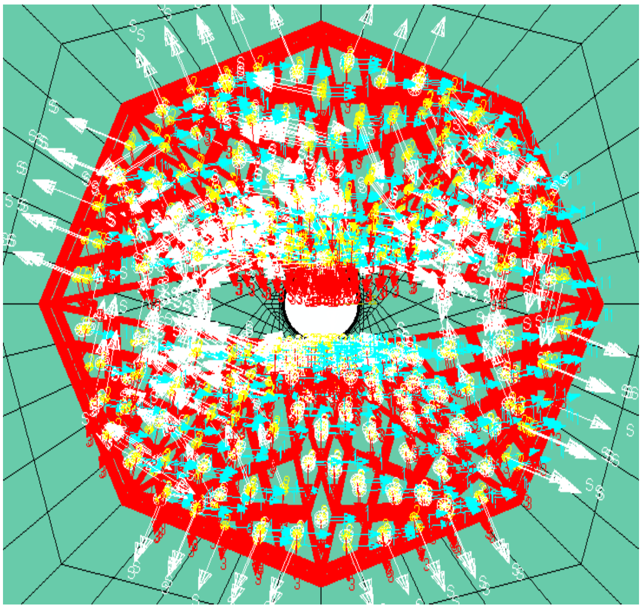

Figure 3.12: Example of material orientation for fibre waviness

3.3 Curing and bridging response under different mode mixity

3.3.1 Curing step results

Mismatch of thermal expansion coefficient between Z-pin and laminate is responsible for interfacial bonding. The curing step partially break the bond between Z-pin and laminate, but the bond leftover will still withstand the mechanical loading.

In the figure 3.13 shown below indicates a Z-pin after thermal step. The CPRESS refers to the contact stress, the positive stress refers to region that completely debonded whereas the negative value means the interface is still active. In QI laminate, the debonding propagate in a horseshoe pattern due to different stacking sequence through the thickness, as the thermal expansion coefficient for different lamina would be different, thus the expansion at different plies after curing would be different.

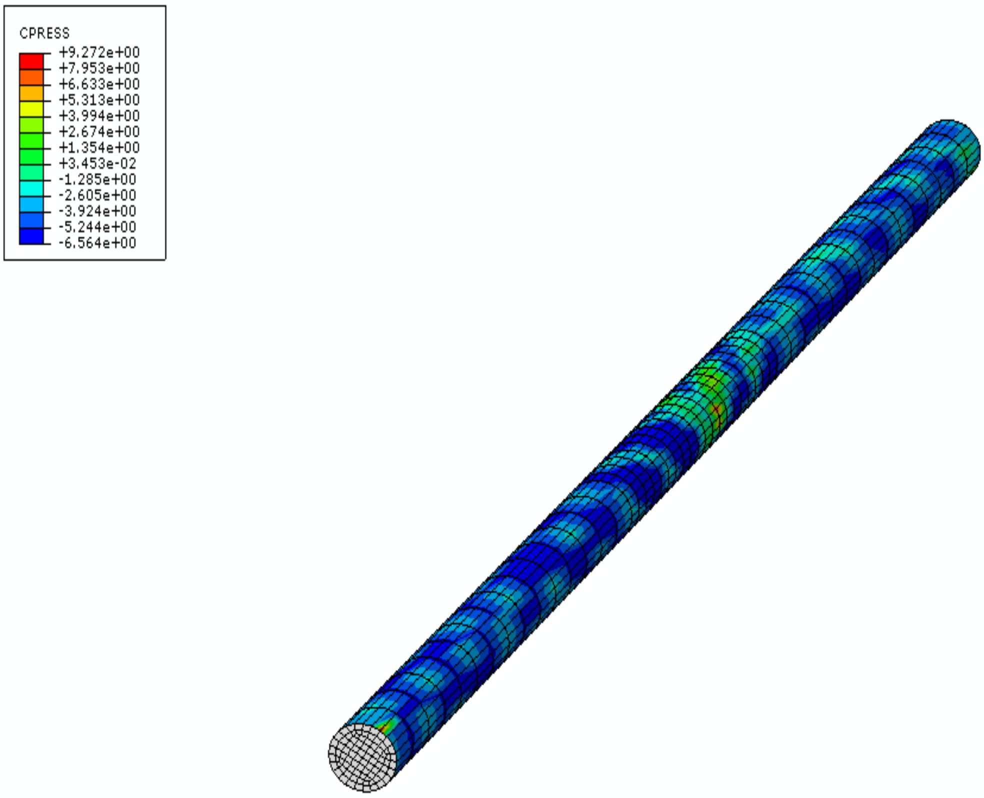

Figure 3.13: Debonding after curing process

3.3.1 Bridging response under different mode mixity

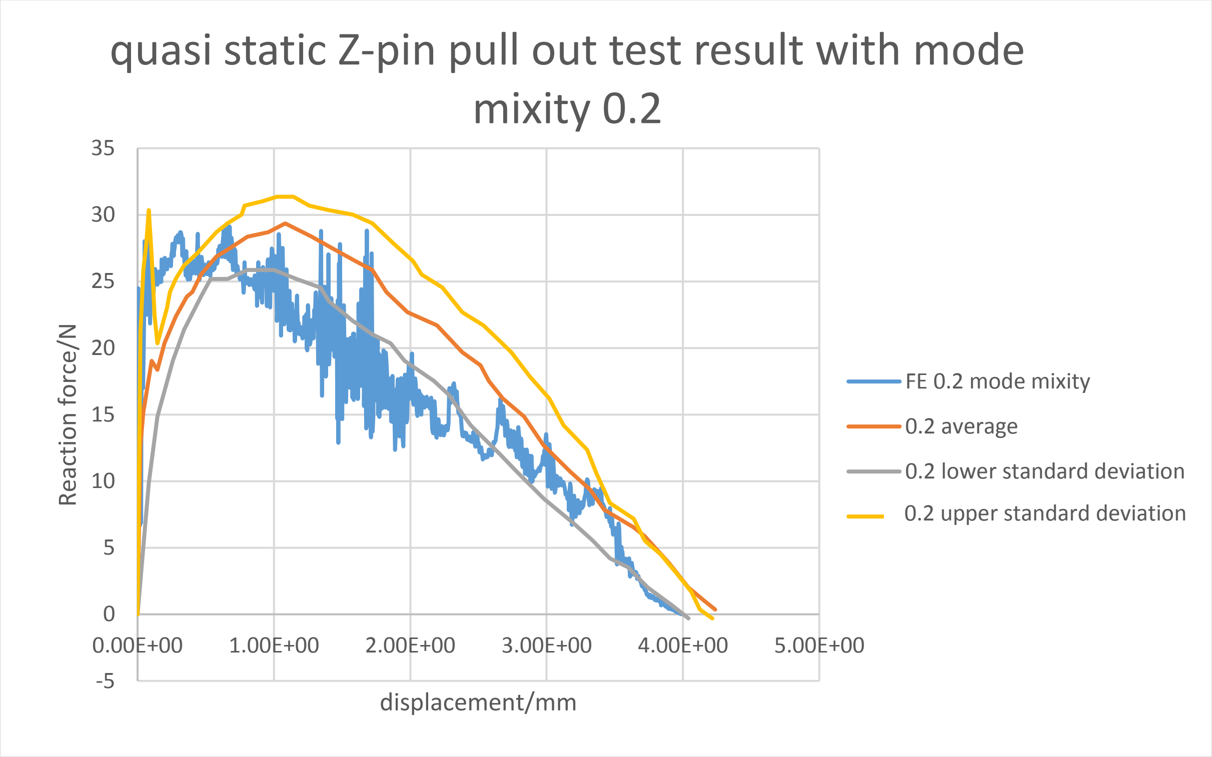

Figure 3.14: mode mixity 0.2 abaqus subroutine vs experimental results.

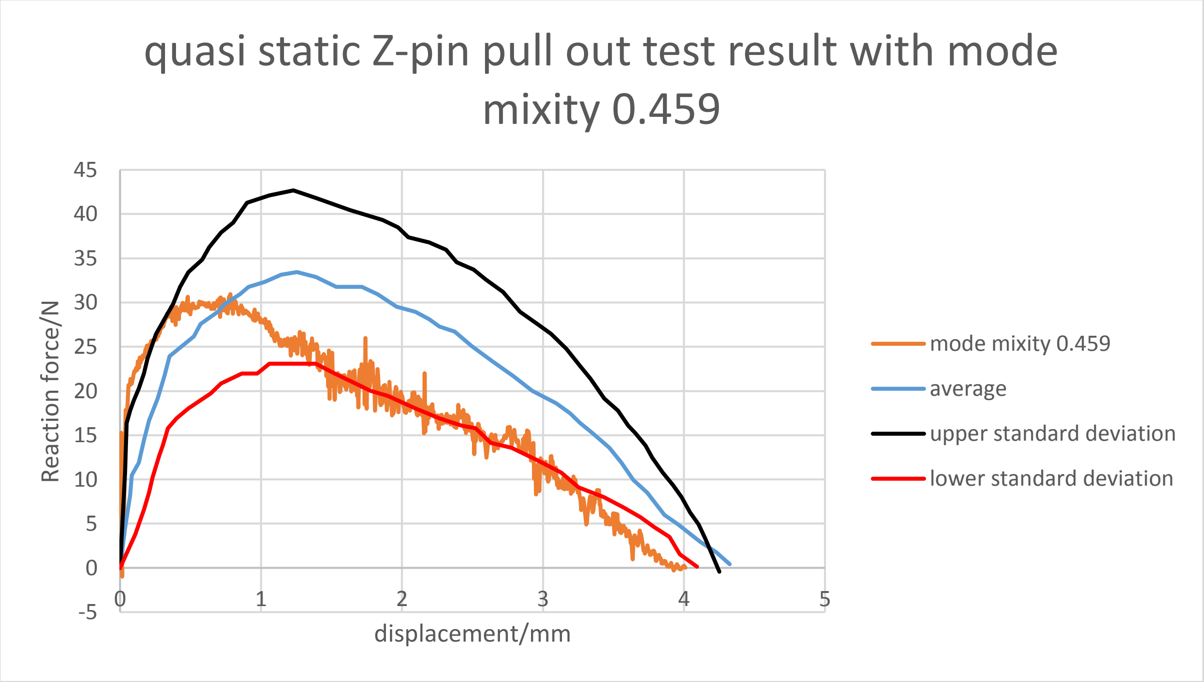

Figure 3.15: mode mixity 0.459 abaqus subroutine vs experimental results.

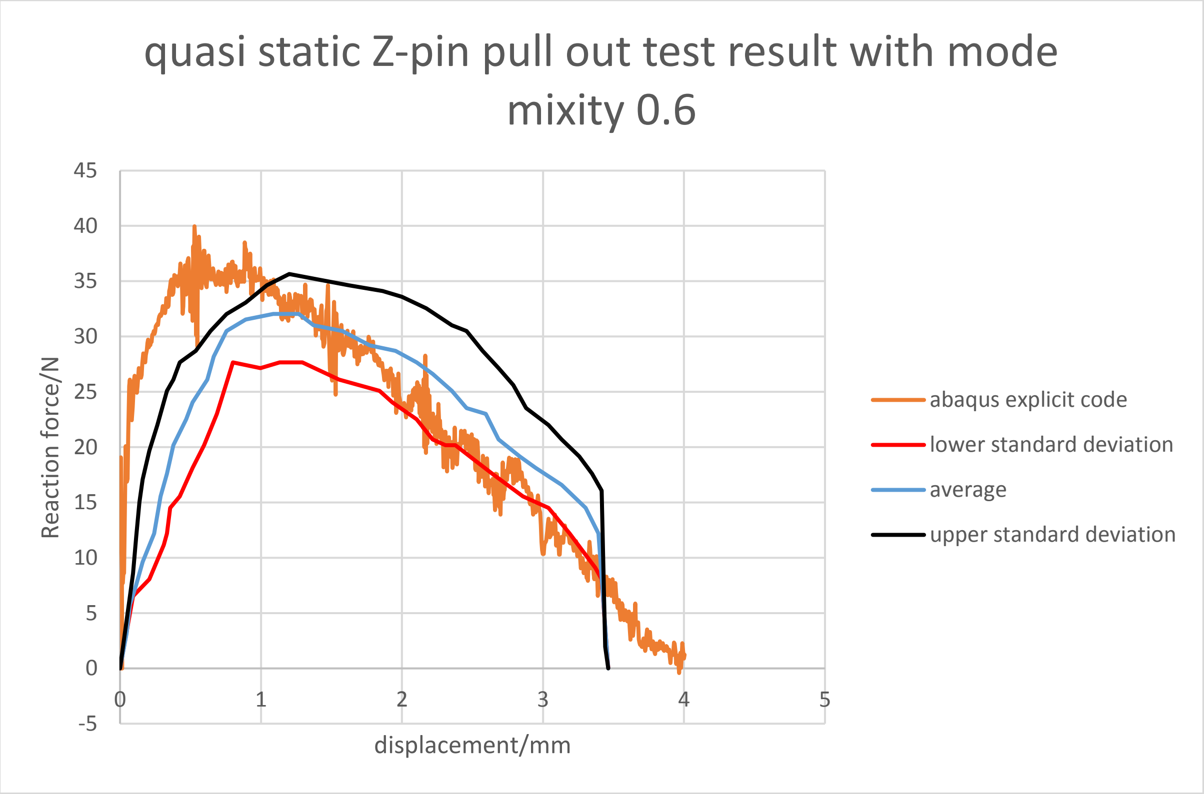

Figure 3.16: mode mixity 0.6 abaqus subroutine vs experimental results.

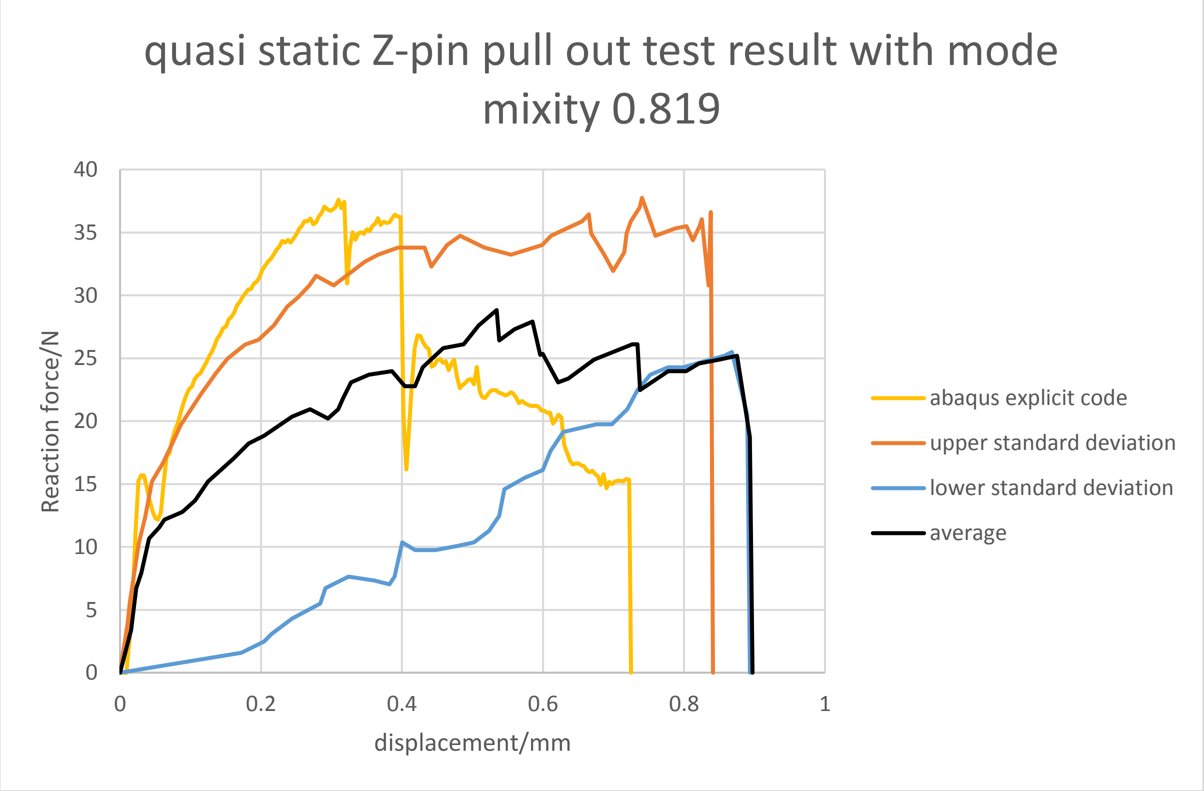

Figure 3.17:mode mixity 0.819 abaqus subroutine vs experimental results.

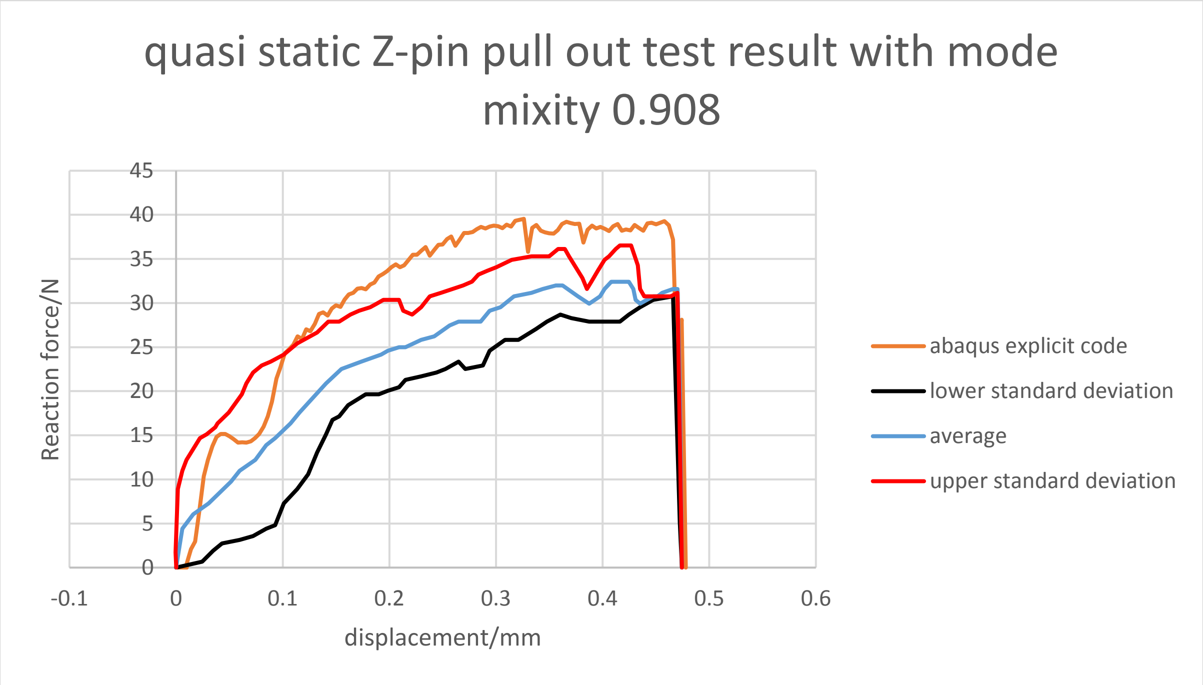

Figure 3.18:mode mixity 0.819 abaqus subroutine vs experimental results.

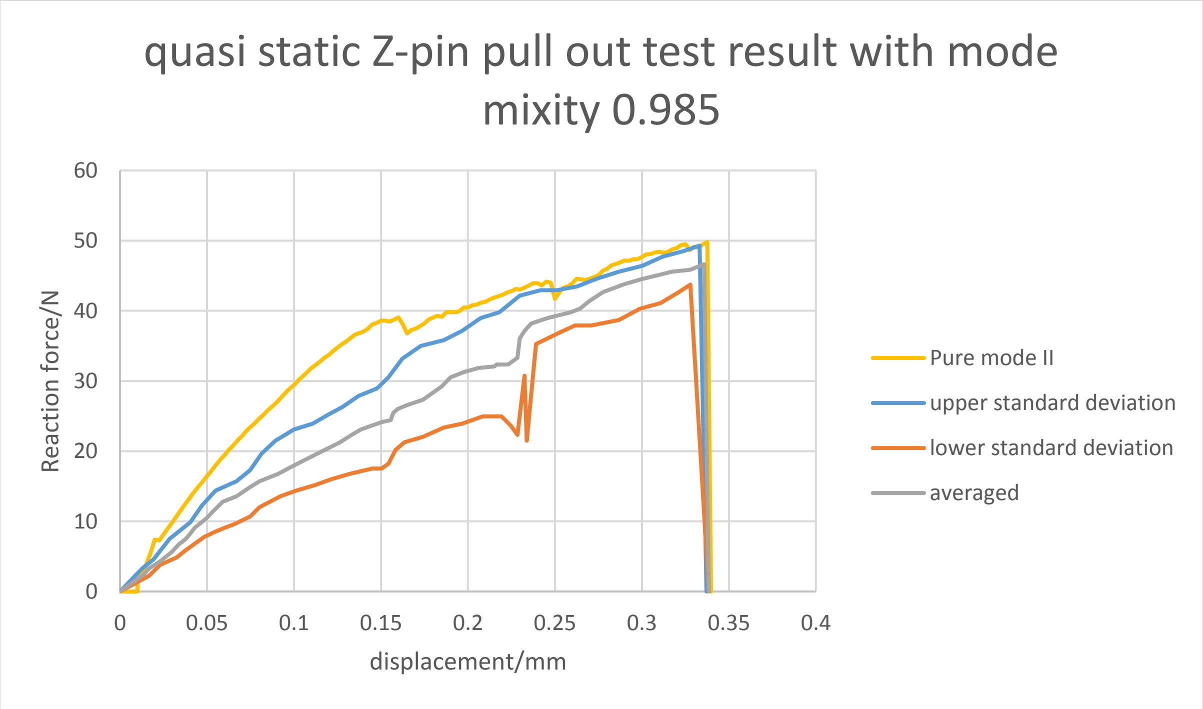

Figure 3.19: mode mixity 0.985 abaqus subroutine vs experimental results.

For the verification of this modelling strategy, pull-out tests with six mode mixites were carried out. The load vs. displacement curves for all the six cases are compared to the experimental results. For low mode mixity from 0.2-0.4, there is an instant increase in the bridging force due to the residual bond left after the curing step. With further loading, the bonding between Z-pin and laminate interface completely broken, and no significant load drop has been observed; that is because the residual stress was added on the top of Coulomb friction. For the mode-mixity region with complete pull-out failure (for mode mixing 0.2 and 0.4) ,both FE simulation and experimental data show that the bridging force rise to a peak value before degrade gradually, the rise of the load is attributed to the "snubbing effect", where an immense pressure is built up because the pin is deflecting, and the friction force in the zone of reflecting is enhanced. As the schematic indicates, an enhanced friction area was demonstrated. The gradual decrease of the bridging force is due to the lessening of the contact area for the intermediate mode-mixity region between 0.6-0.8 mode mixities. Experimental results show large scatter on the bridging force, which is because the probability of survival for each Z-pin specimen is different from each other, whereas the FE Vumat subroutine only considers the universal Weibull parameter and ultimate failure stress. Therefore, there is a discrepancy between modelling results and experimental results; the FE simulation result shows a complete pull-out failure for mode mixity 0.6, whereas the experimental data show a rupture failure. Agreement was seen for mode II tests between experiment and FE results, where a catastrophic failure was seen after the failure stress has been reached, the sudden drop of the bridging force is due to the failure of the fibre strand whereas the others can still withstand the load, and the z-pin has broken completely after progressive strand failure. Furthermore, the displacement is decreasing with the increasing mix-mode ratio.

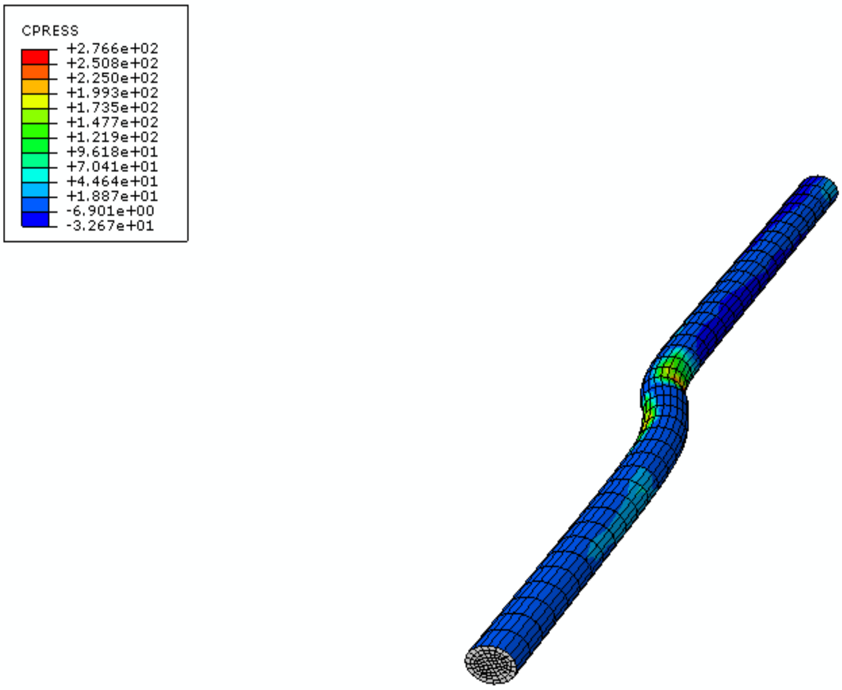

Figure 3.20: Enhanced friction for pin deflecting area

3.3.1 Parametric studies of splitting on Z-pinned laminate under quasi-static loading

Internal splitting occurs when there is high shear stress that appears during the bridging response. Typically, splitting is widely attained within the Z-pin matrix when Z-pin subjects to lateral stress before the ultimate fibre failure. The splits tend to appear in the unsupported region of the Z-pin, i.e., the fragment that has been pulled out of the laminate. The main effect of the splits is to reduce the bending stiffness of the Z-pin during the pull-out.

The presence of splitting was modelled in the current model. Previously, internal splitting was modelled by adding zero thickness cohesive elements into the Z-pin. In the current model, the internal splitting was addressed by modelling another separate cohesive surface contact via the central plane divided the Z-pin into two identical segments.

In the following section, the apparent fracture toughness is compared between FE simulations (the non-splits specimens and the specimen contains one central split) and experiments. All the fracture toughness data in this study is for 2% Z-pin reinforcement, and the value of the apparent fracture toughness can be calculated by:

Equation 3.8

$$G^{*}(\emptyset) = \frac{4\varphi}{\pi D^{2}} G_{pin}$$

Where D denotes the diameter of Z-pin, in this study, the diameter applied is 0.28 mm, refers to an areal density of Z-pins, does the Z-pin dissipate the energy during bridging against delamination, which equals to the integral area under the load vs. displacement curve. Apparent fracture toughness will effectively provide a normalised measure for the fracture toughness of Z-pinned laminate.

As indicated by the figure 3.21, the FE simulations achieved a good agreement with the experimental results. The conflict happens during the transition region, where the failure mode of Z-pin transit from pull-out to pin rupture. In the experimental data, it can be seen that for mode mixity 0.6, a large scatter was presented indicating the Z-pin behave in a volatile manner and majority of pins suffered from pin rupture failure in the end, whereas In the FE simulation, the result obtained indicates apparent pull-out failure thus led to higher fracture toughness. For the cases with high mode mixity (mode mixity excess 0.8), good agreement has been achieved overall.

Comparing the bridging abilities between the z-pin with no splitting and one central splitting. A comparison was drawn, as shown in figure 3.21, Z-pins with no splitting demonstrates higher bridging capabilities for low mode mixity between 0.2 to 0.6. This is since Z-pins with no splitting has larger flexural modulus than the group with splitting. For cases with mode-mixity 0.8 and above. The z-pin with splitting demonstrates higher apparent fracture toughness due to the better capability of sustaining the deformation, thus delay the onset of catastrophic failure.

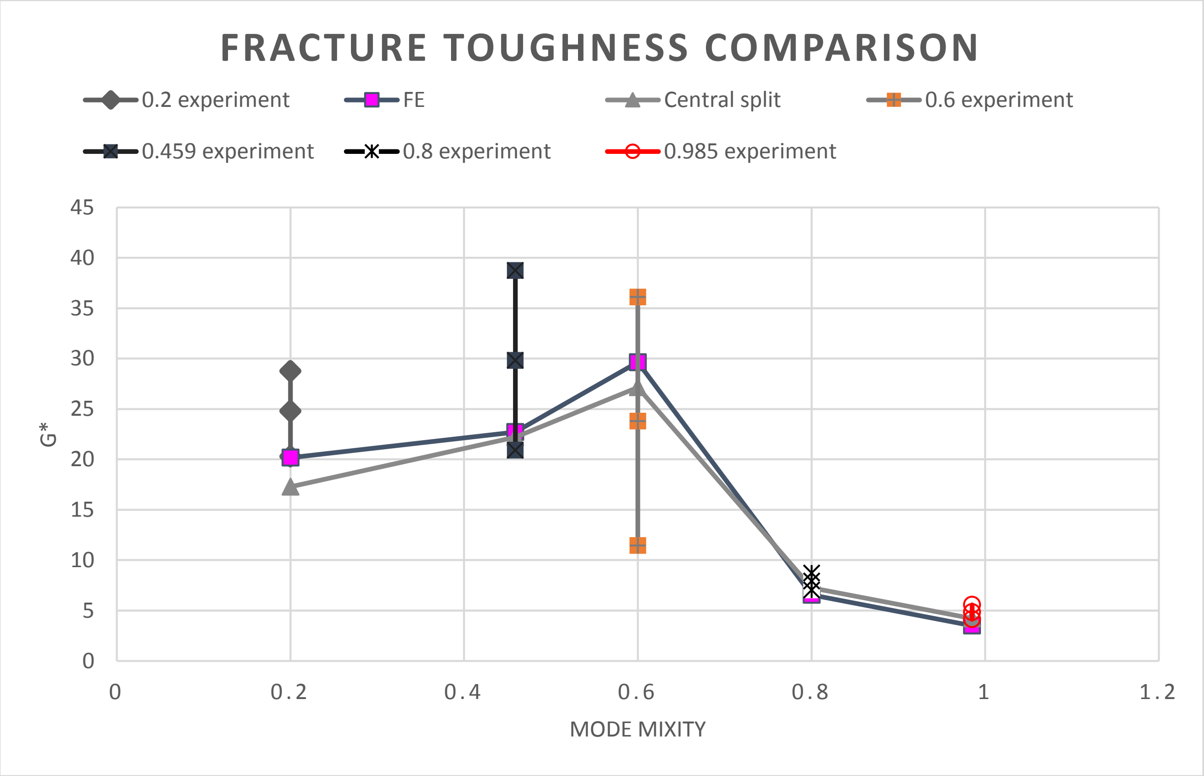

Figure 3.21: Apparent Fracture toughness comparison between experimental result and FE simulation

3.4 Innovative features from establishing a high-fidelity model

This chapter has addressed the development of an innovative three-dimensional high-fidelity FE model for investigation of Z-pinned composite laminate. This modelling approach was based on a versatile ply-level mesh, which explicitly modelled the resin pocket, surrounding laminates and Z-pin misalignment.

A brand-new approach was proposed to address the fibre-waviness in the current study. The material orientation of the fibre surrounding the resin pocket was assigned to be tangential to the curvature of the eyelet resin pocket. And the whole model was partitioned into different parts, including resin pocket, the laminates in the vicinity of the distorted fibre which essentially will be affected by the fibre waviness and the laminate far away from the resin pocket which has the normal material orientation. This approach significantly eases the complexity of the modelling approach, as the previous strategy was to use MATLAB code to enforce a confined field into the fibre-waviness region.

For the verification of this modelling method, a fibrous Z-pin of 0.28 mm diameter and 8mm length was inserted into the laminate. The customised contact subroutine including cohesive contact and frictional contact was successfully implemented to demonstrate the bridging abilities of Z-pin, the user-defined orthotropic material was applied to simulate Z-pin. The modelling approach gives results in great agreement with the experimental results in terms of both mechanical performance and fracture toughness.

The modelling strategy described in the paper is proven to be capable of extending to other Z-pin configurations in terms of stacking sequence or different material.

3.5 Conclusion

In this work, a new cohesive damage model for the prediction of the bridging mechanisms of a single Z-pin under mixed-mode loading was proposed. No cohesive elements were used to model the interface, but instead, cohesive contact was used to model the debonding, and user-defined material was applied to simulate the rupture failure.

In the first part of the section, the modelling methodology and parameters applied were displayed. The simulation strategy explicitly expresses the most significant features of Z-pinned laminates, including the presence of resin pocket fibre waviness and Z-pin/laminate interface. The cohesive contact was described by “cohesive bridging law,” and the interfacial friction was stated by a modified Coulomb friction law.

In the latter section, the bridging forces and apparent fracture toughness from FE modelling were compared with experimental results. The modelling approach gives good agreement in terms of both bridging response and fracture toughness. However, the experimental data shows large scatter, especially in the transitional region when mode mixity varies from 0.4-0.8, and it can be observed from the results presented, for mode mixity 0.6, the experimental result shows that Z-pin surfers from Pin rupture failure whereas the modelling result indicates Z-pin pulled-out successfully with everything intact. In the parametric study, Z-pin with a central splitting was also conducted, and the fracture toughness was compared with both the FE modelling case without splitting and experimental data. Due to the limit of sample size, the difference in between is inconsequential.

In the end, the bridging response was broken into different phases and discussed in detail.

In future work, the case with more splitting density and more mode-mixites should be considered to polish-off the work. Also, the large data scatter in the experimental result reveals that the bridging response is dependent on many factors, including interfacial frictional coefficient, stacking sequences, Z-pin splitting, and residual stress. More parametric studies should be conducted towards these different aspects that may affect the results.

Overall, the present modelling method can be extended to different Z-pinned configurations, and the results obtained regarding the bridging response, and fracture toughness can be used to predict the Z-pinned laminate with different reinforcement arrangement.

Chapter 4 Advanced fidelity model on dynamic bridging test

4.1 Review of published dynamic bridge experimental data

Z-pinning technology has been extensively investigated and developed as a cost-effective method to improve the delamination resistance, and Z-pin is usually made of metals or carbon fibres.

Z-pins have been proven very effective in improving the fracture toughness in all the quasi-static tests, Z-pinned laminate has shown superior performance in the mode I dominated cases compared to Mode II dominated case. The primary reason is due to the difference in the failure mode. In mode I dominated cases, the Z-pins are typically pulled out, and the fracture toughness increases with mode mixites up to a point 0.4. Moreover, the fracture toughness tends to drop if Z-pins are subject to the shear failure mode. Due to the rupture failure mode, it tends to have low energy dissipation because the amount of the displacement it travels is quite small before it is completely broken.

The failure mechanisms of Z-pins also largely depend on other factors like the layup of Composite laminates, the Z-pin insertion angle, and also the insertion length of Z-pin have significant influences on the failure mode as well as the fracture toughness of Z-pins. Furthermore, in the pull-out duration, large lateral deformation can cause the surrounding resin to get damaged or deformed. As a result, both resin and composite laminate are susceptible to strain rate, so it would be of many people's interest to investigate how the mechanical performance of Z-pin pull-out dependent on the loading rate.

The dynamic bridging response of Z-pins is the key for the design, analysis, and certification of composite structures under impact loading, Cui et al.[56] have presented the experimental justification to demonstrate the mechanical response of Z-pins under different loading rate that varies from 0.01mm/s to 12m/s by using a series of samples that have Z-pin embedded in pre-delaminated laminates.

4.2 Single pin dynamic experiments characterisation

The experimental methodology provides a benchmark that the finite element modelling development can follow. The FE modelling work, which will be delineated from section 4.4, was calibrated and validated against the experimental work that has been conducted at the University of Oxford [56]. Thus, the experimental methodology will be introduced from section 4.2 to 4.4 before proceeding to the modelling development.

Figure 4.1 presents the specimens schematic that has been used for the mechanical tests. The Z-pins, which have 0.28 mm diameter, made from T300/BMI material were used in the experiment-pins were inserted in the IM7/8552 pre-preg material, and a layer of PTFE film was inserted at the mid-plane of the layup in order to create pre-existing delamination. Also, the pre-existed delamination will make sure the bridging force was purely from the Z-pins.

The pull-out force applied to a single pin is low, and the data acquisition is quite tricky. To solve the problem, an array of 4×4 pins with evenly spacing in each specimen, which machined from the pinned laminates, to make 10×10 mm blocks and with a thickness of 8 mm. In the investigation. A total pull-out force was obtained from the test and an averaged force was calculated from the total force to investigate the behaviour of a single Z-pin.

A split Hopkinson tension bar system was used for the dynamic tests, and the test speed will reach up to 5.5m/s for this investigation. The failure process was captured with high-speed cameras. A schematic of the split Hopkinson tensile bar system is shown below, and the long projectile can generate stress update within the duration of 1ms. The strain gauge that attached to the bars to measure the strain during the test and therefore enables the force and displacement of the samples to be calculated.

The Z-pins were tested with different combinations of tension and shear loads using aluminium fixtures prepared for alternating the angle between the Z-pin and loading axis. The off-axis angles, β, that the specimens were tested at 0°,15°,30°,45°,60°,75°. Aiming at investigating the transition from pull-out dominated cases to shear dominated failure cases.

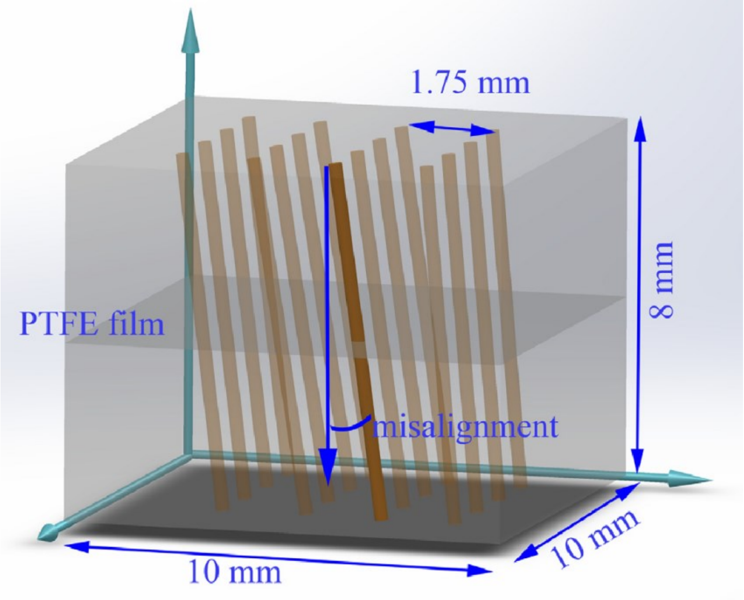

Figure 4.1: Z-pin arrangement in each specimen

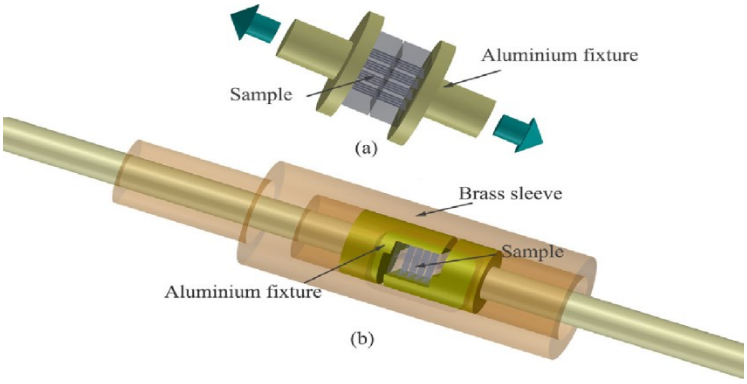

Figure 4.2: Mode I and Mode II Dynamic bridging test configuration

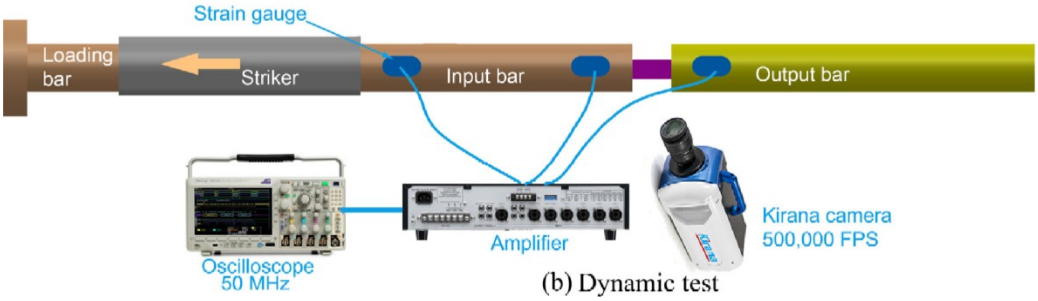

Figure 4.3: Dynamic experimental configuration

4.3 Coupon level dynamic experiments characterisation

4.3.1 Mode I experiment

Coupon level delamination experiments for Z-pinned laminates which under dynamic loading were conducted in [58]. For mode I experiments, wedge-opened double cantilever beam was used to conduct the test. A Split Hopkinson pressure bar was used to make the composite samples reach the prescribed displacement at velocity 4m/s and 7m/s .

The composite samples were made from material IM7/8552 unidirectional prepreg. And the nominal thickness of the sample is 8mm which consists of 64 plies lamina with stacking sequence of $[[0/45/0/-45]_{4s}]_s$. 0.28 mm diameter carbon-fibre Z-pins with a relative spacing of 1.75mm. The Z-pinned zone was placed in front of the initial crack tip.

A strain gauge attached at the back of the laminates, which was used to monitor the bending strain. A schematic contains The WDCB sample is presented below.

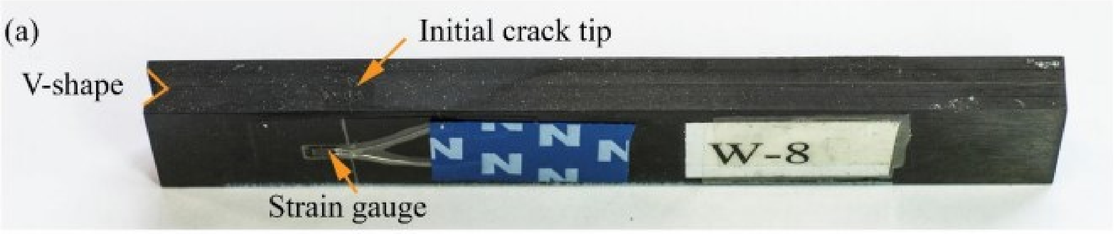

Figure 4.4: WDCB sample with the machining details

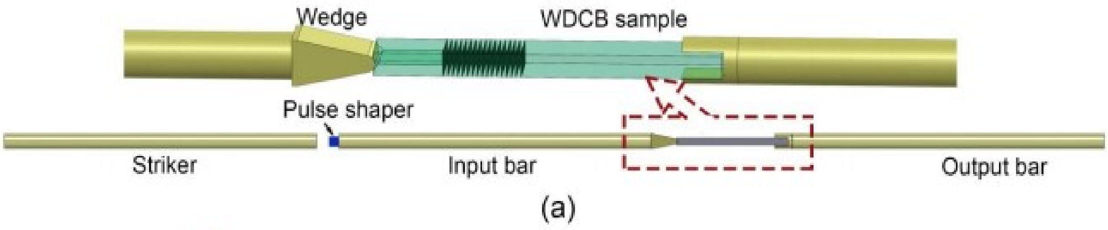

Figure 4.5: Test setup for dynamic WDCB tests

Inevitably, the displacement is not applied at a constant rate, which results in remarkable fluctuations on the dynamic response curves. Comparing to quasi-static test, dynamic cases exhibited less load carrying competency.

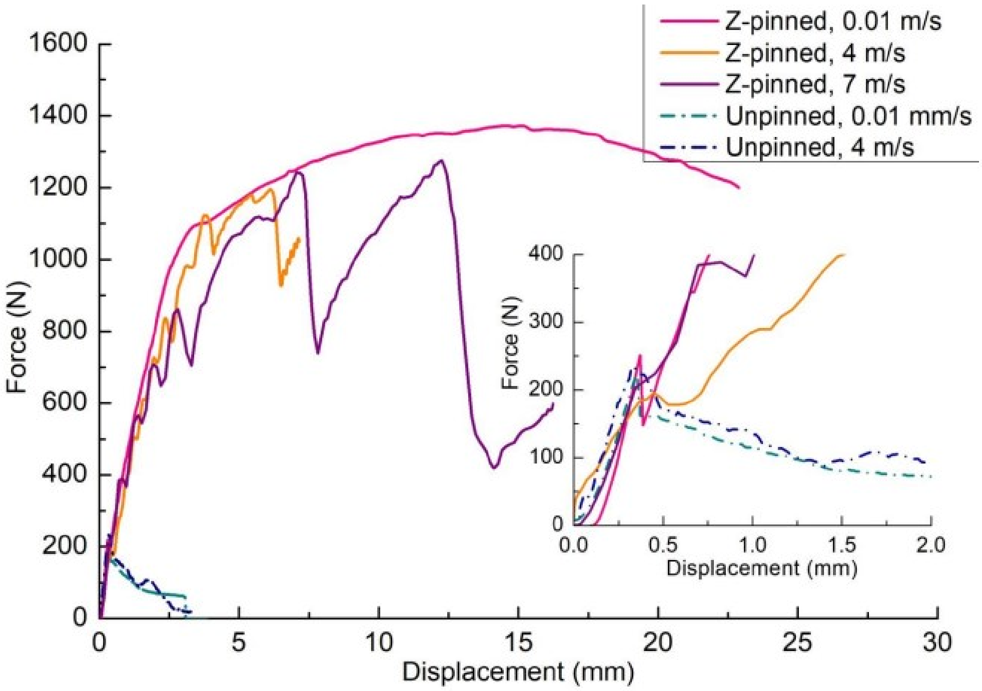

Figure 4.6: Force-displacement curves for WDCB tests

4.3.2 Mode II experiments

Similarly, to Mode I experiment, end notched flexure test was conducted for coupon level mode II test. Under dynamic loading, the crack initiation load for Z-pinned samples were insensitive after crack propagation, whereas the unpinned samples have demonstrated significant oscillations. That is because Z-pins improve the loading capacity when the critical pull-out load has reached.

The responsive reaction force of Z-pinned laminate did not show enough dependency on the loading rate.

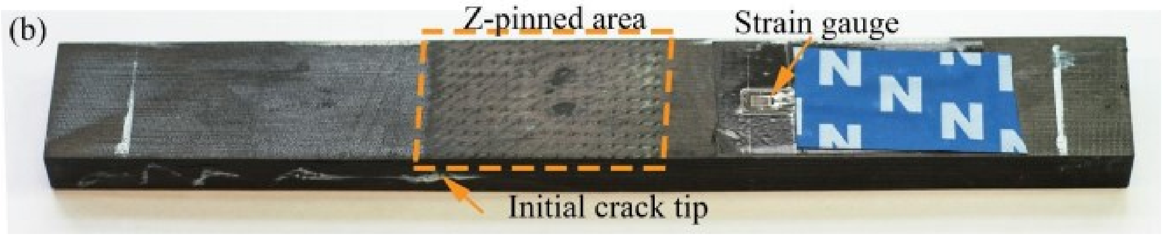

Figure 4.7: Test setup for dynamic ENF tests [58]

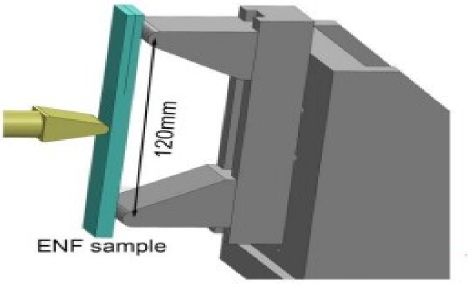

Figure 4.8: Test setup for dynamic ENF tests

Comparing to the delamination resistance improvement for WDCB test for mode I, The presence of Z-pin does not improve the fracture toughness as much. This could be attributed to the fact that there are no pre-cracking from PTFE film, and also the Z-pin insertion have different misalignment

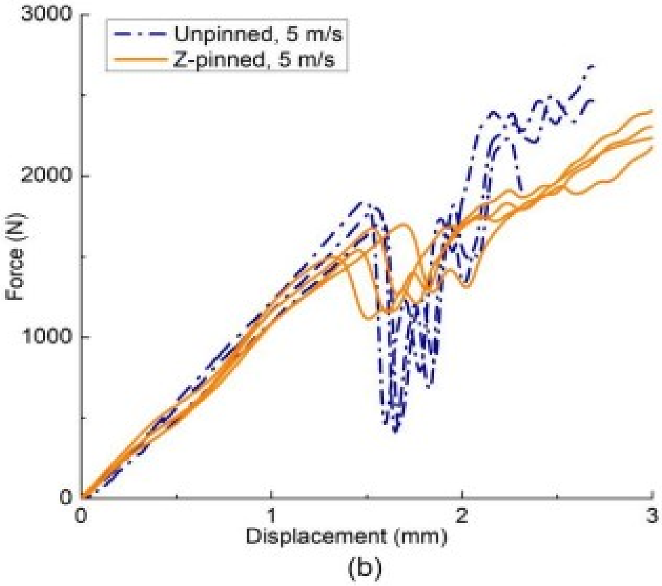

Figure 4.9: Force-displacement curves for ENF tests

4.3.3 Mix-mode experiments

For the coupon level experiment, a single leg bending test were used to characterising the mixed mode delamination behaviour in high loading rate, the schematic shown below gives an idea of a SLB test specimen.

Figure 4.10: SLB sample with the machining details

In SLB tests, the Z-pins were first debonded from surrounding laminates before it finally pulled out. The crack propagation was in a stable manner for SLB test and Z-pinned laminate demonstrate much better capability in carrying load during delamination propagation.

All the pins having the rupture failure mode with the gradual load increase for the dynamic tests, all the failed pins were pulled out partially before they got fully ruptured.

Unlike ENF test, the delamination resistance during the crack propagation stage for SLB test improved significantly by the presence of Z-pins.

4.4.1 Modelling strategy

To address the dynamic bridging FE simulation, the following procedures were considered:

- Again, Ply level mesh was used to model the quasi-isotropic plies to define the fibre direction for different plies.
- Each ply of laminate assigns the material properties of Z-pin, the resin pocket and the surrounding QI laminate.
- The Z-pin/laminate interface in the modelling method is described by the surface based method cohesive contact, whereby it is manually programmed by User subroutine Vuinter. The contact followed by the complete debonding of the cohesive interface was described by a modified coulomb friction law
- Orthotropic user defined material was used to simulate the Z-pin.
- The model definition refers to the experiments set-up in (23). The specimen consists of two blocks each of which comprises 32 IM7/8552 Plies. The nominal thickness of each ply is 0.125 mm, with Z-pin diameter of 0.28mm. the width of the block is 10mm

- In the dynamic bridging test, a loading rate of 5.5 m/s was used to simulate the rapid response. The simulation was conducted in different combinations of tension and shear displacements.

- In the modelling work, a time increment of 8.5e-11 s and a density 1.6e-10 kg/mm^3 was applied

4.4.2 Bridging result

A three-dimensional FE model regarding the single Z-pin specimen was created for Z-pinned composite laminates.

To validate the modelling method, the experimental results of reaction force vs. displacement plots for all the offset angles varies from 0° to 75° conducted by University of Oxford was extrapolate on the graph to calibrate against the modelling result. It can be observed that the bridging force linearly increases to a peak value due to the stiffness of the bonding leftover, and a rapid drop from the top has been denoted due to the fact that the interface has been completely damaged. The bridging behaviour for the following section is mostly dependent on the mode-mixity. The bridging force build-up for the test cases with low offset angles (0° 15° and 30°), whereas for the high offset angles cases, the Z-pins fail prematurely due to the rupture failure as shear stress dominated.

The FE predicted bridging law was compared with the experimental results shown in figure 4.11-16. For the dynamic bridging test cases with no or low offset angles (0°-30°), the observations consist of two stages; The Z-pin deformed elastically until reaching the maximum debonding traction load, followed by a sudden drop of the load. The Z-pin was then pull-out gradually, and the frictional load between Z-pin and laminate will decrease linearly with the pull-out displacement. For the test cases with higher offset angles (45°-75°), the experimental results demonstrate that the Z-pin fails by fibre rupture and has a negligible process of frictional contact, whereas the FE predicted result does show a significant frictional traction load being built up.

It can be seen that good agreement has been reached for the cases with offset angle 30° or less, but regarding the cases with a higher offset angle, the results show less agreement, the modelling tends to underestimate the progress of onset of fibre rupture when the shear failure mode dominates. The change in the bridging response comes from the change of the fracture morphology with the loading rate. In quasi-static tests, the surface roughness plays a more important role than dynamic tests. The rough surface will provide a higher frictional bridging force during the pull-out.

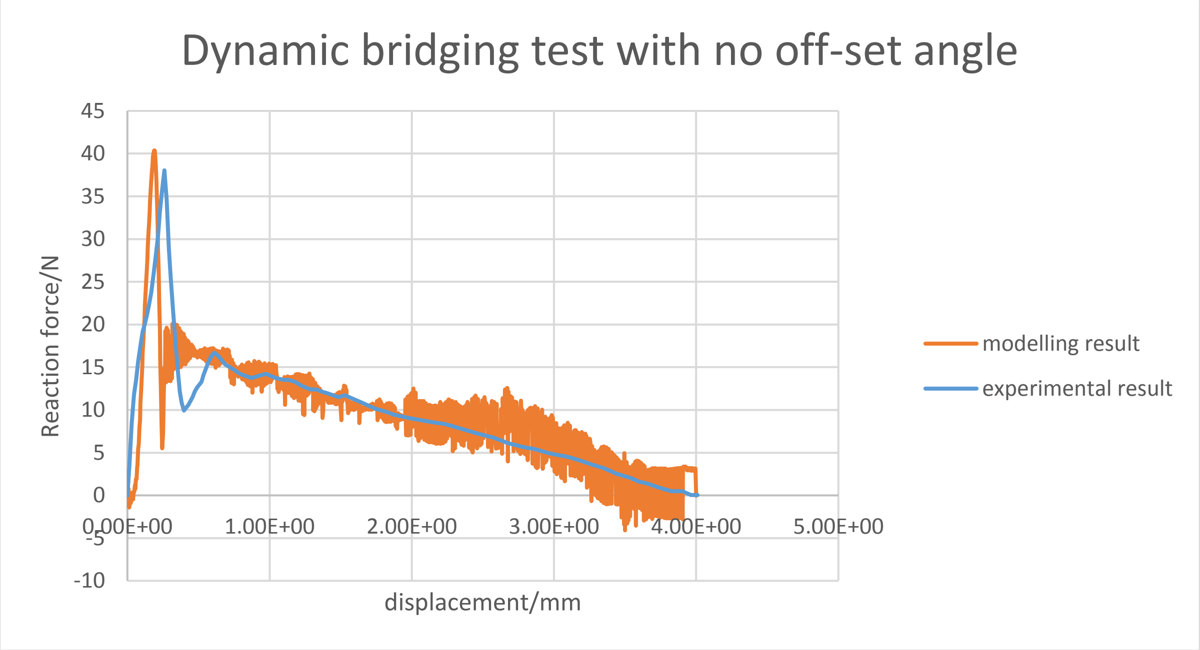

Figure 4.11: Comparison between load-displacement curves of FE models and Experiments with no off-set angle

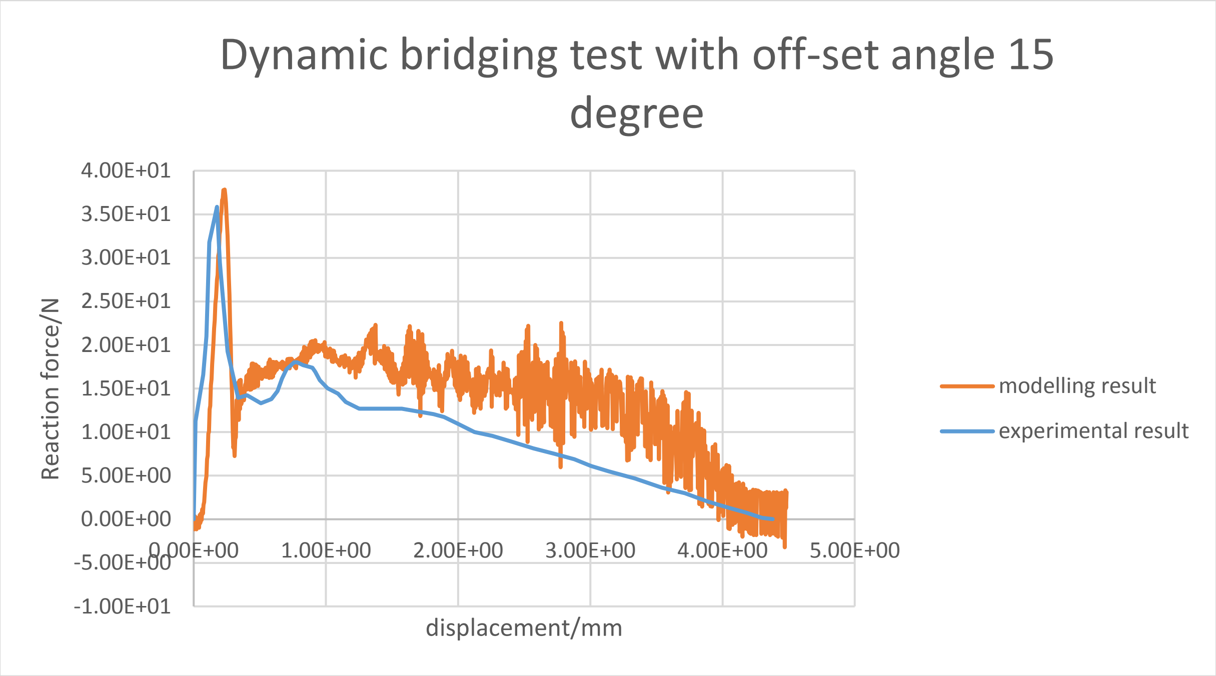

Figure 4.12: Comparison between load-displacement curves of FE models and Experiments with 15° off-set angle

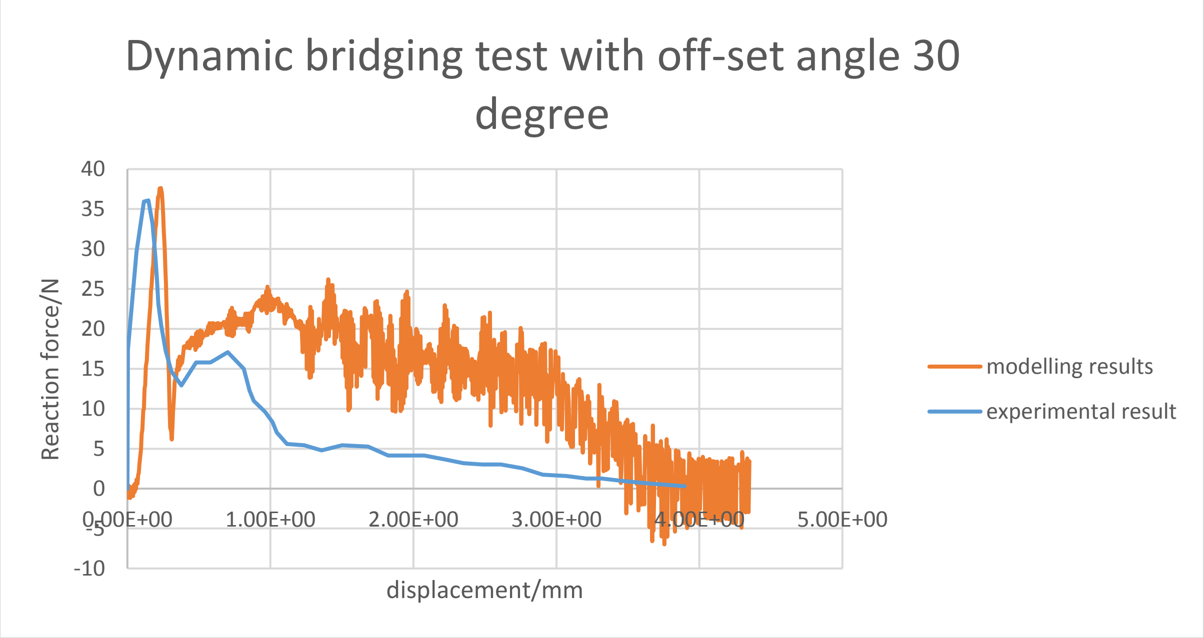

Figure 4.13: Comparison between load-displacement curves of FE models and Experiments with 30° off-set angle

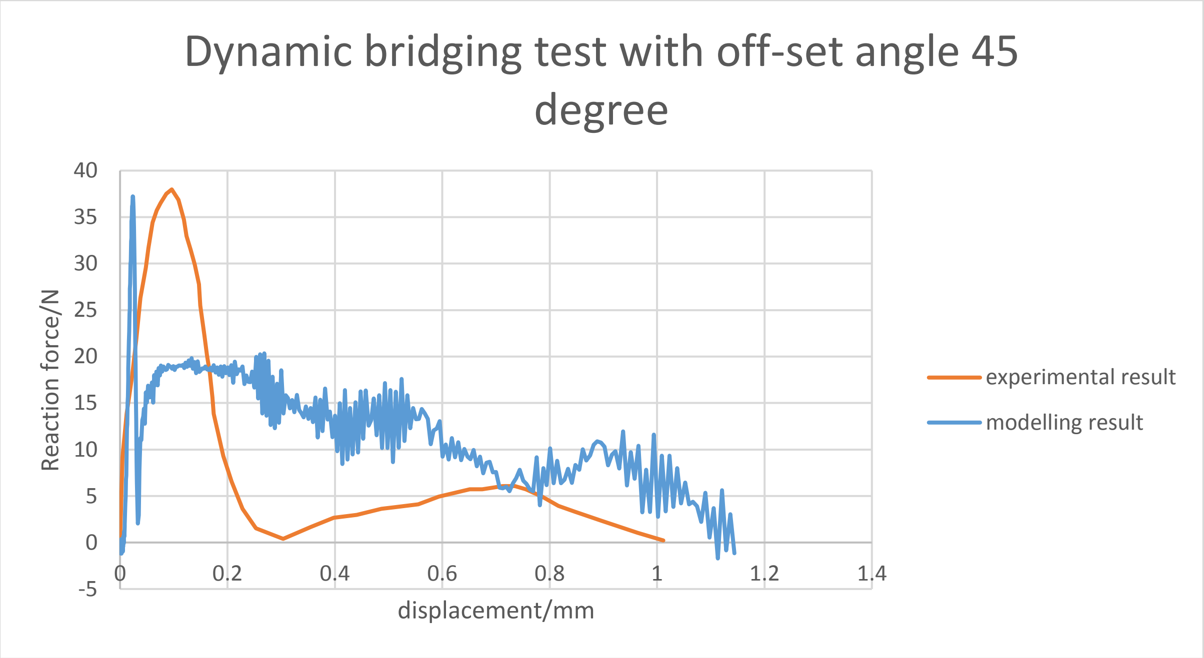

Figure 4.14: Comparison between load-displacement curves of FE models and Experiments with 45° off-set angle

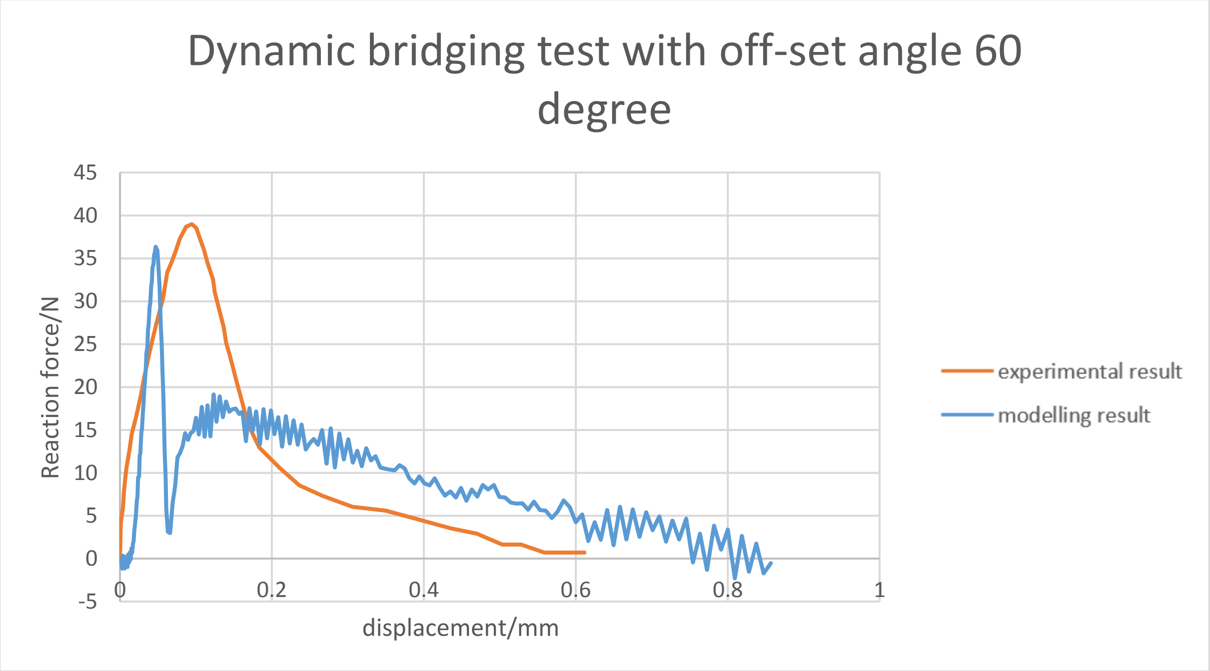

Figure 4.15: Comparison between load-displacement curves of FE models and Experiments with 60° off-set angle

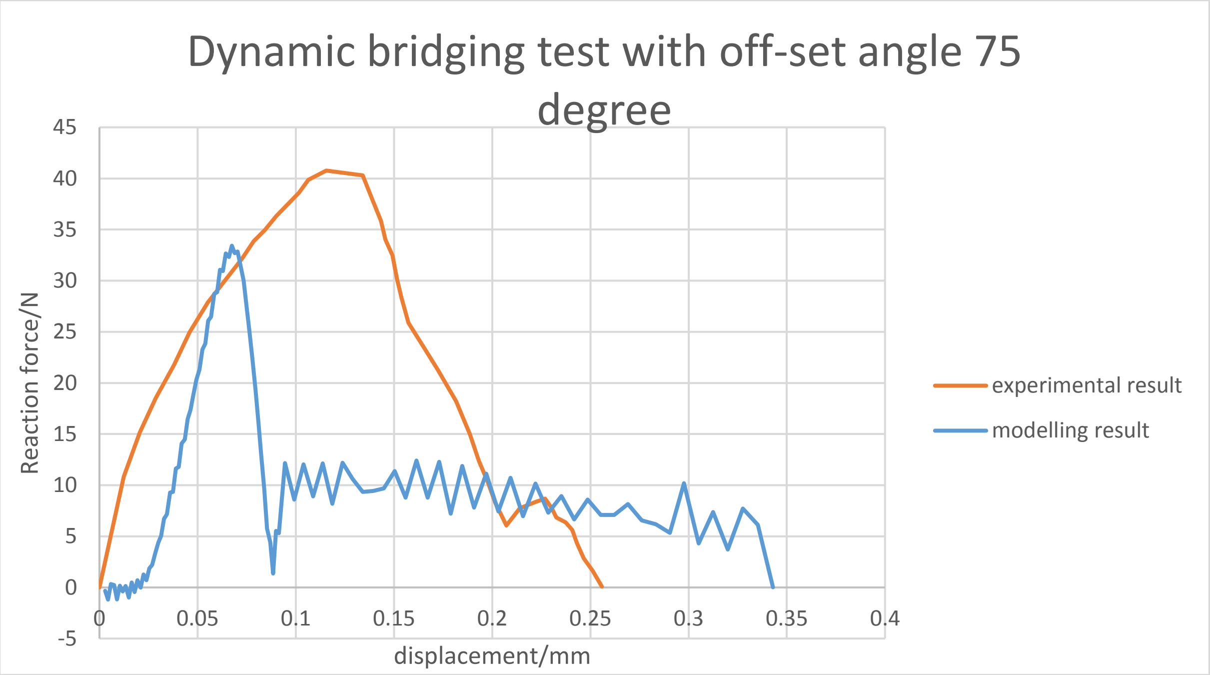

Figure 4.16: Comparison between load-displacement curves of FE models and Experiments with 75° off-set angle

4.4 Parametric studies and comparisons between quasi-static loading and dynamic bridging test

4.4.1 Apparent fracture toughness for Dynamic bridging test

The calculated apparent fracture toughness values are compared with between FE simulations and experiments shown below. Both FE simulation and experimental data behaves in a similar fashion, but it can be seen a large discrepancy was recognised when the offset angle is 30 degrees. The rapid drop of the fracture toughness indicates a transition from pull-out failure to pin rupture. The FE simulations underestimate the onset of failure mode transition. For any other given mode-mixity a good agreement has been achieved.

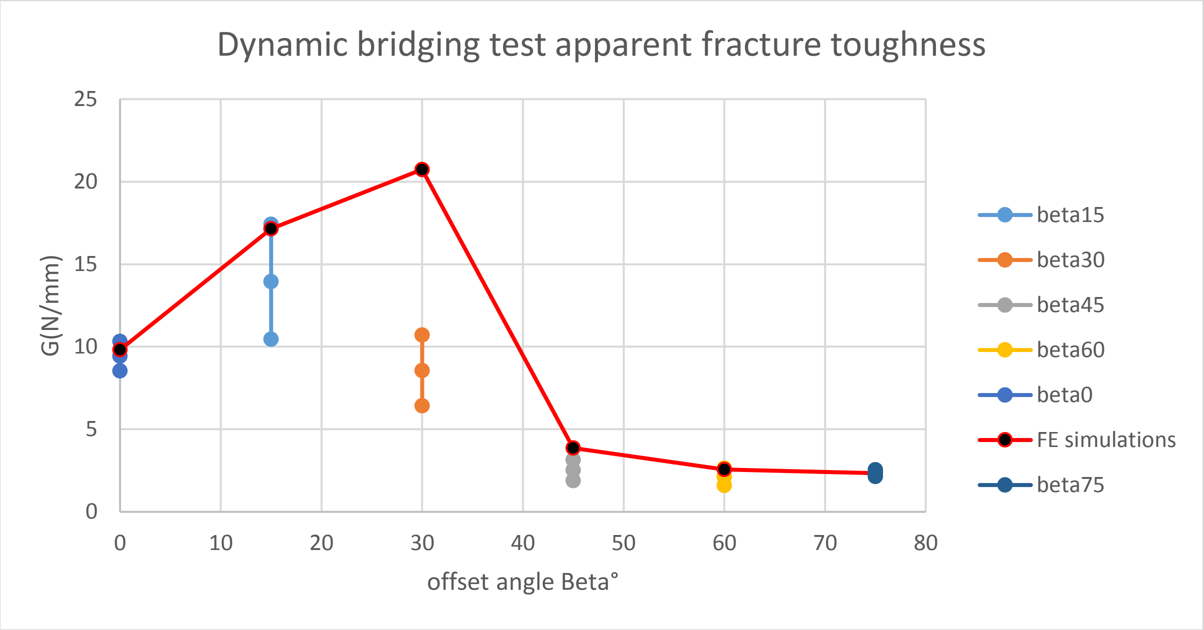

Figure 4.17: Dynamic bridging test apparent fracture toughness

4.4.2 Apparent fracture toughness comparison between dynamic bridging test and quasi-static test

The apparent fracture toughness under quasi-static loading and dynamic bridging test were compared. It can be observed there is an insignificant difference for the mode II dominated test. Because the energy dissipated in the shear dominated failure was much lower than that in mode I tests.

The Z-pin efficiency in resisting mode I delamination for the dynamic test was found lower than that in quasi-static Z-pin efficacy. That is because, for the dynamic test, the fracture due to shear stress was much less rough than that in quasi-static tests, and the rougher frictional interface for quasi-static loading cases increase the Z-pinning efficacy in pull-out. In general, the dynamic bridging test Z-pin insertion shows less efficiency in comparing to the quasi-static test, and the influence of loading-rate on mode II test is inconclusive.

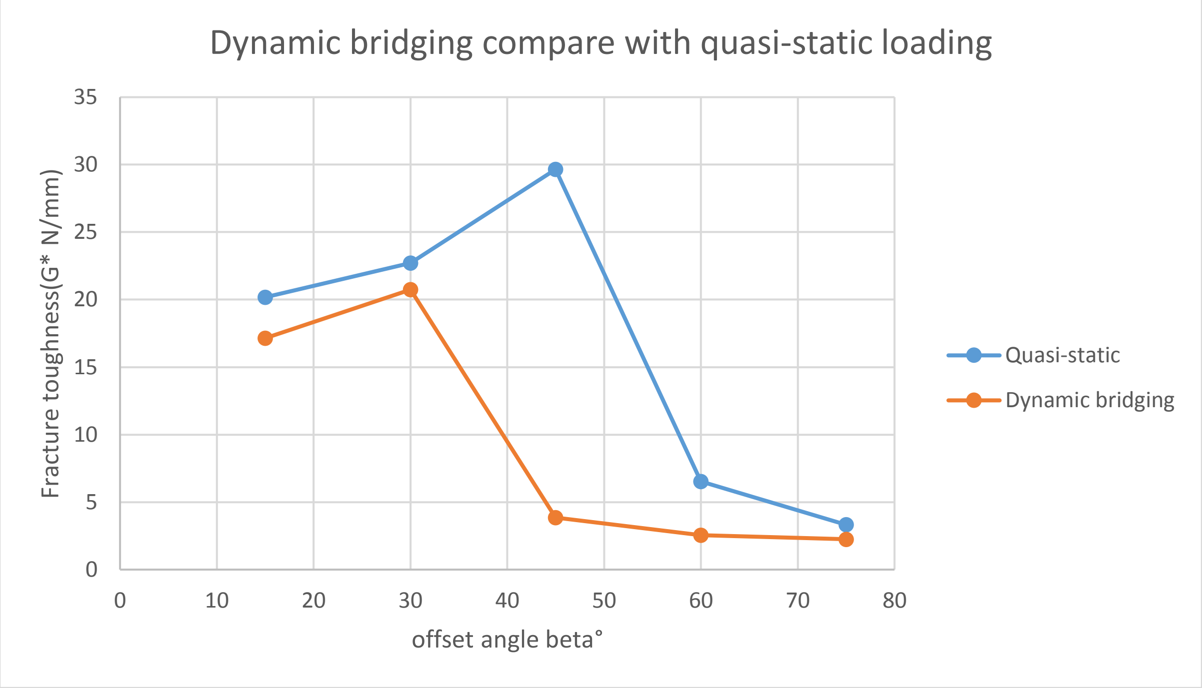

Figure 4.18: Apparent fracture toughness comparison between quasi-static loading and dynamic bridging

4.4.3 Effect of Z-pin/laminate interface frictional coefficient

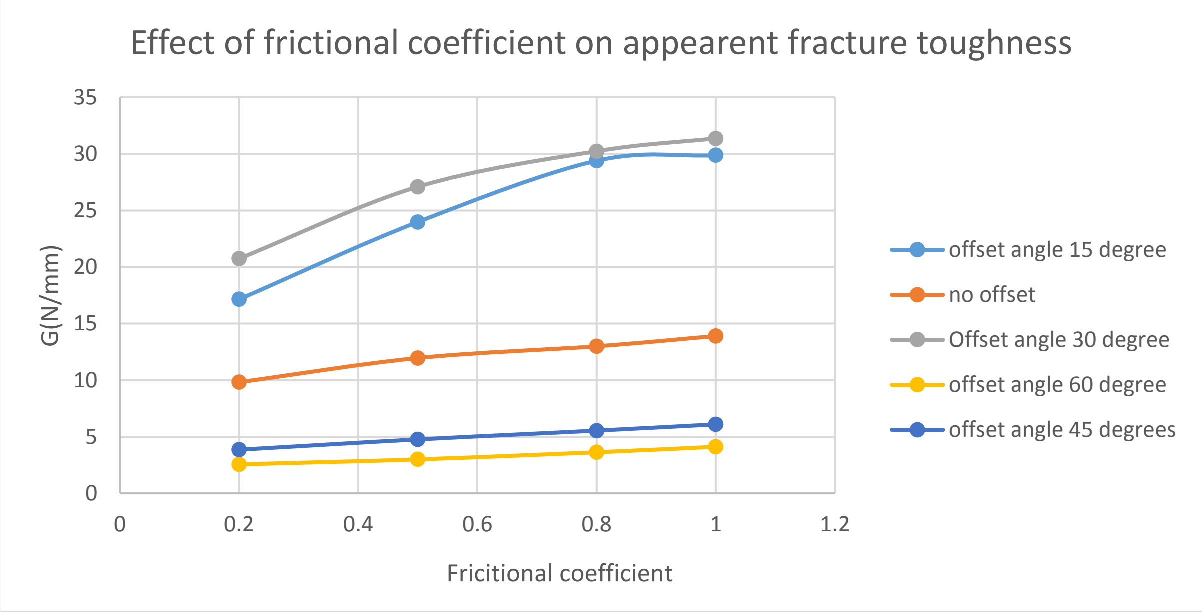

Figure 4.19: Effect of Z-pin/laminate interfacial frictional coefficient on the apparent fracture toughness

The correlation between apparent fracture toughness and the frictional coefficient was shown in figure 4.19. It can be observed that for any given mode mixity, the increase of the frictional coefficient will result in higher apparent toughness. For the case with no offset angle, an increase of the frictional coefficient results in a linear increase of the apparent toughness, whereas for the case with higher mode-mixity, the growth of the apparent fracture toughness is exponential from the beginning. For the cases with a higher offset angle (60°), it can be seen the increase of frictional coefficient does not affect much as the fibre will tend to get ruptured before it can be pulled out so unable to improve the fracture toughness. The apparent fracture toughness increases with μ while the failure mode is pull-out, whereas the effect of μ is somewhat limited for the cases failed by fibre rupture.

4.5 Innovative features and short remarks

It is found in the experiments that the bridging capability of Z-pin can be noticeably different between dynamic and quasi-static test. The bridging response for dynamic loading case with high loading rate is less frequently investigated and has never been predicted by FE modelling work.

In this work a three-dimensional FE model was used to simulate the bridging response under super high loading rate. The same high-fidelity model which was introduced in the Chapter three was used in this chapter. In the dynamic bridging test, a loading rate of 5.5 m/s was used to simulate the rapid response. The simulation was conducted in different combinations of tension and shear displacements.

The biggest difference between the parameters in the quasi-static model and the dynamic model is that the Mass scaling was removed for the test and a minuscule time increment was applied to address the modelling case. That is because the mass scaling parameters used for quasi-static cases would lead to a huge overshoot of the reaction force. Furthermore, a ramp amplitude was also applied to the surface where the loading was applied, as the sudden acceleration from zero to the setpoint loading rate will result in a rapid jump on the reaction force and cause the catastrophic failure of the whole model.

Significant difference has been spotted for the pull-out dominated cases comparing to the fibre-rupture cases, that may be attributed to the rate dependence of the friction and interface properties. It is found that in the simulation results, the model tends to delay the transitioning zone from Pull-out dominated failure to fibre-rupture failure. That may be attributed to the reason that the frictional coefficient used in the model is fixed whereas in practical, the frictional coefficient may be changed during the pull-out process. Thus, the definition of frictional coefficient need to be altered in order to precisely capture the mechanical behaviour before the model can be extended to other dynamic modelling cases.

4.6 Conclusion and discussion

This chapter has addressed the Application of a three-dimensional FE model for Dynamic bridging test. The model has been proved applicable to the model under a high loading rate. Similarly, as compared to the model that has been used for the quasi-static loading case, the model describes the microstructure of Z-pinned laminates, including the features e.g., resin pockets, fibre waviness surrounding the resin pocket and the interface between Z-pin and laminate.

It has been noticed that from the experimental results, the maximum reaction force they reached was around 40 N for all the tests, regardless of the mode mixities that been applied for different cases were different. For the low mode mixities cases, the maximum bridging force reached within a minimal displacement it travels, followed by a rapid drop due to the interface between Z-pin and laminate been broken. A clear bridging force build-up was observed after the complete debonding happened. The nonlinear increase of bridging force may be attributed to the fact the development of a frictional interface with sliding. The bridging force in dynamic tests decreased almost linearly, while the displacement increased.

Comparing to the quasi-static tests, the overall energy dissipation for dynamic tests provided lower energy dissipation. It can be concluded that the capability of Z-pin in terms of improving the delamination resistance decreases with a higher loading rate.

In the latter part of the chapter, the effects of the Z-pin/ laminate interfacial frictional coefficient and the interface debonding were also addressed in detail. These parametric studies aid in terms of identifying the best configuration for improving the apparent fracture toughness.

The present modelling method was proved that ply-level mesh could be applied for the dynamic bridging test with a high loading rate.

Chapter 5 Automatic Z-pin injection machine

5.1 Overview of the Z-pinning insertion system

The traditional Z-pin insertion method like UAZ will lead to significant Z-pin misalignment and unintended Z-pin misalignment is one of the issues the designer should avoid, as different Z-pin insertion angle can affect the apparent fracture toughness of Z-pinned laminate, although a necessary degree of Z-pin misalignment is inevitable, but constrain the scatter of angle into a small and desire range is this proposed method trying to achieve.

The major target of this part of the project is to build up an automatic Z-pin injecting machine with high accuracy, great functionality. The developing phase of this machine can be divided into three sections: Moving system, heating system and Z-pin injecting system.

5.2 Moving system

Moving function is essentially the primary and most important function needed to be achieve for automatic Z-pin injecting machine. The moving function can be achieved by controlling the stepper motor externally using easy drivers. In the toolkit, four Nema 17 stepper motors were given, in this case, A4988 is the easy driver. A4988 is a microchipping driver for controlling bipolar stepper motors which is built-in translator for easy operation. The motion control can be achieved with just two pins on the easy driver, one is for steps and the other is for direction. A diagram regarding connection is illustrated below. VDD and GND pins are needed to connect to the logical power on the Arduino board. 1A , 1B; 2A, 2B are needed to connect to different coils on the stepper motor. For powering the motor, GND and VMOT are needed to be connected to external power supply. A decoupling capacitor is preferred to be connected in between the Arduino board and power supply in order to protect the easy driver from voltage spike. DIR controls the rotation direction of the motor and STEP pin controls the micro steps of the motor. Bridging between Reset pin and sleep pin will enable the driver in a logical high state and function normally. MS1, MS2, MS3 are for selecting one of the five step resolutions according to the table showing on the graph. If they are left disconnected the driver will operate in full step mode.

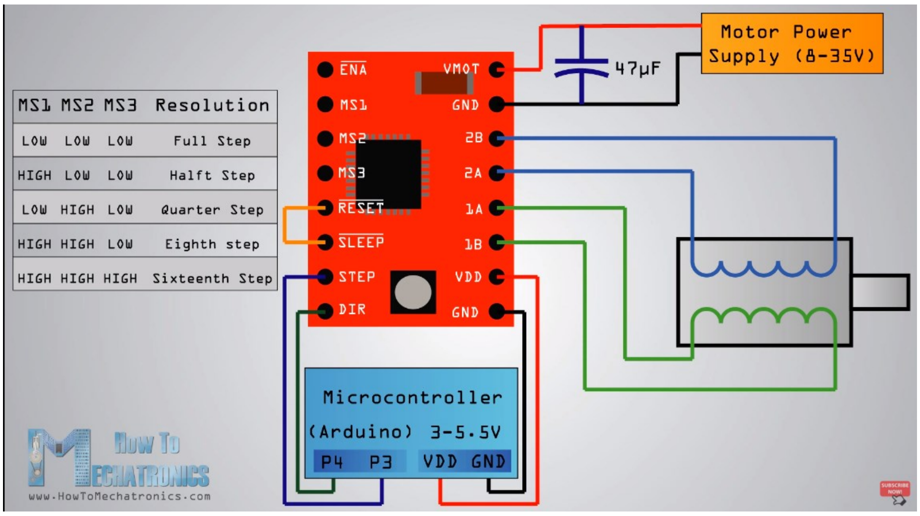

MS1	MS2	MS3	Resolution
LOW	LOW	LOW	Full Step
HIGH	LOW	LOW	Halft Step
LOW	HIGH	LOW	Quarter Step
HIGH	HIGH	LOW	Eighth step
HIGH	HIGH	HIGH	Sixteenth Step

Figure 5.1: Connection of easy driver a4988

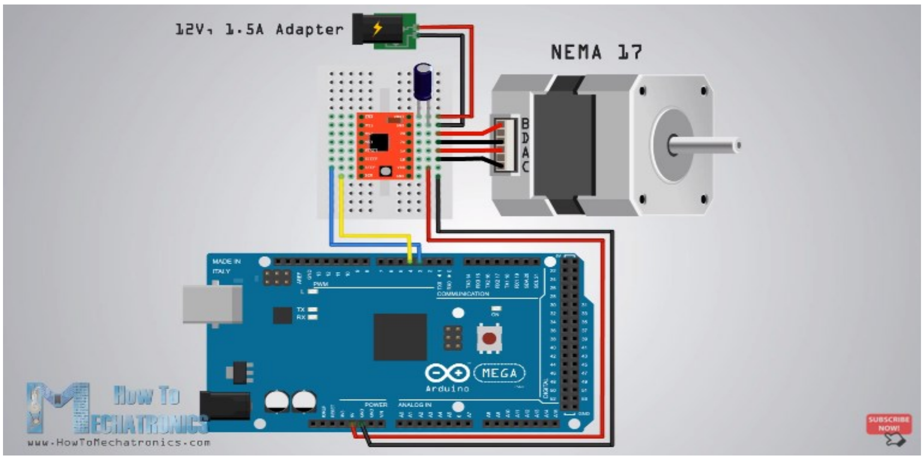

Figure 5.2: Complete circuit schematic

5.2.1 Manual control of the stepper motors

LabVIEW (Laboratory Virtual Instrument Engineering Workbench) is a visual programming language developed by National Instruments, was used to command the stepper motors.

Input the pin number to the subvi stepper for the sake of telling labview which digital pins are engaged for the motion control. And command the speed, steps, acceleration with manual input to describe the required motion.

the motion of the motor is controlled by a high/low state of the control values. Anything other than zero will enable the function of the motor while 0 will disable the function

5.2.2 Automatic stepper motor control

The stepper motor should recognise the location entered and moving accordingly. To achieve such a function, a converter between coordinate in the unit of mm and the steps required. In LABVIEW, a VI is a visual programming language block containing the key information to pass into mechanical components. A Subvi denotes the language block subject to the VI at higher hierarchy.

A VI contain the steps converter is shown below, the function of it can be split into several steps:

1. Input the predetermined coordinates into the system and using the excel reading Subvi to extract all the coordinates
2. Considering the coordinates consists of X,Y,Z components, the displacement that has been made for each execution is equals to the X,Y,Z coordinates in every new location subtract the coordinates in the preceding location.
3. However, after completion of one cycle, the value you obtain is a scalar, instead of an array. It is equals to the discrepancy between last coordinate and the second last coordinate.
4. Executing the for loop once again and incorporate with a while loop, the problem will be sorted. A list of displacements the printer should be moving are obtained.
5. Multiplying a factor of 5(roughly) will transfer the displacement into the number of steps required to execute the command.
6. Using a flat sequence to determine the priority of the moving order

Incorporating the subvi into the major VI will achieve the automated function

5.2.3 Limit switch and Home function

Limit switch is playing a role like an external Boolean control, it bridges the software and hardware which enable the printer to be switch on/off externally. And every time before putting the printer into use, all the position should be readjusted and send back to original position. The following subvi is used to read the status of the limit switch, it will stop when the limit switch is pressed. An indicator is used to update the status of the limit switch to other systems.

Do the same to other axis and combine everything together in a flat sequence structure will allow the homing function to be executed one by one.

5.3 Heating system

5.3.1 Heat transistor

The core of the heating system is the device which can provide the power to the machine .N-channel mosfet is by far the most popular choice to apply as a heat transistor, the pins on mosfet are kindly defined as gate, drain and source. Mosfet is work by voltage, when voltage is applied between gate and source, the current is allowed to flow between drain and source. Gate is the control port; drain is where the current will drain into and source is where the current is coming out again. The resistance of mosfet is subject to the amount of voltage applied, the resistance from drain to source is inversely proportional to the voltage. That is implying, when the voltage is very low, the resistance extremely high like the switch is open. After the voltage has been altered and exceed the voltage threshold, the resistance drops quickly which enables more current pass through.

5.3.2 Thermistor

A thermistor is playing the role of measuring the temperature of the heating bed in Celsius. Thermistors are resistors that the inner resistance vary with temperature. A 10k ohms resistor is used to protect the thermistor. The resistance R of a thermistor at a certain temperature T can be modelled by：

Equation 5.1

$$R = R_R E^{\left(B\left(\frac{1}{T}-\frac{1}{T_R}\right)\right)}$$

Where R_R is the resistance at a reference temperature T_R $(25°C)$ and B is a constant. The temperature is measured in Kelvin. In our case, the resistance R_R is 10000 ohms at the reference temperature 25°C. Rearranging the equation above in terms of T as a function of resistance yields:

Equation 5.2

$$T = [\frac{1}{T_R} + \frac{1}{B}\ In\ (\frac{R}{R_R})]^{-1}$$

Vcc is a fixed logical power of 5V.

The equation for output voltage is therefore:

Equation 5.3

$$V = V_i \frac{R}{R_i + R}$$

Rearranging the equation we would get an expression of R:

Equation 5.4

$$R = \frac{R_i V}{(V_i - V)}$$

Substitute the expression back into the equation stated above, we can obtain an expression in terms of voltage and resistance.

Equation 5.5

$$T = [\frac{1}{T_R} + \frac{1}{B} In\left(\frac{R_1 V}{R_R(V_i - V)}\right)]^{-1}$$

Which can give us a temperature in terms of Kelvin, and subtract 273 will result a temperature in units of Celsius.

5.3.2 Power control (PID controller)

When the heating system is planned to be implemented to the whole control system of the 3D printer, maintaining the temperature to stay within an appropriate range will be one of the most essential goals to achieve. Incorporating a PID controller will be considered as one of the accessible approach.

5.3.2.1 Introduction to PID controller

PID control is a control method that was used extensively in the fields of control engineering. It has a simple structure, excellent stability and convenient adjustability. As its name indicates, it utilizes proportion, derivative and integral to work out controlled quantity based the system errors. Users can choose any of the three methods as combination, which is very flexible.

5.3.2.2 P-control(Proportional control)

If the output of the controller is proportional to the error, which is :

Equation 5.6

$$u(t) = K_p e(t)$$

The proportional controller will play a role as a variable gain amplifier, by changing the proportional action factor K_p the proportional controller can help to adjust the output. However, there will always be a steady-state error between output and the value of expectation. Merely adjusting the value of K_p will not only cause the stability of the system to deteriorate but also will lead the oscillation of the system more frequently. So, there are systematic error cannot be overcome by solely introduce the proportional control.

5.3.2.3 I-control (integral control)

The difference between set-point and process variable is defined as steady state error. Steady state is an important section that needs to be addressed. The integral term will integrate the error and increase over time. So the controller will keep working as long as there is an error still exist. Increasing the output of the controller can help reduce the steady state error to zero.

5.3.2.4 D-control (Differential control)

D control can help the whole system improve its dynamic property though adjusting the change rate of error signal. It is often used to accommodate the overshoot and setting time of the system.

For a PID controller, the output is:

Equation 5.7

$$K_p e(t) + K_i \int_0^t e(t)dt + K_d \frac{d}{dt} e(t)$$

Labview provides PID control toolkit used in Labview, which ease the difficulty of building up a digital PID controller

5.4 Cutting mechanism

A customised Z-pin insertion head is proposed in the following section. The insertion head need to meet a few requirements simultaneously. Feed pins in a designed length with a certain velocity, generate enough cutting force to cut them into a designed size.

In order to meet all these requirements, the insertion head should be comprised as three parts: a pin feeding driver, a director and a cutter.

5.4.1 Pin feeding and directing device

Two pulleys were used to drive the z-pin to predetermined location. Essentially, there will be a pulley directly connected with stepper motor that used as actuator to initiate the motion of rotation and there will be another pulley driven by the primary pulley to provide enough frictional force to pull down the Z-pin. A slot will be generated on the surface of one pulley in order to guide Z-pin to correct location. The width of that slot is designed to be slightly larger than the diameter of Z-pin whereas the depth is slightly smaller than the diameter to provide enough contact stress.

5.4.2 Z-pin Cutter

The mechanism proposed here is aimed to transfer the rotational motion provided by stepper motor to a linear cutting motion executed by the cutter. A gear after carefully sizing is chosen to help achieve this function. The radius of the gear must be large enough to generate enough force to cut off the z-pin fibre. The cutter will cut the Z-pin against the wall

5.4.3 The assembly of insertion head

The designing procedures can be found in Appendix C, which including the AutoCAD drawing for each component.

After deliberately designing, the whole insertion system is presented below:

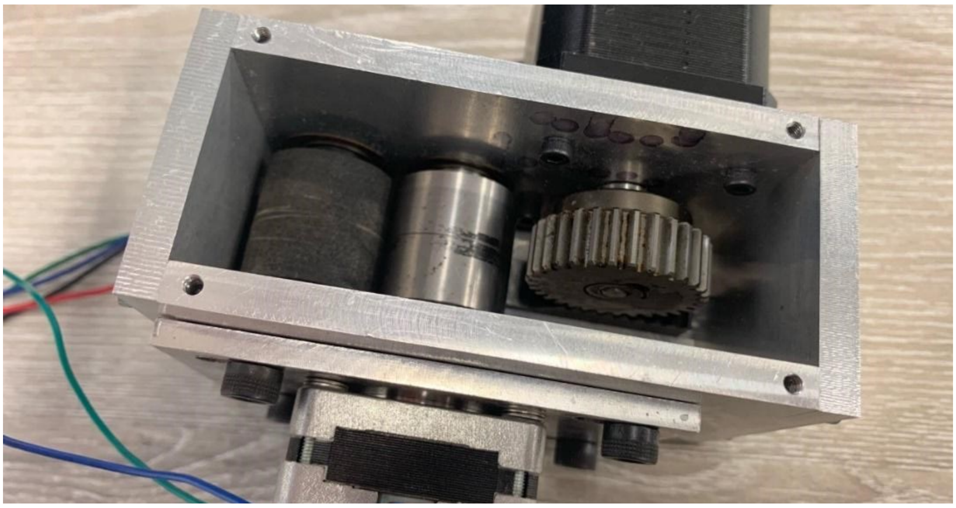

Figure 5.3: The assembly of Z-pin insertion head

However, there is a critical issue with this design. The driven pulley does not provide enough torque to drive the cutter to cut successfully. And furthermore, due to the weight penalty, the insertion head is too hard to drive smoothly. It requires more than demanded steps to input into the stepper motor to move the insertion head a certain distance, thus significantly affect the necessary degree of accuracy.

5.5 Conclusion

The Control and heating systems were working as required but the insertion head is still subject to the next level of refinement work to apply it into practical insertion case.

Chapter 6 Conclusions and future work

6.1 Conclusions of the finite element modelling approaches

A micro-mechanical FE modeling strategy that applies to a surface-based cohesive contact model has been developed and presented in the thesis. This modeling strategy contains two separate sections, the user-defined contact subroutine that describes cohesive contact and frictional contact plus the user-defined material subroutine, which implements Weibull theory to simulate the progressive fibre failure analysis of Z-pin. The cohesive contact is used for modeling glued surface behavior; it starts with an elastic stretching phase before the quadratic stress criterion is met and followed by a power-law criterion for failure evolution. The interface friction is defined by a modified Coulomb friction law, which adds additional shear stress on the top of standard coulomb law in order to characterize the geometrical irregularities and the surface roughness of the Z-pin surface. The FE simulation results have been compared with the benchmark test, including DCB/ENF/MMB/tensile test characterizations; excellent agreements have achieved between the numerical results and the experimental results. This allowed the code to be carried forward to the high fidelity FE model; the model simulates single Z-pin reinforced composite laminates. A versatile mesh considering the resin-pocket, stacking sequence, and fibre waviness were introduced in the thesis. The validity of the modeling strategy has been exhibited by having an excellent agreement between numerical results and experimental results, both in terms of bridging force and apparent fracture toughness. The significant discrepancy lies in the transitional region when mode mixity varies from 0.4 to 0.8, and the possible factors which might affect the results including the Z-pin splitting, Z-pin/laminate bonding, Z-pin/laminate frictional coefficient, and residual stress. Due to the insufficient time, only internal splitting was addressed in the thesis. In the next part of the thesis, the modeling approach was extended to the dynamic bridging test. In this section, a fundamental investigation of rate effects on the pin-laminate interaction has been conducted for single pinned laminate. In the comparison between experimental data and numerical results, some discrepancies were realized. The experimental results have shown that Z-pin efficacy in improving the delamination resistance decreased with the increase of mix mode ratio, whereas the modeling work shows the delamination resistance improving up until the offset angle reaches 30 degrees and decreased in a similar fashion as compared to the experimental results. In general, the Z-pin efficacy in dynamic tests has been found to be lower than that in quasi-static tests for higher loading rate, and the difference was found more significant for the mode I dominated cases than that in mode II dominated cases.

6.2 Conclusion for automatic Z-pin insertion machines

An automatic z-pin insertion machine was proposed in this study; the finalised assembly consists of a control system, a heating system, which can be controlled by LabVIEW and Z-pin cutting mechanism.

The design took advantage of the foundation of a 3D printer; all the axis can be activated and controlled by stepper motors. The LabVIEW can help to program the axis to move into the desired location via designate a list of coordinates. The heating system enables the heating platform to be able to use at high working temperatures; thus, the prepreg can be in a soft condition during the Z-pinning process. Z-pin cutting mechanism contains pin feeding mechanism, pin driven mechanism, and pin cutter.

However, due to practical issues, the actuator does not provide enough torque to drive the cutter to complete the cut.

6.3 Future works

First of all, more parametric studies should be done on both quasi-static loading and dynamic bridging test cases, as stated in the previous section, the factor may affect the bridging response including splitting, interface bonding strength, interface frictional coefficient, residual shear stress. All these parameters should be investigated in further detail. It is worth noting that the surface-based cohesive contact method is too complicated for modelling internal splitting. Compared to adding zero thickness cohesive elements into the Pins, the proposed strategy needs the contact surface between fibre strands to be modelled in advance. If 15 splitting were considered, it means the Z-pin must be divided into 16 small sections and assemble together, plus each individual contact surface has to be defined in advance in order to achieve the cohesive contact.

Regarding the micro-mechanical model, the refinement work can be extended into a few fields. First off, the micro-mechanical model can be extended to model pins with different geometries, e.g., rectangular Z-pins. It is reported that rectangular pins of the same volume as standard circular Z-pins can result in better fracture toughness. To apply rectangular Z-pins, features including the resin pocket, fibre waviness will be different from that in standard circular Z-pin case; some modifications should be done in order to address the changes.

Secondly, in this study, only fiber-reinforced Z-pins were considered. Other materials like metallic Z-pins should be included in future work. Employing of metallic pins in the model means strain-based failure criteria need to be considered. The current star level mesh and features can be readily extended to that for metallic Z-pins.

For automatic Z-pin insertion machines, a new reiteration loop should be conducted on reducing the weight penalty of the current structure, i.e., the mainframe of the current insertion machines is made of steel, which is excessively heavy for the design. Also, another stepper motor that provides enough torque to the Z-pin cutter should be considered to replace the previous one.

Appendix A

Bibliography

1. Chang P. The mechanical properties and failure mechanisms of z-pinned composites. PhD Dissertation, RMIT University, 2006.

2. Partridge IK., Cartie D.D.R, T.Bonnington - Manufacture and Performance Of Z-Pinned Composites , Advanced Polymeric Materials, 2003

3. Partridge IK, Cartié DDR. Delamination resistant laminates by Z-Fiber® pinning: Part I manufacture and fracture performance. Compos Part A Appl Sci Manuf 2005;36:55–64.

4. Lander JK. Designing with Z-pins: Locally reinforced composite structures. Phd Dissertation Cranfield University, 2008

5. Lefebure P. Assembly of dry carbon performs by a z-pining technology. Proc.SAMPE Eur. Tech. Conf. Toulouse:2006.

6. Knaupp M, Scharr G. Manufacturing process and performance of dry carbon fabrics reinforced with rectangular and circular z-pins. J Compos Mater 2013.

7. Johnson DW, Garrett SA, Hook JM, Moyers SG. Method of inserting Z-axis reinforcing fibers into a composite laminate. US 20050006023 A1, 2005.

8. Boyce JS, Roland R. Wallis J,Bullock DE. Composite structure reinforcement. US 4808461 A, 1989

9. Choi IH, Ahn SM, Yeom CH, Hwang IH, Lee DS. Manufacturing of Z-pinned composite laminates. Proc. ICCM 17 Conf., Edinburgh: 2009.

10. Song Qinghua, Li Yong. Study on an automatic multi-pin insertion system for preparing Z-pin composite laminates. Chinese Journal of Aeronautics. 2014

11. A.P. Mouritz Review of composite laminates. Composite part A : Applied science and Manufacturing 2007,page 2383-2397

12. Steeves CA, Fleck NA. In-plane properties of composite laminates with through-thickness pin reinforcement. Int J Solids Struct 2006; 3197-212

13. P.Chang , A.P Mouritz, B.N. Cox. Flexural properties of z-pinned laminates. Composites: part A 38. 2007

14. S. Kravchenko, O. Kravchenko. Composite toughness enhancement with interlaminar reinforcement. Composite part A, 2013.07.006

15. D5528. Standard test method for mode I interlaminar fracture toughness of unidirectional fibre-reinforced polymer matrix composites. ASTM stand 2007.

16. Cartie DDR, Troulis M, Partridge IK. Delamination of Z-pinned carbon fibre reinforced laminates. Compos Sci Technology 2007;66:855-61

17. D6671/D6671M. Standard test method for mixed Mode I-Mode II interlaminar fracture toughness of unidirectional fiber reinforced polymer matrix composites. ASTM Stand 2006.

18. Rugg KL, Cox BN, Massabo R. Mixed mode delamination of polymer composite laminates reinforced through the thickness by z-fibers 2002;33:177–90.

19. L. Francesconi, F. Aymerich Effect of Z-pinning on the impact resistance of composite laminates with different layups , Composites Part A 114(2018) 136-148

20. A. Rezai, D. Cartie, I.Partidge, P.Irving, T.Aston, P. Negre, J. Langer. Interlaminar damage resistance of Z-fibre TM reinforced structural CFRP. In: Proceedings of the 13th International conference on composite materials,June,2001, Beijing

21. Zhang X, Hounslow L, Grassi M. Improvement of low-velocity impact and compression-after-impact performance by Z-fibre pinning. Comps Sci Technol 2006; 66(15);2785-94

22. Knaupp M, Baudach F. Franck J, Scharr G. Impact and post-impact properties of CFRP laminates reinforced with rectangular Z-pins. Compos Sci Technol 2013;87:218-23

23. E.Greenhalgh, A.Lewis, R.Bowen, M.Grassi. Evaluation of toughening concepts at structural features in CFRP- part I: Stiffener pull-off.2006,Composite: Part A,V37.

24. B.N Cox. Snubbing effects in the pull-out of a fibrous rod from a laminate. Mechanics of Advanced Material and Structures, volume 12, 85-98,2005.

25. M.Yasaee,L.Bigg. G.Mohamed. S. Hallett. Influence of Z-pin embedded length on the interlaminar traction response of multi-directional composite laminates, Material & Design, Volume 115, 2017, 26-36

26. HY. Liu WY Yan. XY Yu, YW Mai. Experimental study on the effect of loading rate on mode I delamination on Z-pin reinforced laminates. Composite Science and Technology. Volume 2007. Page 1294-1301

27. Beene.M S.Gannon M.Yasaee Mode II delamination resistance of composites reinforced with inclined Z-pins. Material & Design,Volume 94, 2016, 565-572

28. Beene.M, M.Yasaee Effective use of metallic Z-pins for composites through-thickness reinforcement. Composites Science and Technology 175 (2019) 77-84 .

29. Julian. H, Gerhard.S Pull-out performance of rectangular Z-pins in hot-cured carbon fibre reinforced laminates. Composite Structure 186 (2018) 62-67e

30. F.Pegorin, K. Pingkarawat, A.P. Mouritz. Electrical-based delamination crack monitoring in composites using Z-pins. Composites: Part A 104 (2018) 120-128

31. Zhang B, Allegri G, Hallett S.R. An experimental investigation into multifunctional Z-pinned composite laminates, Mater Des 2016; 108; 679-88

32. Jain LK, Mai Y-W. On the effect of stitching on Mode I delamination toughness of laminated composites. Compos Sci Technol 1994;51:331–45

33. Cox BN. Constitutive model for a fibre tow bridging a delamination crack. Mech Compos Mater Struct 1999;6:117-38

34. Cox BN, Sridhar N. A traction law for inclined fibre tows bridging mixed-node cracks. Mech Adv Mater Struc 2002;9:299-331

35. Robinson P, Das S. Mode I DCB testing of composite laminates reinforced with z-direction pins: a simple model for the investigation of data reduction strategies. Eng Fract Mech 2004;71:345–64.

36. G.Allegri. M.Yasaee.I.K Partridge and S.R. Hallett A Novel model of delamination Bridging via Z-pins in composite laminates. ACCIS, University of Bristol,2014

37. Fert-MM, An investigation of the mechanical performance of Z-pin reinforced composites. phd-thesis,2016

38. J.Jokinen. The simulation of a double cantilever beam test using the virtual crack closure technique with the cohesive zone modelling. International Journal of Adhesion and Adhesive 88(2019)

39. H.Cui. YL.Li S.Koussios L.Zu Bridging micro mechanism of Z-pin in mixed mode delamination, Composite Structures 93(2011)

40. B.Zhang, G.Allegri, S.R.Hallett High-fidelity FE modelling of Z-pins in quasi-isotropic Laminates - 2014, ECCM16

41. Jiang. S.R.Hallett A concise interface constitutive law for analysis of delamination and splitting in composite materials and its application to scaled notched tensile specimens. Int J. Numer. 2007

42. S.T. Pinho, L, lannucci, P. Robinson Modelling delamination in an explicit FE code using 3D decohesion elements CompTest 2004,

43. S.pinho Modelling failure of laminated composite using physically-based failure models, Phd Thesis, 2005

44. S.T.Pinho. P. Robinson Formulation and implementation of decohesion elements in an explicit finite element code. In press Composites Part A, 2005

45. S.R Hallett, P.W. Harry Cohesive zone length in numerical simulations of composite delamination. Engineering Fracture Mechanics, 2008,75(16),4774-4792

46. Z.P.Bazant , Size effect on structural strength: a review. Archive of Applied Mechanics, November 1999, Volume 69, pp 703-725

47. Scaling effects in notched composites. M.R. Wisnom, S.R. Hallett, C. Soutis. Journal of Composite Materials, 2009

48. X. Zhang, A cohesive zone model for predicting delamination suppression in Z-pinned laminates. Composites Science and Technology 71(2011) 1898-1907

49. X. Zhang, F. Bianchi. Predicting mode II delamination suppression in Z-pinned laminates. Composites Science and Technology 72(2012) 924-932

50. B.Zhang G.Allergi. Micro-mechanical Finite element analysis of single Z-pin pull-out,SIMULIA UK Regional User meeting, 2013.

51. G.Allegri. M.Yasaee.I.K Partridge and S.R. Hallett A Novel model of delamination Bridging via Z-pins in composite laminates. ACCIS, University of Bristol,2014

52. M.Yasaee,J.K Lander, G Allegri. Experimental characterisation in mixed mode traction-displacement relationships for a single carbon composite z-pin, Composites Science and Technology, 2014

53. Hallett SR, Green BG, Jiang WG, Wisnom MR. An experimental and numerical investigation into the damage mechanisms in notched composites. Compos Part A Appl Sci Manuf 2009;40:613–24.

54. Marlett K, Ng Y, Tomblin J. Hexcel 8552 AS4 unidirectional prepreg at 190 gsm & 35 % RC qualification material property data report. 2011.

55. ISO/DIS 15114. Fibre-reinforced plastic composites - Determination of the mode II facture resistance for unidirectionally reinforced materials using the calibrated end-loaded split (C-ELS) test and an effective crack length approach 2012:1–16.

56. Composites M, Precision WS. Standard Test Method for Mixed Mode I-Mode II Interlaminar Fracture Toughness of 2010:1–14.

57. H. Cui, M. Yasaee, G. Kalwak Bridging mechanisms of through thickness reinforcement in dynamic mode I&II delamination. Composites: Part A 99(2017)

58. H.Cui YL.Li S.Koussios A.Beukers Mixed mode Cohesive law for Z-pinned composite analysis,Computational Material science 75(2013) 60-68

59. H.Cui , M. Yasaee , S.R.Hallet , Dynamic bridging mechanism of through-thickness reinforced composite laminates in mixied mode delamination. Composites Part A: Applied Science and Manufacturing, Volume 106,March 2018, Page 24-33

Appendix B : Visual code for LABVIEW

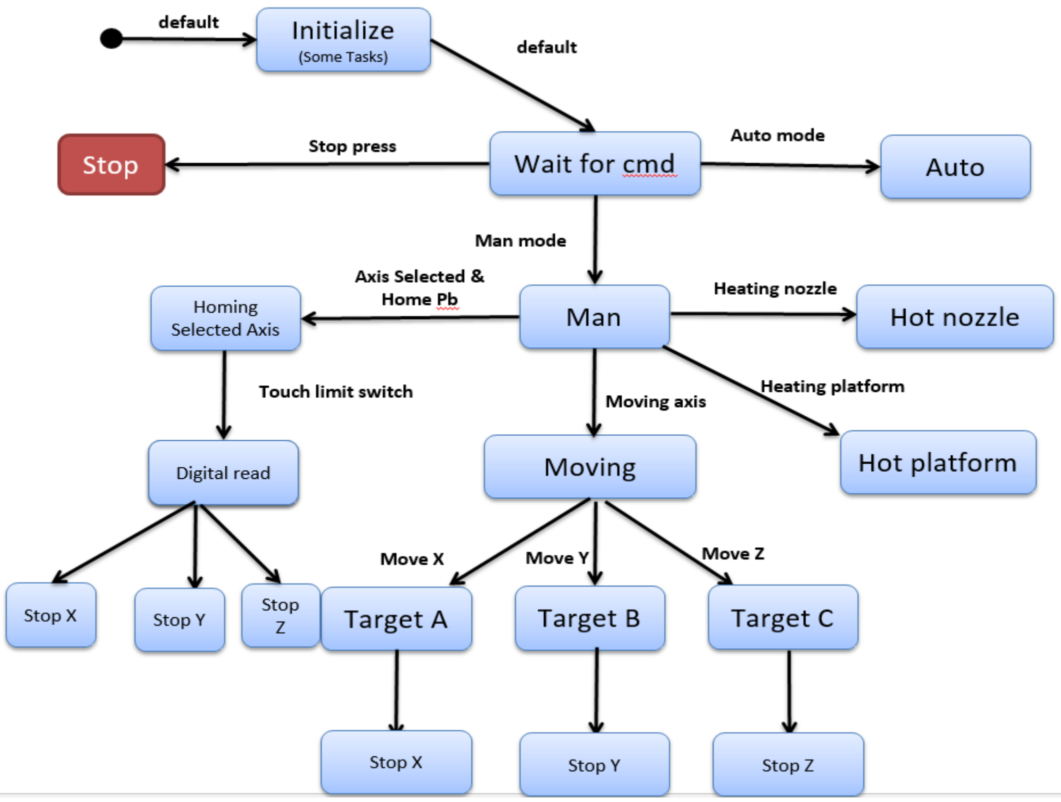

Appendix B . 1: *Overview of the Z-pin injecting machine design*

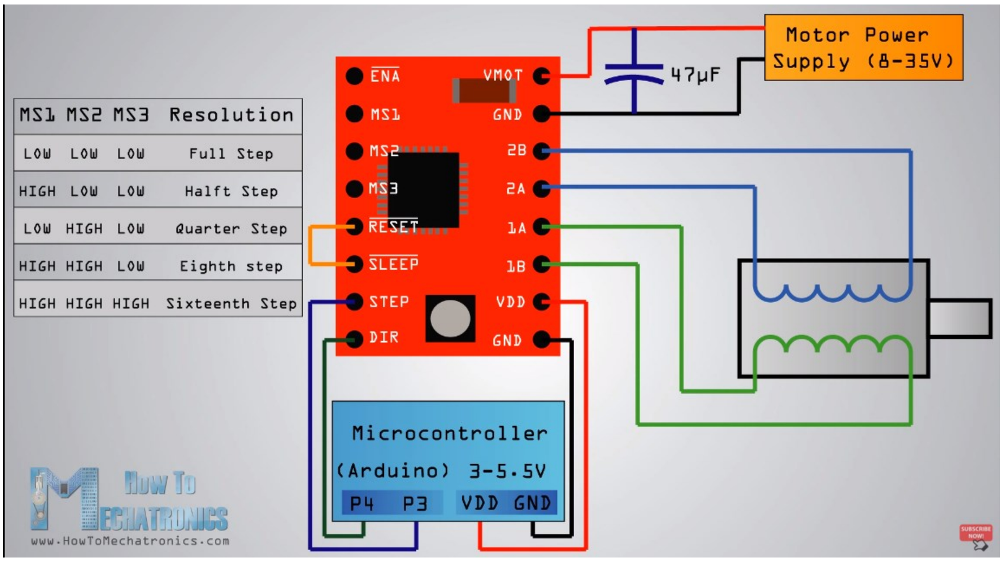

MS1	MS2	MS3	Resolution
LOW	LOW	LOW	Full Step
HIGH	LOW	LOW	Halft Step
LOW	HIGH	LOW	Quarter Step
HIGH	HIGH	LOW	Eighth step
HIGH	HIGH	HIGH	Sixteenth Step

Appendix B . 2: Connection of easy driver a4988

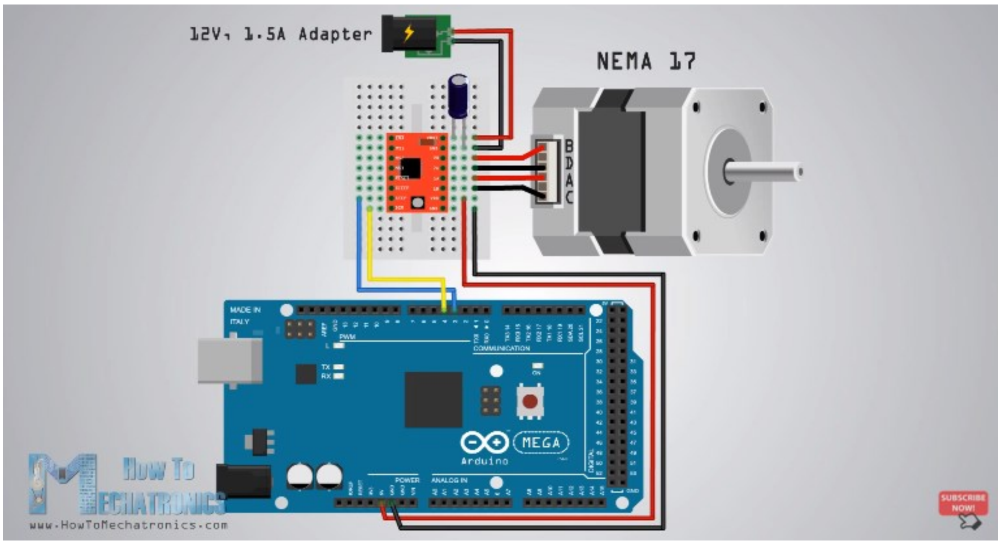

Appendix B . 3: Complete circuit schematic

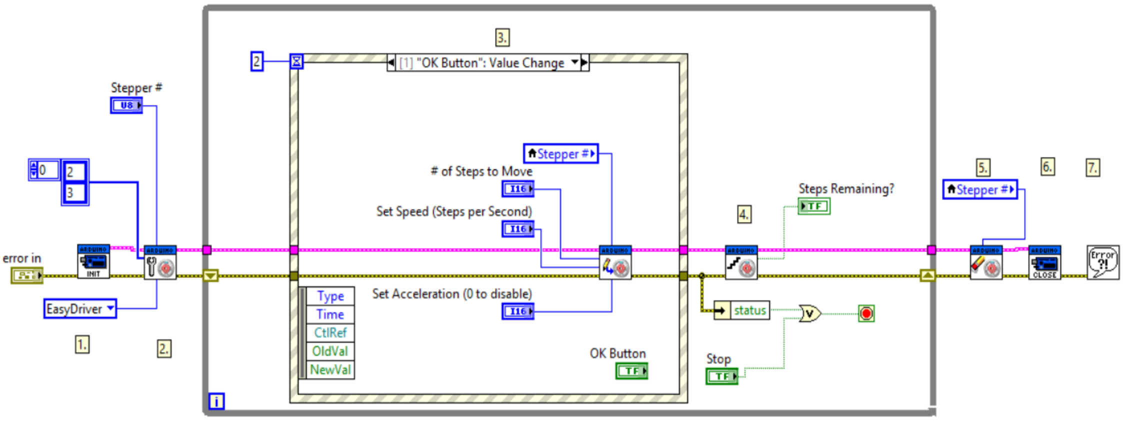

Appendix B . 4: Vi for single stepper motor

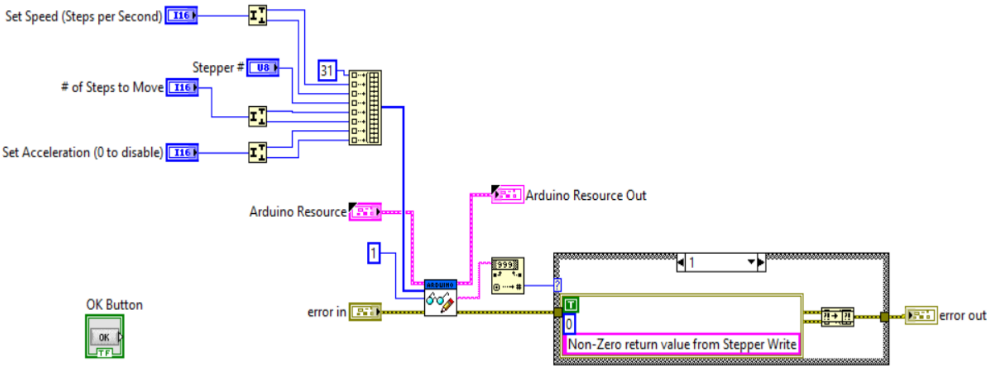

Appendix B . 5: VI for stepper write

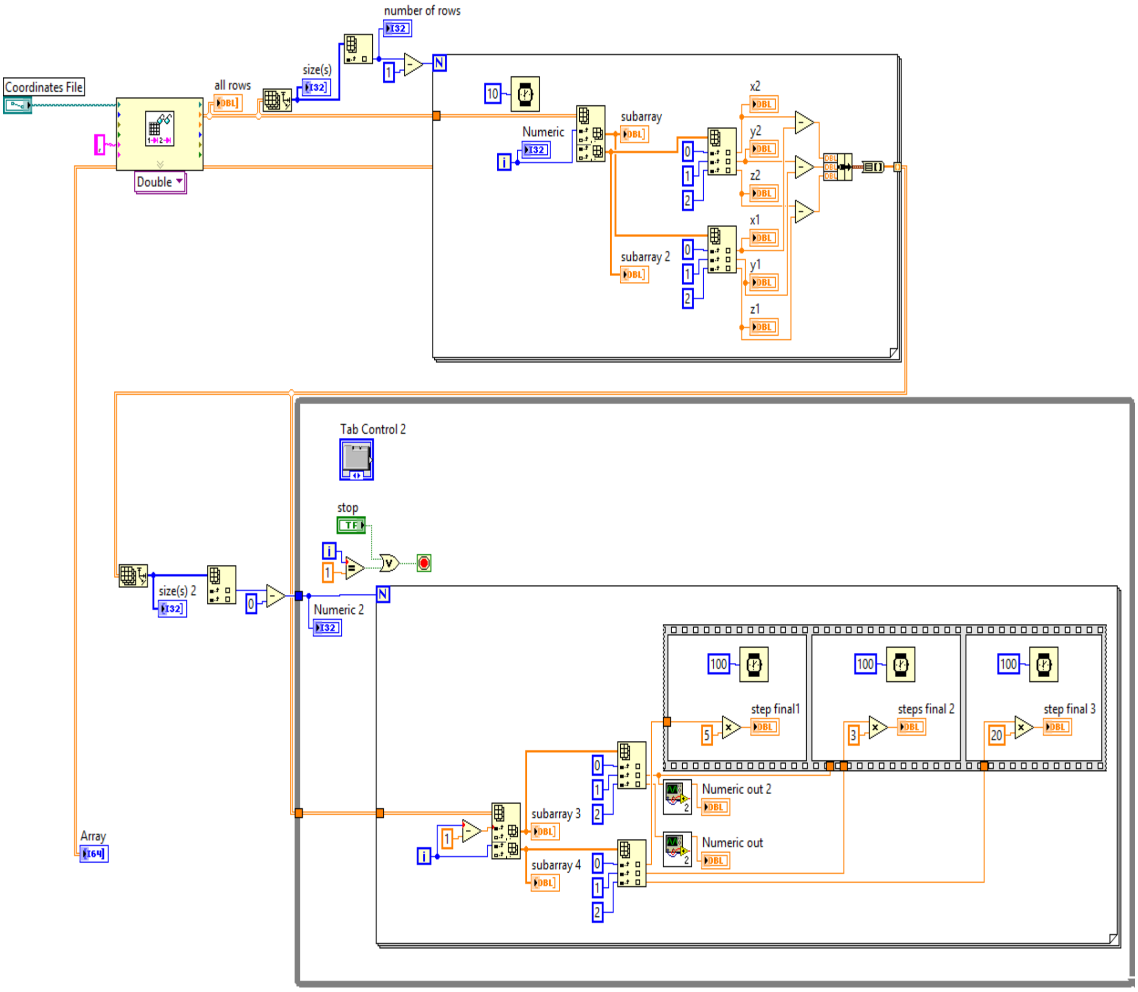

Appendix B . 6: Automatic coordinate input file

Incorporating the subvi into the major VI, the printer is alive!

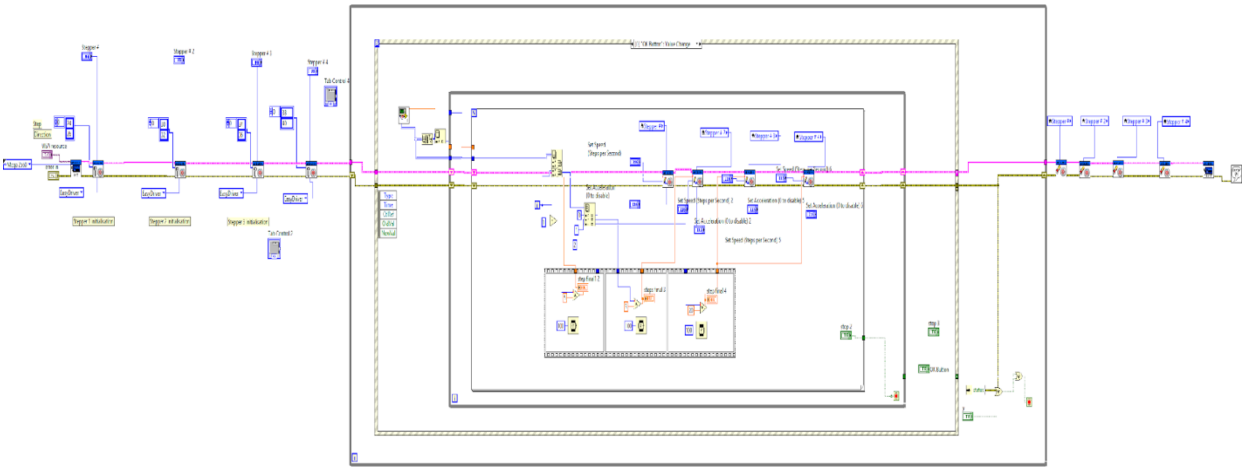

Appendix B . 7: Multiple motors auto control

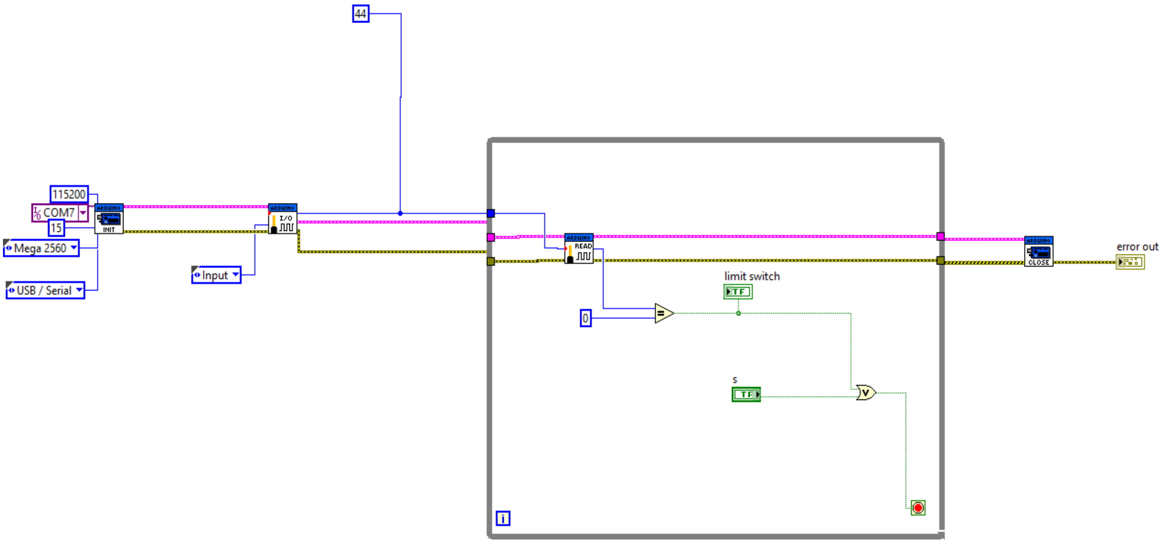

Appendix B . 8: Limit switch digital read

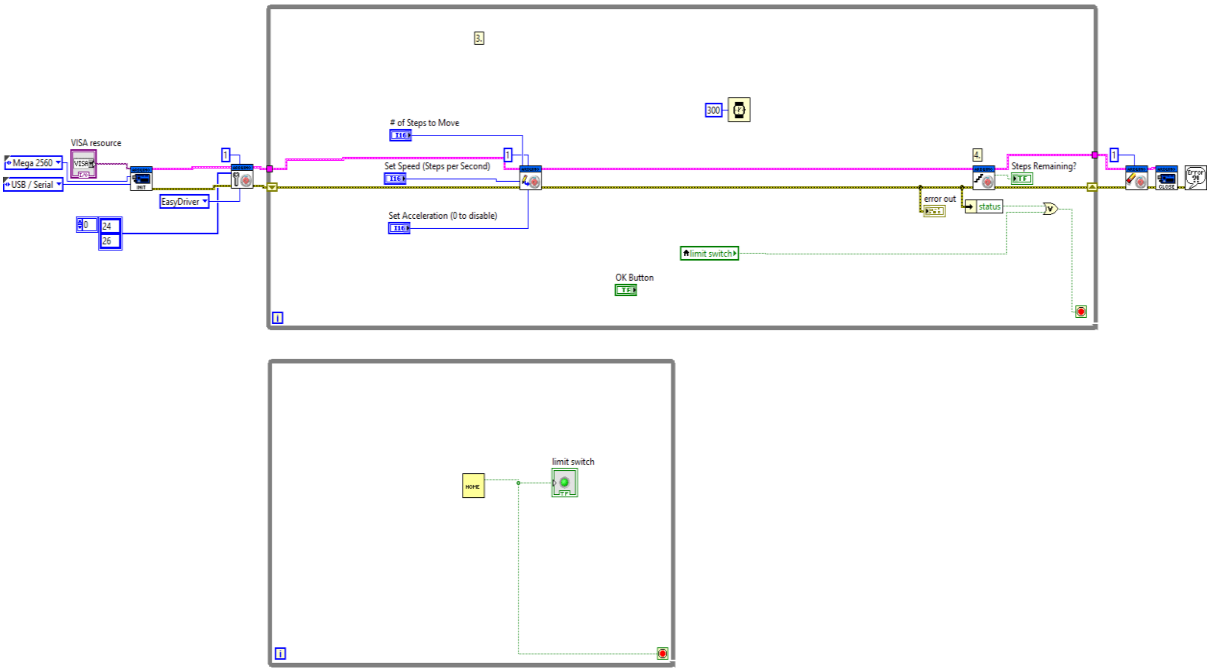

Appendix B . 9: Limit switch stopping an axis

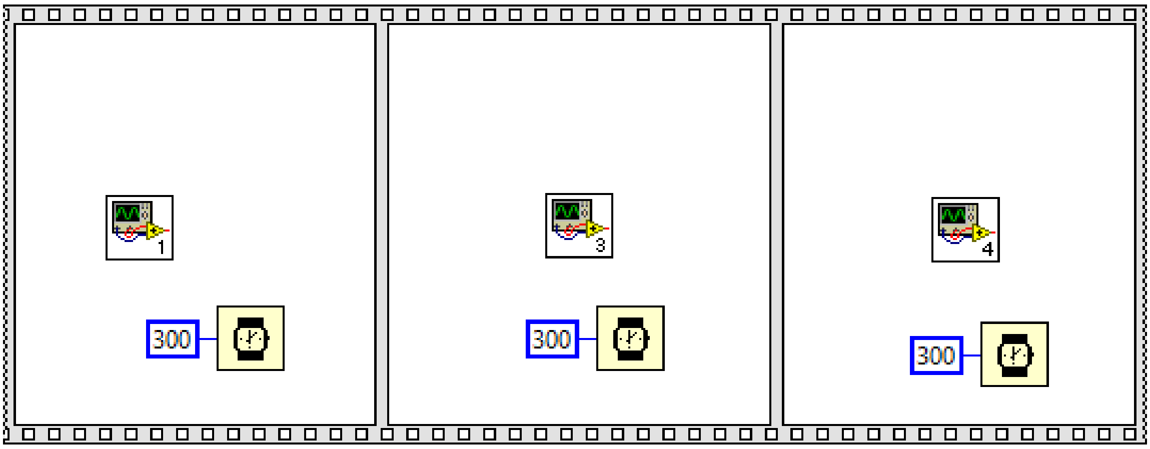

Appendix B . 10 :Limit switch stopping an axis

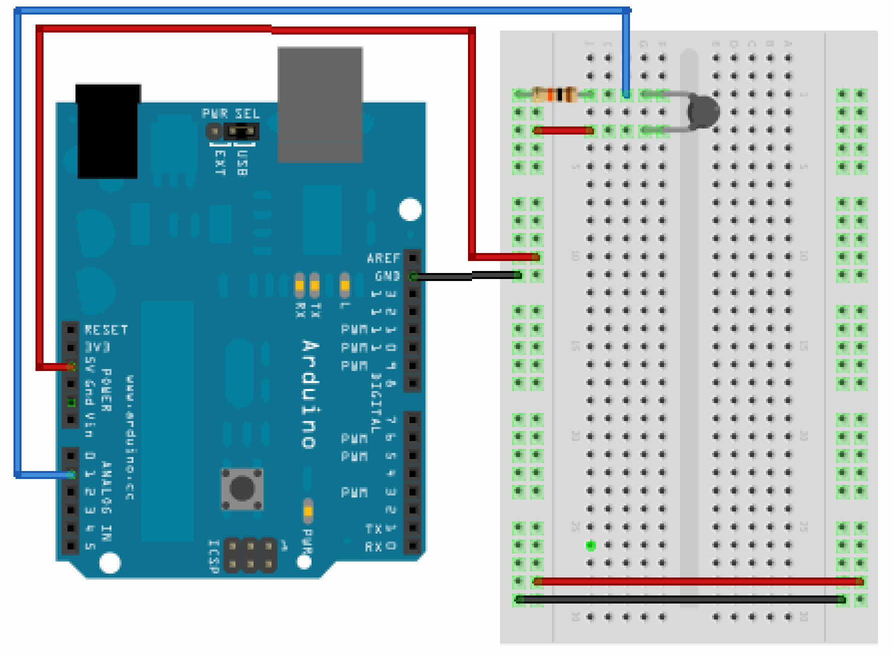

Appendix B . 11: Thermistor connection to Arduino board

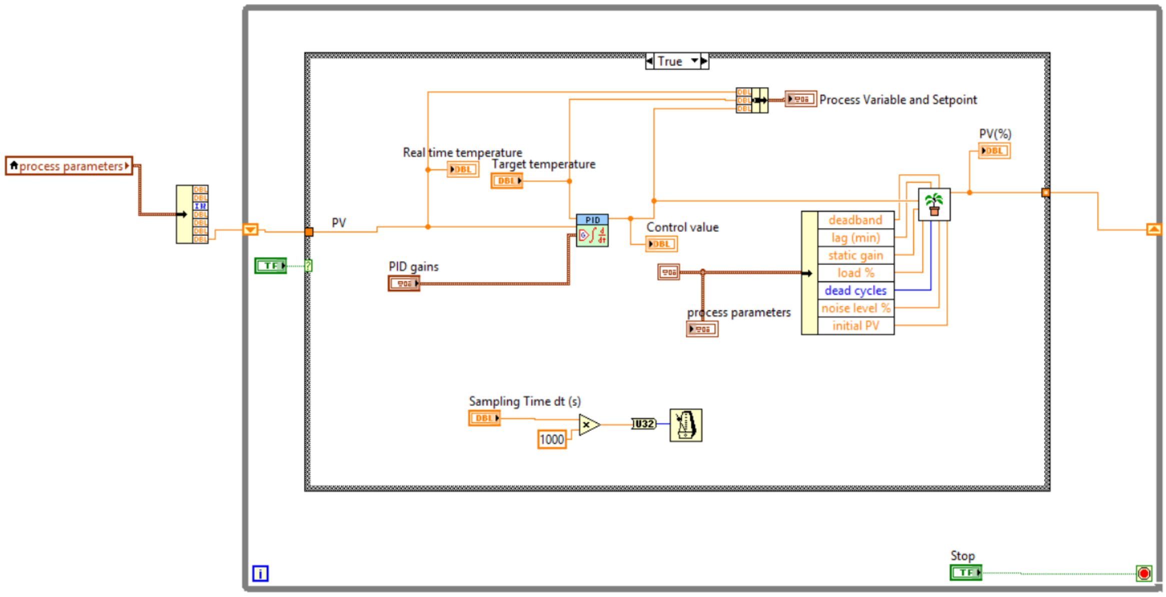

Appendix B . 12: A PID controller for temperature stabilising control

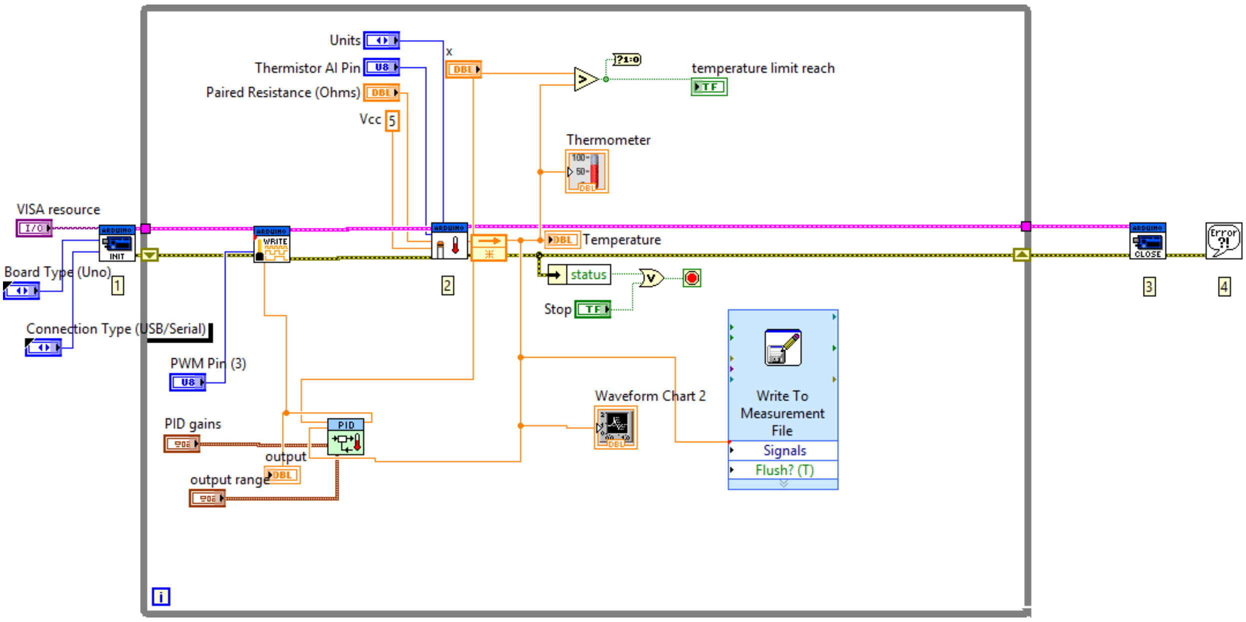

Appendix B . 13:A PID controller for temperature stabilising control

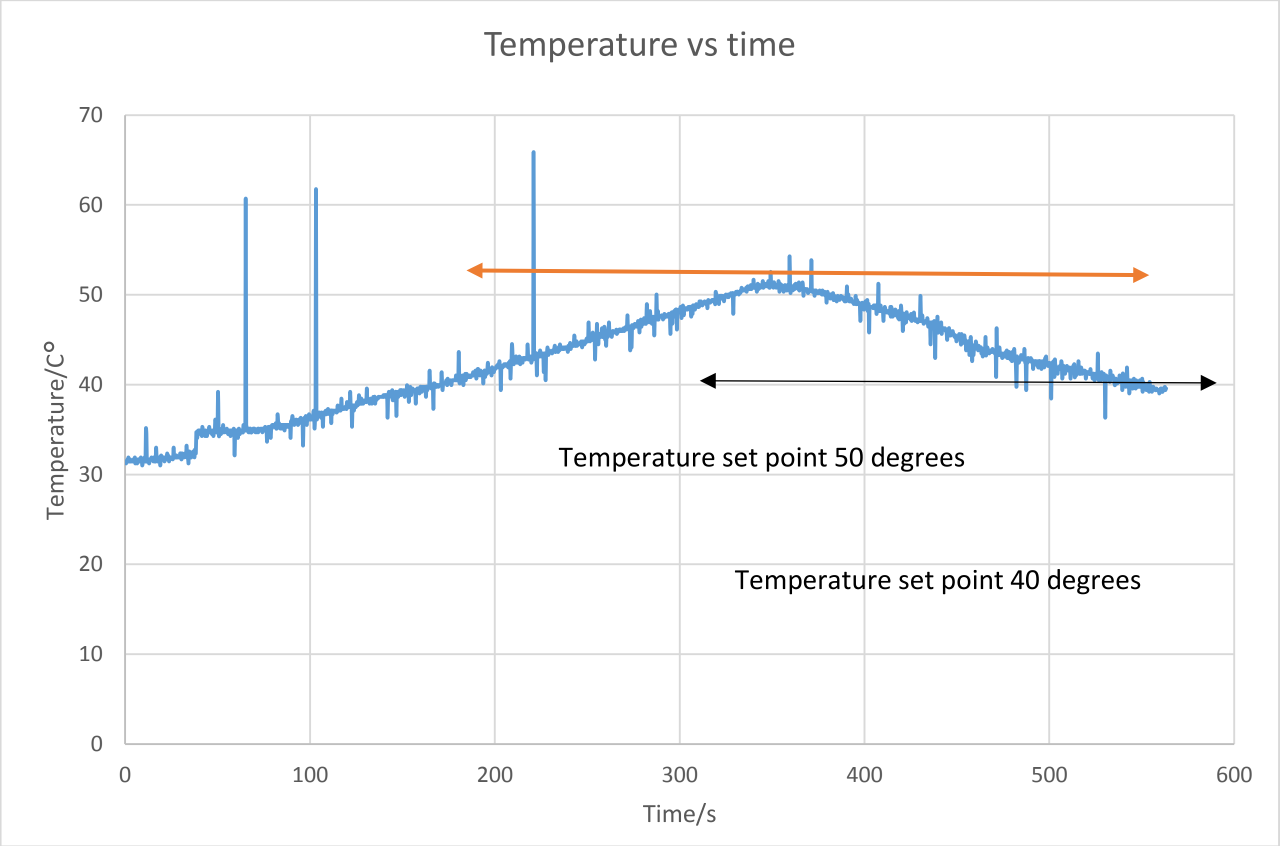

Appendix B . 14: Heating temperature vs Time

Appendix C : AutoCAD drawing for Z-pining insertion head components

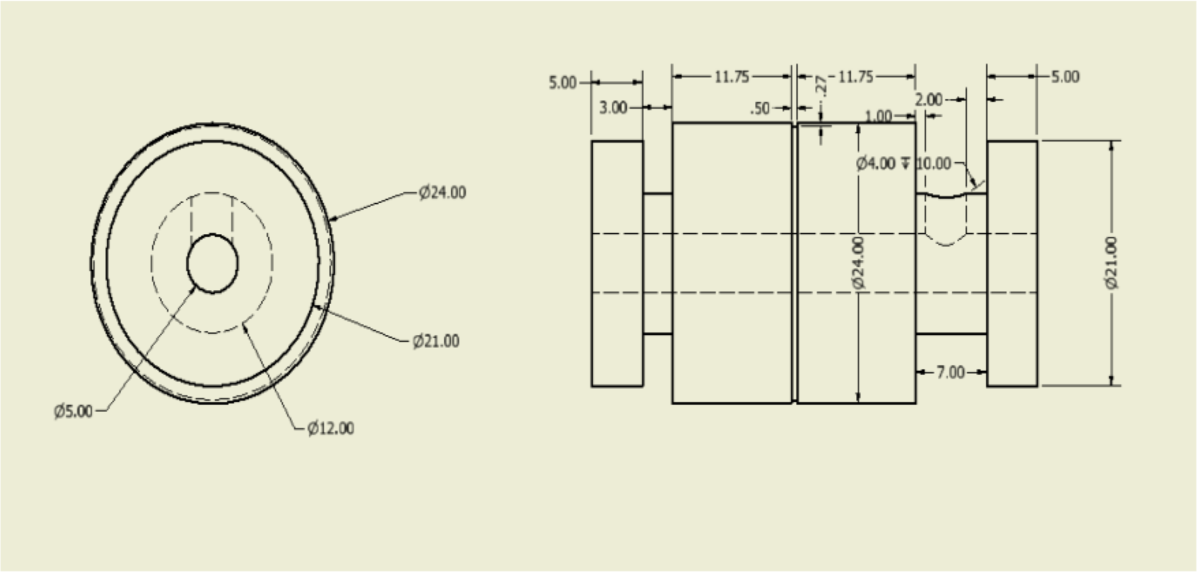

Appendix C . 1: Metal driven pulley and shaft

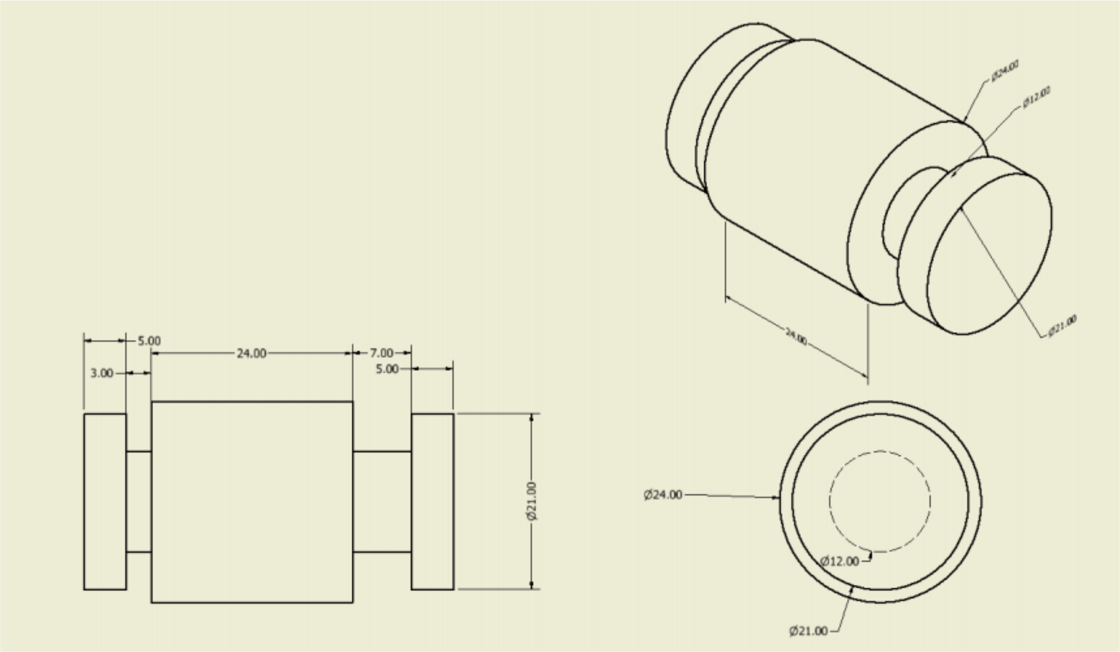

Appendix C . 2: The 3D printed fixed pulley and shaft

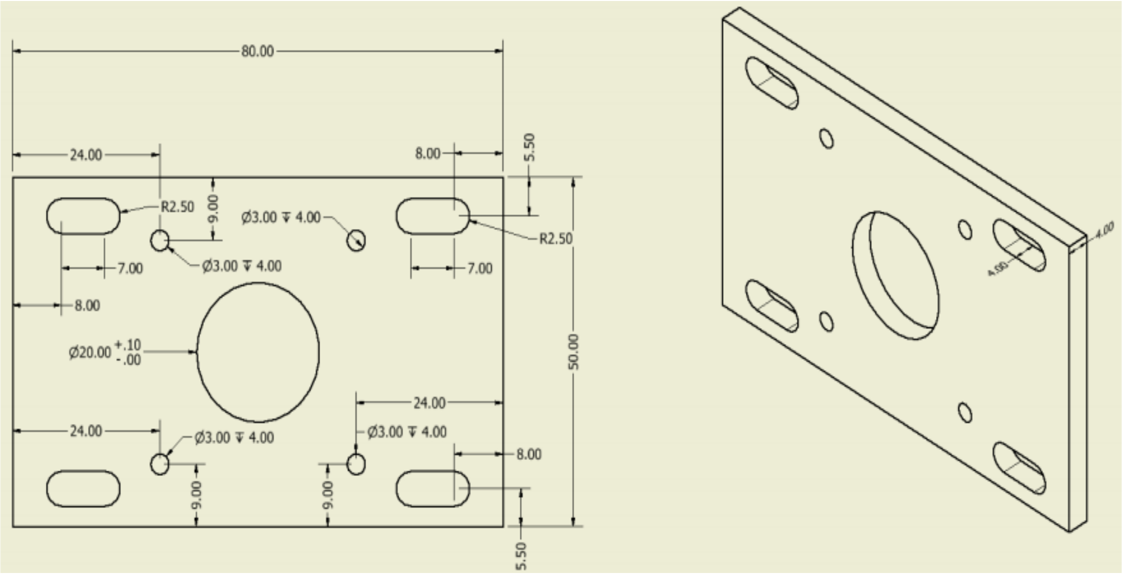

Appendix C . 3: The sliding wall attached outside of the insertion box in order to move the pulley

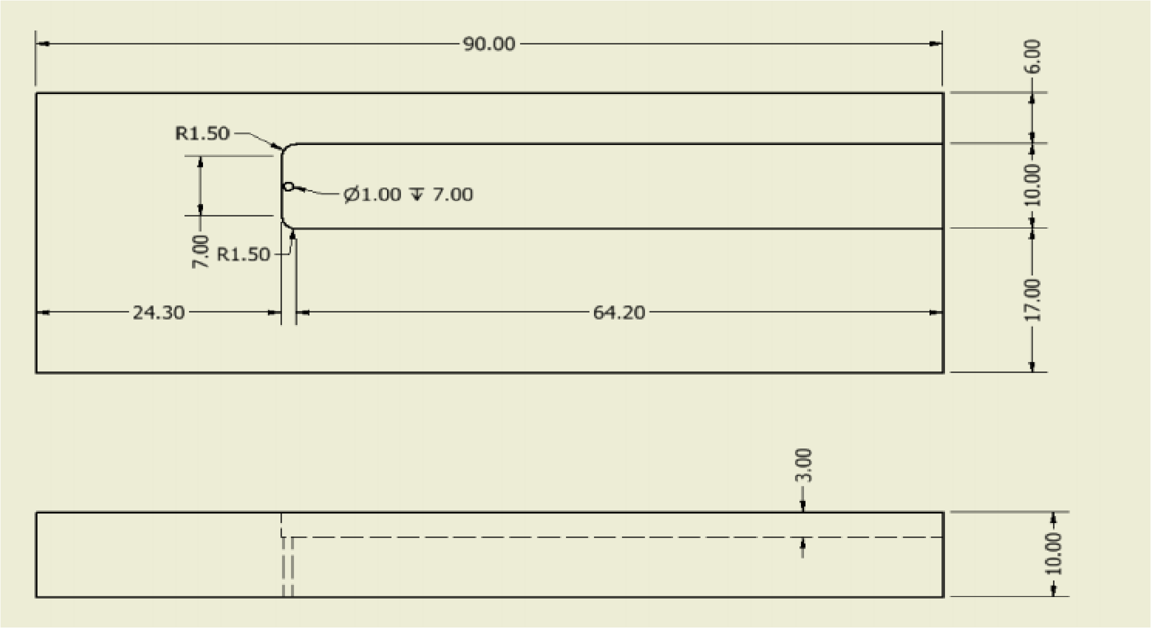

Appendix C. 4: The bottom wall which was made by steel

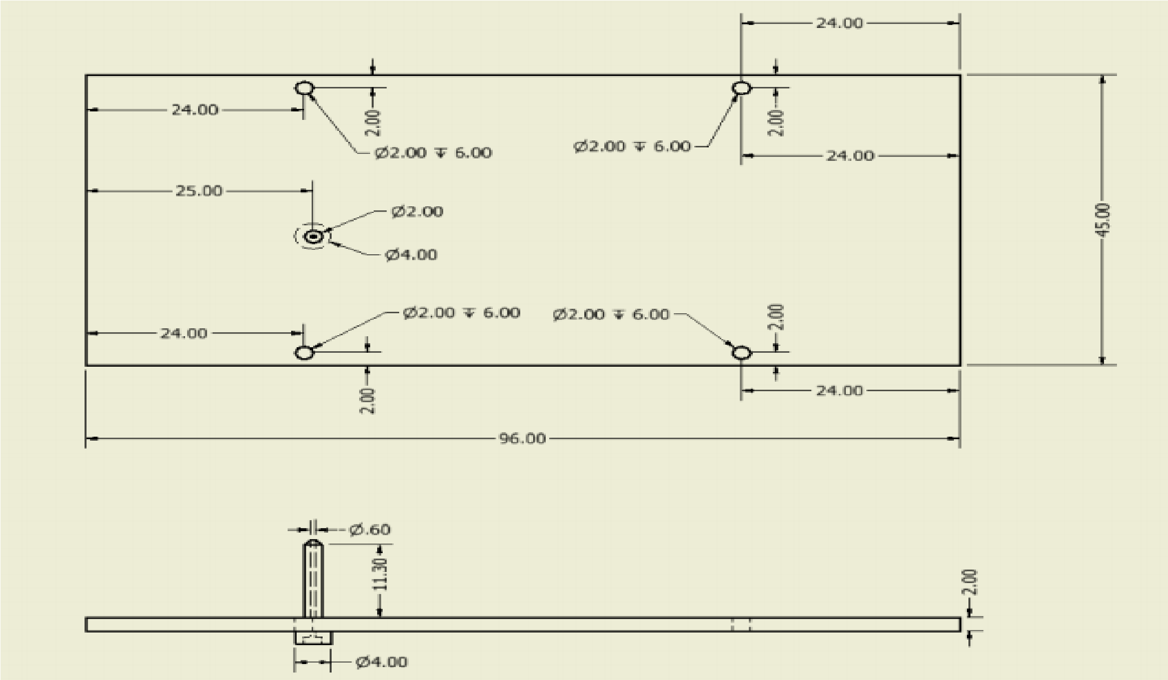

Appendix C. 5: The plastic Z-pin top wall with Z-pin insertion hall

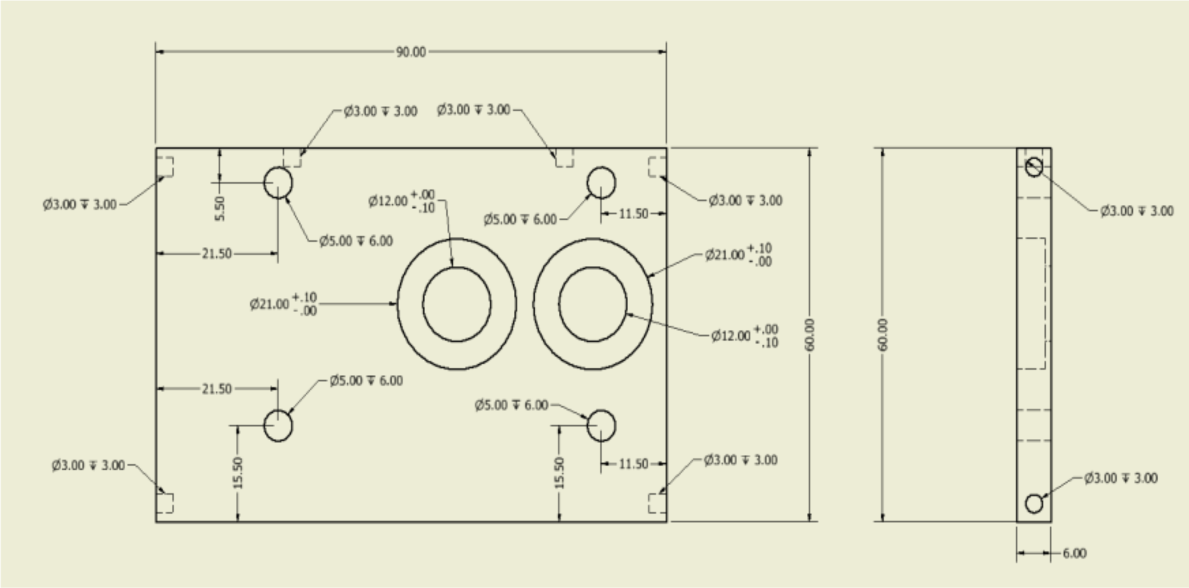

Appendix C. 6: The aluminium front wall

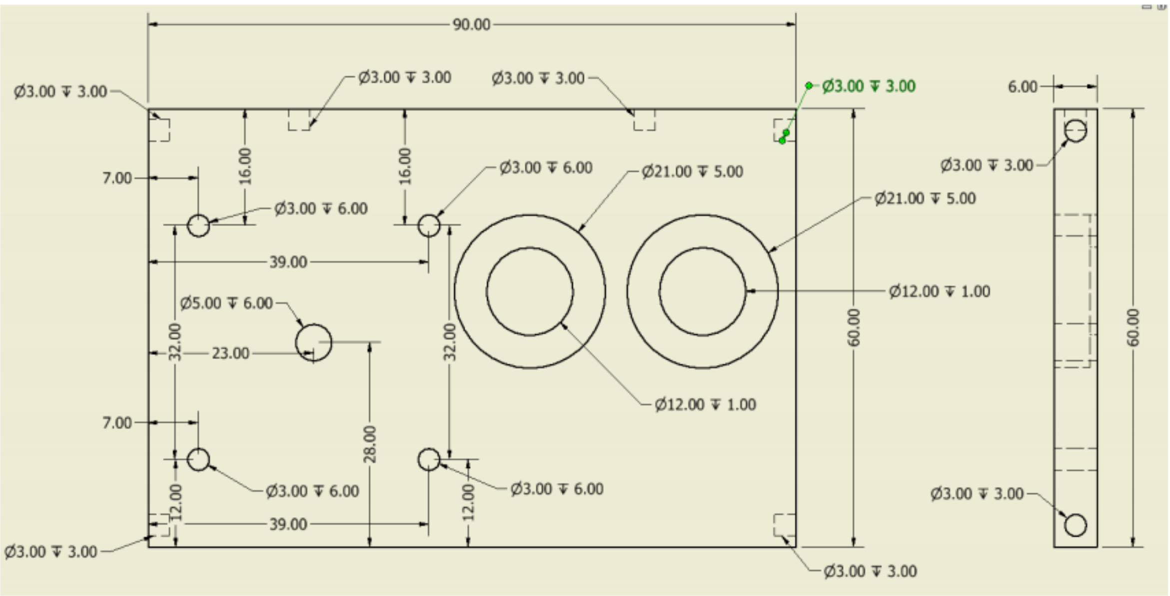

Appendix C. 7: The aluminium back wall